NORTHWESTERN UNIVERSITY

The Role of Alpha-Synuclein Aggregation in Endoplasmic Reticulum Protein Folding and Homeostasis

A DISSERTATION

SUBMITTED TO THE GRADUATE SCHOOL

IN PARTIAL FULFILLMENT OF THE REQUIREMENTS

for the degree

DOCTOR OF PHILOSOPHY

Field of Neuroscience

By

Iva Stojkovska

EVANSTON, ILLINOIS

December 2021

ABSTRACT

Protein homeostasis, or proteostasis, is essential for preserving all cellular functions and involves a balance of protein synthesis, folding, trafficking, and degradation. A collapse in proteostasis is a common feature of many neurodegenerative disorders that are characterized by the accumulation of insoluble protein aggregates in the brain. Parkinson's disease (PD) is a neurodegenerative disorder characterized by large protein aggregates primarily composed of alpha-synuclein (α-synuclein), but how these aggregates perturb the proteostasis pathways is not well understood. To this end, we developed and characterized novel PD patient-derived midbrain dopaminergic neuron models that naturally accumulate and aggregate α-synuclein through endogenous *SNCA* triplications. It is well established that α-synuclein disrupts proper protein trafficking and lysosomal function. Here, we show that α-synuclein aggregates perturb the earlier stages of the proteostasis network by inducing dramatic fragmentation of the endoplasmic reticulum (ER) and compromising ER protein folding capacity. Subsequently, this leads to the misfolding and aggregation of immature lysosomal β-glucocerebrosidase (GCase) in the ER causing downstream lysosomal dysfunction. Despite these ER phenotypes, PD neurons fail to initiate the unfolded protein response, indicating that α-synuclein disrupts the ability of neurons to sense perturbations in ER protein folding. Importantly, these pathogenic phenotypes can be partially attenuated using rescue strategies that target the ER and enhance ER folding capacity. Specifically, we found that ER proteostasis enhancers promote soluble, functional GCase, while co-application with protein trafficking enhancers enhances lysosomal function and reduces pathological α-synuclein levels. Our studies suggest that protein aggregates perturb the ability of neurons to sense misfolding in the ER, and that synergistic enhancement of multiple branches of the proteostasis pathway may provide therapeutic benefit in PD and other synucleinopathies.

Acknowledgements

Receiving a PhD is the greatest honor and the ultimate educational achievement of my lifetime. I wouldn't be able to accomplish this dream of mine if it wasn't for the unconditional support and encouragement from those that came along with me on this grand adventure. This is for you all.

I would like to express my sincere gratitude to my advisor, Dr. Joe Mazzulli, for his continuous support, thoughtful scientific ideas, and guidance throughout the last five years. His insightful feedback pushed me to sharpen my critical thinking skills and showed me what high-quality scientific research should look like. Most importantly, he also taught me to be confident in my work, to not be afraid, and to take chances. I am very thankful that he took a chance on me as his first PhD graduate student. I would also like to thank my thesis committee members, Dr. Gabriela Caraveo-Piso, Dr. Liming Li, and Dr. James Surmeier, for their incredibly valuable input on my project and guidance throughout my graduate training.

I am deeply grateful to my lab mates, former and current, for making my time at Northwestern unforgettable: Stefanos Aivazidis, Karan Sharma, Caleb Pitcairn, Laetitia Francelle, Nandkishore Belur, Kristina Fredriksen, Eilrayna Gelyana, Tino Morella, Naomi Murata, Willayat Wani, and Frieda Zunke. I would like to give a special shoutout to Stefanos for being the best life coach in and outside of the lab, to Karan for putting up with my loudness and bad jokes, and to Caleb for being a fantastic lab desk and apartment building neighbor. Thank you, Laetitia, for sharing your delicious baked goods and for being a source of inspiration on how to be an amazing scientist while also juggling life outside of the lab. Nandkishore, thank you for being a great "co-worker" and for letting me bother you with science questions ever since day one in the lab. Let's not forget the original third musketeer, Kristina, who adventured

with us throughout Chicago and kept lab incredibly entertaining with all that mouse chasing. And lastly, I'd like to thank Frieda for her endless patience as she was showing me the ropes when I first joined the lab and for being an incredible scientific role model. Thank you everyone for being the best science family and the greatest of friends. This would not have been possible without all of you.

My PhD journey began with the greatest roommate ever, Katie Evans. I am so glad that we got to transition into this phase of our life together. Thank you for keeping me sane throughout the last few years and for pushing me to try new things. I will forever cherish our grand adventures in windy San Francisco, spontaneous trips to Target and Coldstone, and our luxurious blanket forts.

My time at Northwestern would not have been as memorable without the best PhD cohort the world has ever seen: Edward Kim, Rummi Ganguly, Kristen Warren, Hayley White, Schnaude Dorizan, Matt Mullen, Migz Ramirez, and Neto Josh. You all are the funniest and craziest oddballs I have ever met, and I could not have asked for a better group of people to go through a PhD with. Some of the greatest memories I will have from this chapter of my life will be the times we spent together. Thank you for teaching me how to do all the stuff I should have learned in college and for making the Mambo No. 5 weekend the best camping trip that has ever existed. I already can't wait to "NUIN" with you all again in our favorite state.

The greatest thank you of all is to my family. To my loving parents, you have celebrated every successful experiment and milestone and endured every failure and stress of graduate school with me. Thank you for always being alongside me as I went through this PhD. I am eternally grateful for your endless love, encouragement, and advice. You have always steered me in the right direction, and I know that I would not be where I am nor who I am today without

you. I dedicate this PhD to my grandparents, Uranija and Vangel, who are the primary reason that I decided to pursue neuroscience and to devote my life to researching neurodegenerative diseases. I hope I have made you proud.

Finally, a big thank you to my partner, Max Garhammer. Even as you began your own PhD, you were and continue to be my greatest cheerleader and have been there for me every step of the way. Your constant source of inspiration and positive energy has helped to push me forward and survive the toughest parts of graduate school. Words cannot express how thankful I am for your unconditional love and support. I am so grateful to science for bringing us together and I can't wait to see where we go together next.

Dedication

Za

Uranija Babinkostova

i

Vangel Babinkostov

LIST OF ABBREVIATIONS

4-MU-Gluc	4-Methylumbelliferyl-β-D-Glucopyranoside
6-OHDA	6-Hydroxydopamine
ATP	Adenosine triphosphate
AD	Alzheimer's disease
ANOVA	Analysis of variance
α-syn	Alpha-synuclein
ATF6	Activating transcription factor 6
BafA1	Bafilomycin A1
BCA	Bicinchoninic acid
BDNF	Brain derived neurotrophic factor
BFA	Brefeldin A
BSA	Bovine serum albumin
cAMP	Cyclic adenosine monophosphate
CANX	Calnexin
Cas9	CRISPR-associated protein 9
CBE	Conduritol-β-epoxide
cDNA	Complementary deoxyribonucleic acid
CICR	Calcium-induced calcium release
Con-A	Concanavilin-A
CRISPR	Clustered regularly-interspaced short palindromic repeats
DA	Dopamine
DANT	Dantrolene
DAPI	4′,6-Diamidino-2-phenylindole
DDSA	Dodecenyl succinic anhydride
DHBP	1,1'-diheptyl-4,4'-bipyridinium dibromide
DILT	Diltiazem
DLB	Dementia with Lewy bodies
DMP-30	2,4,6-tris(dimethylaminomethyl)phenol
DMSO	Dimethyl sulfoxide

DNA	Deoxyribonucleic acid
DOX	Doxycycline
EDEM	ER degradation-enhancing alpha-mannosidase-like protein
EDTA	Ethylenediaminetetraacetic acid
eIF2α	Eukaryotic initiation factor 2-alpha
ELISA	Enzyme-linked immunosorbent assay
EndoH	Endoglycosidase H
Epox	Epoxomicin
ER	Endoplasmic reticulum
ERAD	ER-associated degradation
ETC	Electron transport chain
FBS	Fetal bovine serum
FGF8a	Fibroblast growth factor 8a
FISH	Fluorescence *in situ* hybridization
FTI	Farnesyl transferase inhibitor
GAPDH	Glyceraldehyde 3-phosphate dehydrogenase
GBAP	*GBA1* pseudogene
GCase	β-Glucocerebrosidase
GD	Gaucher's disease
GDNF	Glial cell-derived neurotrophic factor
GluCer	Glucosylceramide
gRNA	Guide RNA
GRP78	Glucose-regulated protein 78
GRP94	Glucose-regulated protein 94
GSL	Glycosphingolipid
GWAS	Genome-wide association studies
H4	Human neuroglioma
HEK	Human embryonic kidney
HEPES	4-(2-hydroxyethyl)-1-piperazineethanesulfonic acid
Hex B	Hexosaminidase B

HPLC	High-performance liquid chromatography
HR	Homologous recombination
HSB	High salt buffer
IF	Immunofluorescence
iPD	Idiopathic Parkinson's disease
iPSCs	Induced pluripotent stem cells
iPSn	Induced pluripotent stem cell-derived neurons
IRE1	Inositol-requiring enzyme 1
KD	Knock-down
kDa	Kilodalton
Klf4	Kruppel-like factor 4
LIMP2	Lysosomal integral membrane protein 2
L-DOPA	l-3,4-Dihydroxyphenylalanine; levodopa
MAM	Mitochondria-associated membranes
MOI	Multiplicity of infection
MPP+	1-methyl-4-phenylpyridinium
mRNA	Messenger ribonucleic acid
MS	Mass spectrometry
Mut	Mutant
NAC	Non-amyloid component
NaF	Sodium fluoride
Na_3VO_4	Sodium orthovanadate
NGS	Normal goat serum
NMA	N-methylaniline
Oct3/4	Octamer-binding transcription factor 3/4
OsO_4	Osmium tetraoxide
PBS	Phosphate buffered saline
PCR	Polymerase chain reaction
PD	Parkinson's disease
PDI	Protein disulfide isomerase

PDL	Poly-D-lysine
PERK	Protein kinase (PKR)–like ER kinase
PFA	Paraformaldehyde
PFB-FDGluc	5-(Pentafluorobenzoylamino)fluorescein di-b-D-glucopyranoside
PIC	Protease inhibitor cocktail
PLA	Proximity ligation assay
PMI	Post-mortem index
PMSF	Phenylmethylsulfonyl fluoride
PURM	Purmorphamine
PVDF	Polyvinylidene fluoride
qPCR	Quantitative real-time polymerase chain reaction
RNA	Ribonucleic acid
RNAseP	Ribonuclease P
ROS	Reactive oxygen species
RT-PCR	Reverse transcriptase polymerase chain reaction
RyR	Ryanodine receptor
SD	Standard deviation
SDS	Sodium dodecyl sulfate
SDS-PAGE	Sodium dodecyl sulfate polyacrylamide gel electrophoresis
SEM	Standard error of the mean
SHB	Sucrose HEPES buffer
SHH	Sonic hedgehog
shRNA	Short hairpin ribonucleic acid
SIM	Structured illumination microscopy
SMAD	C. elegans Sma gene and Drosophila mothers against decapentaplegic proteins
SNARE	Soluble N-ethylmaleimide-sensitive factor (NSF) attachment protein receptor
SNpc	Substantia nigra pars compacta
Sox2	Sex determining region Y-box 2
SSEA4	Stage-specific embryonic antigen 4
TEM	Transmission electron microscopy

TBS	Tris-buffered saline
TBS-T	Tris-buffered saline with 0.2% Tween-20
Tg	Thapsigargin
TGFβ-3	Transforming growth factor β-3
TH	Tyrosine hydroxylase
TRA1-60	T-cell receptor alpha locus
UPR	Unfolded protein response
UPS	Ubiquitin proteasome system
WT	Wild-type
XBP1	X-box binding protein 1

TABLE OF CONTENTS

Co-authored publications

LIST OF FIGURES

CHAPTER 1

CHAPTER 2

CHAPTER 3

LIST OF TABLES

Supplementary Tables

CHAPTER 1

Introduction

Preface. The introductory chapter of this dissertation has been adapted largely from Stojkovska et al., 2017, a peer-reviewed review article on the "Molecular mechanisms of α-synuclein and *GBA1* in Parkinson's disease" published in the journal *Cell and Tissue Research*.

1.1 Parkinson's disease: hallmark symptoms, pathology, and current treatments

Parkinson's disease (PD) is the most prevalent motor disease and second most common neurodegenerative disorder affecting approximately 1% of people over the age of 60 (Nussbaum and Ellis, 2003) and over 4% of people by age 85. Although PD is commonly thought of as an age-dependent disorder with an average age of onset of 60, rare early-onset cases can occur with diagnosis at age 40 or younger as a result of genetic mutations (Quinn et al., 1987). The clinical features of PD include motor deficits such as a distinctive resting tremor, slowness of movement (bradykinesia), rigidity of the limbs or trunk, and impaired balance and coordination. However, the majority of PD patients also experience non-motor symptoms such as dementia, as well as depression, psychoses, sleep disruption, and gastrointestinal dysfunction.

Although the cause of the non-motor symptoms in PD remains elusive, the motor symptoms of PD are thought to occur as a result of decreased dopamine neurotransmitter levels due to a progressive loss of dopaminergic neurons within the substantia nigra pars compacta (SNpc) region of the midbrain. In addition to the SNpc, neurodegeneration has also been documented in many other regions of the nervous system, including the cortex, hippocampus, locus coeruleus, amygdala, and parts of the autonomic nervous system (Alexander, 2004).

Pathologically, PD is characterized by the presence of insoluble protein inclusions called Lewy bodies and Lewy neurites, located in the cytoplasm and neurites, respectively, within surviving neurons (Spillantini et al., 1997). Classic Lewy bodies appear spherical in shape, with an 8-30 μm diameter and a dense eosinophilic core surrounded by a clear surrounding halo (Forno, 1996). Initial studies consistently identified filamentous structures within Lewy inclusions that contain cross-β sheets and exhibit properties similar to other disease-linked amyloid proteins including amyloid-β and tau. However, for many years, the biochemical composition of Lewy inclusions remained largely debated. It is now widely accepted that the primary component of Lewy inclusions is the protein alpha-synuclein (α-syn). α-Syn immunoreactivity has now become the best tool to identify Lewy inclusions in the nervous system and has allowed for the discovery of a family of neurodegenerative diseases defined by α-syn inclusions, termed synucleinopathies.

The recognition of the role of dopamine in PD led to the development of the dopamine precursor levodopa (L-DOPA) in 1961 (Birkmayer and Hornykiewicz, 1961) as dopamine replacement therapy for patients. However, as the disease advances, the increase in dosage and prolonged use of L-DOPA causes patients to experience side effects of the drug, including dyskinesias (spontaneous, involuntary movements) and hallucinations. Although research in the area of PD has been extensive, the current treatment options ameliorate only the symptoms of PD. Currently, no therapy exists for treating the underlying neurodegeneration and progression of PD. Therefore, there is an urgent need to gain a better understanding of the molecular mechanisms behind PD pathology.

1.2 Genetics of Parkinson's disease

A genetic component to PD was long thought to be unlikely because the majority of PD cases occur sporadically. However, it is now widely accepted that a subset of PD cases, approximately 5-10%, have a hereditary etiology. Sporadic and familial PD patient brains are usually pathologically indistinguishable in that they both contain Lewy inclusions. This suggests that both sporadic and familial PD cases share a common pathogenic mechanism.

The first clues into the molecular etiology of PD occurred as a result of genetic analysis of a family, called the Contursi kindred, with autosomal dominant inheritance of PD. This led to the identification of a mutation at residue 53 from alanine to threonine (A53T) in the *SNCA* gene that encodes α-syn (Polymeropoulos et al., 1997; Spillantini et al., 1995), a small 140 amino acid pre-synaptic protein (Figure 1-1). Critical to the pathogenic mechanism of α-syn, A53T and other familial-linked point mutations (e.g., A30P, E46K, H50Q, G51D, A53E) (Figure 1-1) result in accelerated oligomerization or fibrillization of the protein (Conway et al., 1998; Cullen et al., 2011; Ghosh et al., 2013; Greenbaum et al., 2005; Rutherford et al., 2014), indicating a probable gain-in-toxic function mediated by protein aggregation.

Since the initial discovery of *SNCA* mutations, additional rare monogenic forms with autosomal recessive modes of inheritance have been identified as causative factors for PD. Mutations in Parkin, *PINK1*, *ATP13A2*, and DJ-1 are known to lead to early-onset PD and their recessive mode of inheritance indicates that neurodegeneration likely occurs through a loss-of-function mechanism (Scott et al., 2017). Interestingly, the putative normal functions of these genes all converge on the mitochondrial and lysosomal systems. For instance, both Parkin and *PINK1* play important roles in initiating clearance of damaged mitochondria via lysosomes, termed mitophagy (Youle and Narendra, 2011). *ATP13A2* is thought to be essential for proper

functioning of the lysosome (Schultheis et al., 2013; Tsunemi and Krainc, 2014), and DJ-1 is thought to protect mitochondria from oxidative damage (Guzman et al., 2010). Mutations in leucine-rich repeat kinase 2 (*LRRK2*), such as G2019S, represent the most common form of familial PD. Previous studies have identified interactions of *LRRK2* with multiple Rab proteins, which are key mediators of protein trafficking (Cookson, 2016; Steger et al., 2016), leading to defects in vesicular transport and the lysosomal clearance pathway. Consistent with the importance of disrupted protein trafficking in PD pathogenesis, mutations in a distinct trafficking component called *VPS35* that mediates endosome-to-Golgi trafficking also causes autosomal dominant PD (Vilarino-Guell et al., 2011; Zimprich et al., 2011). Together, genetic analyses of familial PD have implicated a role for mitochondria, protein trafficking, and lysosomes as key pathways involved in disease progression.

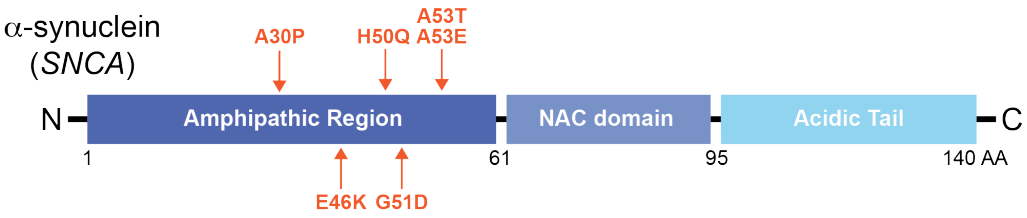

Figure 1-1. Schematic diagram of α-synuclein and common PD-linked mutations. *SNCA* encodes α-synuclein (α-syn), a small 140 amino acid (AA) protein that is approximately 14 kilodaltons (kDa) in size. α-Syn is comprised of three distinct domains: (1) an N-terminal amphipathic region, which contains the six missense mutations known to cause familial PD as well as seven evolutionarily conserved KTKEGV motifs that give α-syn its ability to interact with membranes, (2) a central hydrophobic non-amyloid component (NAC) domain that is responsible for the increased propensity of the protein to form aggregates, and (3) an acidic C-terminal tail that contains mostly negatively charged amino acids and is largely unfolded.

1.3 Physiological and pathological roles of α-synuclein

α-Syn is an abundantly expressed protein in neurons, where it is localized at presynaptic

terminals (Maroteaux et al., 1988), particularly in the striatum, hippocampus, neocortex, thalamus, and the cerebellum (Iwai et al., 1995). Although the normal physiological function of α-syn is not completely understood, the ability of α-syn to interact with synaptic proteins (Burre et al., 2014) suggests that it plays a regulatory role in synapses, particularly in regard to synaptic plasticity (Clayton and George, 1999), neurotransmitter release (Emanuele and Chieregatti, 2015), presynaptic vesicle pool maintenance (Murphy et al., 2000), and the assembly of SNARE complexes at presynaptic terminals (Burre et al., 2010; Chandra et al., 2005).

Aside from *SNCA* point mutations, it is also known that the overabundance of wild-type α-syn can be detrimental. Certain features of PD can be mimicked by the overexpression of human wild-type α-syn *in vivo*, including α-syn inclusion formation and motor deficits (Giasson et al., 2002; Kahle et al., 2000; Masliah et al., 2000; Matsuoka et al., 2001). Perhaps the most critical genetic evidence for a role of α-syn in PD pathogenesis comes from the identification of PD patients that harbor multiplications in the *SNCA* genomic region (Chartier-Harlin et al., 2004; Singleton et al., 2003) leading to the overexpression of the wild-type α-syn protein.

The first description of a family with an *SNCA* multiplication was in 2003, where the genetic cause was determined to be a triplication (3X) in the *SNCA* genomic region (Singleton *et al.*, 2003) resulting in a total of four copies of *SNCA*. The extent of the genomic triplication region was determined to be 1.61 to 2.04 Mb in size (Singleton *et al.*, 2003). Importantly, the region of triplication contained 16 other annotated or putative genes aside from *SNCA*. Although studies have not eliminated the other 16 genes as contributors for this PD form, *SNCA* is thought to be the causative factor primarily due the significant role it plays in PD. Autosomal dominant PD patients with a duplication (2X) in *SNCA*, resulting in a total of three *SNCA* copies, were identified shortly thereafter (Chartier-Harlin *et al.*, 2004). Genetic analyses have revealed widely

variable sizes of the *SNCA* duplicated regions, ranging from 0.2 to 41.2 Mb, and containing anywhere from 2 to 150 genes (Chartier-Harlin *et al.*, 2004). Interestingly, the severity of the clinical phenotype of *SNCA* multiplication patients is dependent on α-syn dosage (Singleton and Gwinn-Hardy, 2004). By contrast with *SNCA*-2X patients whose phenotype closely resembles sporadic PD patients, *SNCA*-3X patients have an early age-of-onset and a more rapid disease progression (Fuchs et al., 2007; Singleton *et al.*, 2003). Moreover, patients with *SNCA* multiplications display the classical Lewy pathology, indicating that a mere overabundance of the wild-type protein leads to a neurodegenerative condition. However, the molecular mechanism by which wild-type α-syn overexpression leads to neurotoxicity and contributes to PD pathogenesis remains unknown. The overarching research goal of this dissertation was to identify this molecular mechanism.

1.4 Lysosomal dysfunction as a contributor to Parkinson's disease pathology

Protein homeostasis, or proteostasis, involves the balance of synthesis, folding, trafficking, and degradation of proteins. Many neurodegenerative diseases, including PD, are characterized by a collapse in proteostasis. The soundly documented feature of Lewy inclusions composed of aggregated α-syn is direct evidence that the mechanisms responsible for α-syn clearance are disrupted in the PD brain.

The degradation of α-syn occurs through autophagy via lysosomes (Cuervo et al., 2004; Webb et al., 2003). Lysosomes are acidic compartments within a cell that contain hydrolytic enzymes responsible for the digestion of macromolecules such as misfolded proteins, as well as organelles and other cell debris. Genome-wide association studies (GWAS) in PD patients have identified several PD risk genes, most of which have key roles in autophagy and lysosomal

function (Chang et al., 2017; Nalls et al., 2019; Nalls et al., 2014; Simon-Sanchez et al., 2009). Perhaps the most critical evidence for lysosomal dysfunction in PD came from the clinic, where parkinsonian symptoms were observed in patients with the lysosomal storage disorder, Gaucher disease (GD) (Neudorfer et al., 1996). Most patients with type I GD present with visceral symptoms including enlargement of the spleen and liver, anemia, bone abnormalities, and macrophages containing accumulated lysosomal substrates (Grabowski, 2008). At the time, the finding of neurological involvement in these GD patients was unusual since the majority of type I GD patients were not widely known to present with neurological symptoms. However, more severe forms of GD have been classified as types 2 and 3 with infantile or adolescent onset and often present with prominent neurodegeneration (Grabowski, 2008). Patients with GD have loss-of-function mutations in the *GBA1* gene that encodes the lysosomal hydrolase, β-glucocerebrosidase (GCase), a hydrolase that catalyzes the breakdown of the lipid glucosylceramide (GluCer) into glucose and ceramide (Brady et al., 1965). Since many of the known *GBA1* mutations, including N370S, L444P, and 84GG, reduce the stability and / or enzymatic function of the enzyme (Grace et al., 1994), lysosomes accumulate the undigested substrate GluCer and other lipids which leads to compromised lysosomal function.

After the discovery of PD symptoms present in type I GD patients, clinicians also noted that first-degree relatives of GD patients with heterozygous mutations in *GBA1* presented with Parkinsonism at a higher-than-expected frequency, suggesting that heterozygote carriers were also at risk (Goker-Alpan et al., 2004). Validation studies were subsequently performed on a large population of sporadic PD patients, demonstrating that 5–10% of patients harbored at least one *GBA1* mutation (Sidransky et al., 2009). The clinical progression of PD patients with *GBA1* mutations is often more rapid compared to patients without mutations, and there is a greater risk

for cognitive impairment (Brockmann et al., 2011; McNeill et al., 2012; Neumann et al., 2009; Sidransky *et al.*, 2009; Tan et al., 2007). Like sporadic PD, the pathology of *GBA1*-PD patient brains also involves the loss of nigral dopamine neurons and the presence of Lewy bodies and neurites (Westbroek et al., 2011).

It is now widely accepted that *GBA1* mutations represent one of the strongest genetic risk factors for the development of PD. Interestingly, *GBA1* mutations have also been linked to another synucleinopathy, dementia with Lewy bodies (Nalls et al., 2013), further establishing the relationship of *GBA1* to synucleinopathies. Lewy body inclusions composed of α-syn have been documented in the brains of GD patients with neurological symptoms (Wong et al., 2004), strongly suggesting that α-syn also plays a key role in the neurodegenerative process of GD patients.

1.5 Defects in protein trafficking play a role in Parkinson's disease pathology

Aside from mutations in lysosomal components, genetic analyses indicate that defects in another critical component of the proteostasis network, vesicular trafficking, also contribute to PD pathogenesis (Hunn et al., 2015; Martin et al., 2014). Disruptions in protein trafficking such as due to mutations in *LRRK2* or *VPS35* have been strongly implicated in PD pathology (refer to section 1.2). Moreover, various models of PD pathology indicate that α-syn can disrupt numerous intracellular trafficking steps, including those at the early and late endosomes (Outeiro and Lindquist, 2003) as well as lysosomes (Chung et al., 2013; Mazzulli et al., 2011). Although α-syn is largely a disordered protein, one hypothesis for how α-syn can disrupt vesicular trafficking comes from studies of its biophysical properties which identified that α-syn has a propensity to bind lipid membranes (Burre *et al.*, 2014; Theillet et al., 2016).

The proper maturation of lysosomal proteins, including GCase, requires their trafficking from the endoplasmic reticulum (ER) to the Golgi portion of the secretory pathway prior to their delivery to lysosomes. Previous work from our group and others has shown that α-syn can impair ER-to-Golgi protein trafficking (Cooper et al., 2006; Gitler et al., 2008; Gosavi et al., 2002; Thayanidhi et al., 2010), resulting in reduced lysosomal function due to the accumulation of immature lysosomal proteins in the ER (Cuddy et al., 2019; Mazzulli *et al.*, 2011; Mazzulli et al., 2016). Specifically, α-syn overexpression has been shown to lead to its direct binding and disruption of ER-Golgi SNARE proteins, such as ykt6, which are vital for mediating membrane fusion (Cuddy *et al.*, 2019; Thayanidhi *et al.*, 2010). Additionally, overexpression of several ER-Golgi trafficking components, such as Rab1, can suppress α-syn-induced toxicity (Cooper *et al.*, 2006), further demonstrating the importance of proper ER to Golgi transport for normal cellular function.

1.6 Cellular maintenance of endoplasmic reticulum protein homeostasis

The ER is a large intracellular organelle that forms an extensive interconnected network composed of branching tubules and flattened cisternae. It is a highly dynamic structure whose morphology is regulated by membrane fission and fusion events. These structural features support the remarkable number of functions that the ER performs, including protein folding, lipid synthesis, and calcium regulation.

Perhaps the most critical functions of the proteostasis network take place in the ER compartment. Approximately one-third of the cell's proteome is synthesized, folded, and processed in the ER. Calcium-dependent molecular chaperones are proteins that aid in the proper folding of newly synthesized proteins and therefore play a pivotal role in maintaining ER

proteostasis. The calcium-dependent ER lectin chaperones, calnexin (CANX) and calreticulin (CALR), are particularly important for maintaining proper protein folding and quality control by binding partially folded or misfolded monoglucosylated proteins including GCase and other lysosomal hydrolases (Ou et al., 1993; Tan et al., 2014). Improperly folded proteins can rebind CANX or CALR for additional folding cycles, however if the folding attempts are unsuccessful, terminally misfolded proteins will be removed from the ER by retro-translocation and degraded by the ubiquitin proteasome system (UPS) via a process called ER-associated degradation (ERAD).

Another important group of ER chaperones are the glucose-regulated proteins (GRPs). GRPs are members of the heat shock protein family of chaperones and are constitutively expressed proteins that can be induced under stressful conditions. Of all the GRP chaperones, GRP78 is considered to be the master regulator of the ER. In addition to facilitating protein folding, GRP78 is also responsible for controlling the activation of transmembrane ER stress sensors (Figure 1-2) and for retrograde transport across the ER membrane of aberrant proteins destined for degradation by the UPS.

Disrupted protein trafficking and accumulation of unfolded or misfolded proteins in the ER overwhelms the folding machinery, invariably leading to ER stress and initiation of the unfolded protein response (UPR) (Figure 1-2). The UPR constitutes a series of signaling pathways in an attempt to restore ER proteostasis by decreasing overall protein synthesis, reinforcing protein folding and quality controls, and / or enhancing protein degradation mechanisms. The three main stress sensors that initiate the UPR include inositol-requiring enzyme 1 (IRE1), double-stranded RNA-activated protein kinase (PKR)–like ER kinase (PERK), and activating transcription factor 6 (ATF6) (Figure 1-2). Under normal conditions, GRP78 is

directly bound to IRE1, PERK, and ATF6. In the presence of an unfolded or misfolded protein, GRP78 dissociates from the three stress sensors in order to aid the misfolded protein. This dissociation leads to the subsequent activation of PERK, IRE1, and ATF6, each of which induce rapid signals to the nucleus for transcriptional upregulation of quality control machinery and expansion of the ER to accommodate excess protein load (Figure 1-2). The UPR provides the cell with time and the proper equipment to deal with and recover from ER stress. However, prolonged or chronic ER stress can lead to the activation of apoptotic pathways mediated by PERK and IRE1 (Ron and Walter, 2007), suggesting that time is an important factor for determining cell fate.

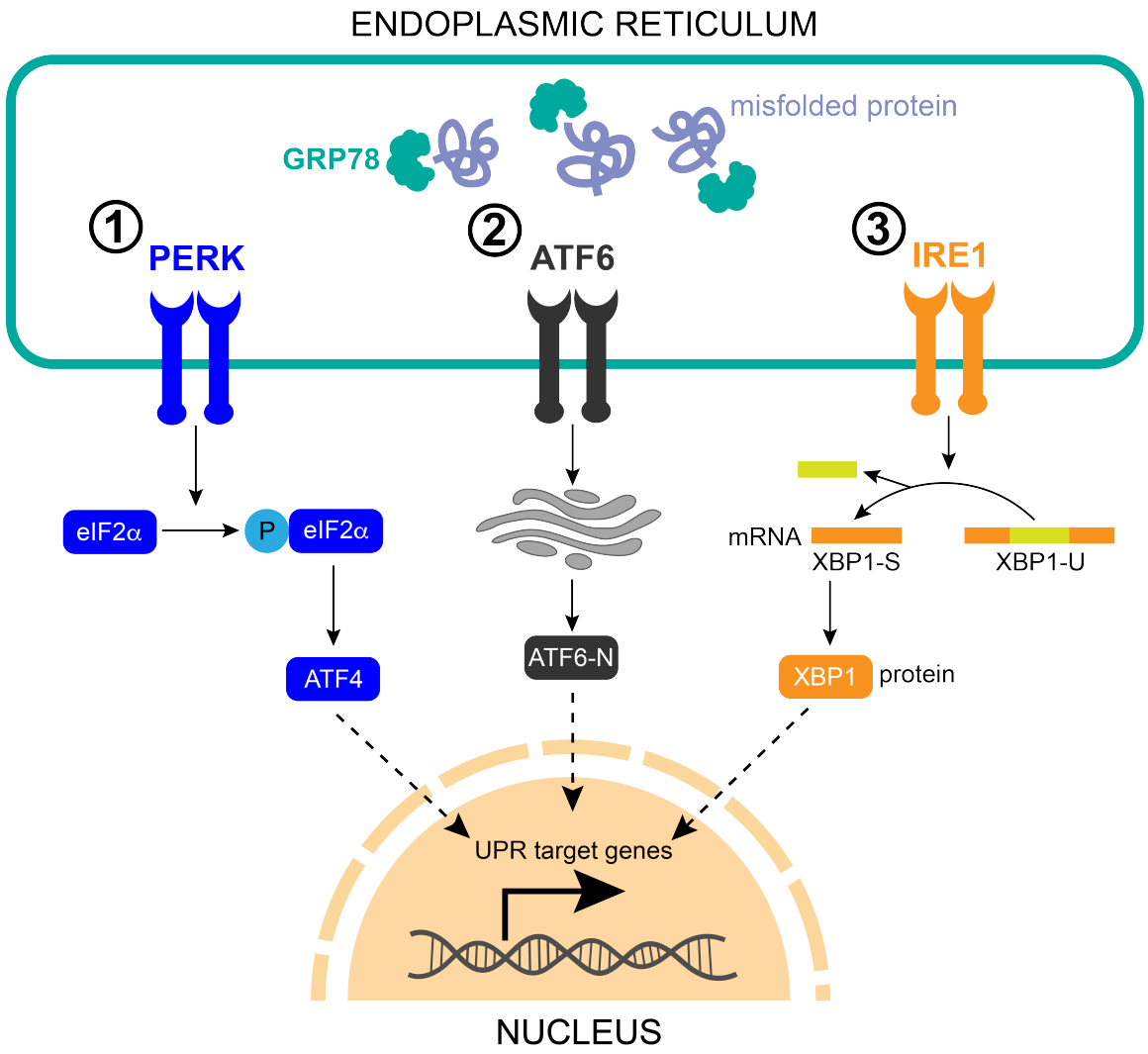

Figure 1-2. Overview of the UPR signaling pathways initiated during ER stress.

(1) Activation of PERK leads to the phosphorylation and subsequent inactivation of the eukaryotic initiation factor 2 alpha (eIF2α) that is normally required for initiating protein translation, thereby decreasing the cell's protein load. In addition, the PERK UPR arm allows for the selective translation of several mRNAs including activating transcription factor 4 (ATF4), which translocates to the nucleus to regulate genes involved in stress adaptation.

(2) ATF6 activation leads to its translocation from the ER to the Golgi where it is cleaved by proteases to generate an N-terminal fragment, ATF6-N, which acts as a transcriptional activator for ER chaperones and components necessary for ERAD.

(3) Activation of IRE1 stimulates its endoribonuclease activity leading to the splicing of X-box-binding protein 1 (XBP1-U) mRNA. Translation of the spliced XBP1-S mRNA results in an activated transcriptional activator XBP1 that translocates to the nucleus to activates genes important for protein folding and ERAD.

1.7 Dissertation overview

A fundamental question that remains open in the neurodegeneration field is how insoluble α-syn aggregates, which are the primary component of Lewy body and neurite inclusions, lead to neurodegeneration. Genetic studies have identified mutations in *SNCA* that lead to the development of PD. More recently, multiplications in the wild-type *SNCA* gene were also identified to be responsible for PD, indicating that a mere increase in α-syn dosage is directly related to PD pathogenesis. However, the molecular mechanism by which wild-type α-syn overexpression contributes to neuronal toxicity and contributes to PD pathogenesis remains unknown. Therefore, the main goal of this dissertation was to gain mechanistic insight into this biological process.

Based on many current findings that describe in detail the mechanistic connection of lysosomal dysfunction to PD pathogenesis, we hypothesized that wild-type α-synuclein overexpression leads to an imbalance in proteostasis and contributes to PD pathogenesis by perturbing the proper functioning of the endoplasmic reticulum (ER) compartment. To test this hypothesis, we developed and characterized novel PD patient iPSC-derived midbrain dopaminergic neuron models that naturally develop α-syn pathology through *SNCA* triplications.

In Chapter 2, we describe the generation and characterization of our PD models in detail. In addition, we show that the PD models accumulate and aggregate α-syn and demonstrate lysosomal dysfunction due to defects in ER-Golgi trafficking of lysosomal hydrolases such as GCase. We additionally aimed to determine whether lysosomal GCase dysfunction occurs specifically due to α-syn accumulation. Therefore, we created *SNCA*-3X isogenic control iPSCs by targeted disruption of the *SNCA* gene using a dual nickase CRISPR/Cas9 strategy.

Collectively, our findings indicate that disruption of wild-type GCase function occurs specifically through α-syn accumulation.

In Chapter 3, we identify an unusual and unexpected proteostasis phenotype, the aggregation of immature wild-type GCase in the ER compartment. Using our PD neuronal models, we show that this GCase phenotype is associated with ER fragmentation. Despite the dramatic morphological alterations of the ER, we were surprised to find that the classical ER stress phenotypes, previously observed in numerous models of PD as well as in GD, were absent in the *SNCA*-3X neuronal models. Additionally, we propose a molecular mechanism by which α-syn may lead to these alterations.

In Chapter 4, we use innovative therapeutic strategies to target GCase and determine whether these strategies are sufficient in rescuing α-syn pathology. By simultaneously enhancing protein folding in the ER and ER-Golgi trafficking via small molecule modulators, we show that restoring ER GCase solubility, trafficking, and downstream lysosomal GCase function can rescue pathological α-syn levels. Our results suggest that comprehensive strategies that target multiple branches of the proteostasis pathway may be beneficial to patients with PD and other proteinopathies.

Lastly, Chapter 5 presents a summary and examines the significance of our findings. The limitations of our work and suggestions for future scientific studies are also discussed.

The data presented in Chapters 2-4 was adapted from my first-author original research manuscript titled “Rescue of α-synuclein aggregation in Parkinson’s patient neurons by synergistic enhancement of ER proteostasis and protein trafficking”. This manuscript, which took a collaborative research effort, is under peer review at the time of this writing.

CHAPTER 2

Novel Parkinson's disease iPSC-derived midbrain models demonstrate α-syn accumulation and lysosomal dysfunction.

Preface. The work presented in this chapter of the dissertation has been adapted largely from Stojkovska *et al*., 2021, an original research manuscript titled "Rescue of α-synuclein aggregation in Parkinson's patient neurons by synergistic enhancement of ER proteostasis and protein trafficking" that is currently under peer review.

OVERVIEW

Human somatic cells can be reprogrammed into induced pluripotent stem cells (iPSCs) by the overexpression of four transcription factors, Oct4, Sox2, Klf4, and c-Myc, collectively termed Yamanaka factors (Takahashi and Yamanaka, 2006). Upon introduction of the Yamanaka factors, the cells begin to form compact colonies that resemble pluripotent stem cells. These colonies can be identified based on their well-defined edges and near circular morphology, and are comprised of cells with a large nucleus with less cytoplasm in the cell body. Pluripotent stem cells have an unlimited self-renewal capacity. Importantly, they have the potential to differentiate into any of the three germ layers and can therefore give rise to any cell type in the body. Moreover, iPSCs are a promising source of cells for regenerative medicine and are increasingly being used as models for investigating mechanisms of patient-specific diseases.

Numerous protocols have been developed for the differentiation of iPSCs into various human cell types. For instance, in order to more accurately model Parkinson's disease (PD) and the associated pathology, a well-established protocol has been developed for the derivation of authentic midbrain dopamine (DA) neurons that exhibit molecular, chemical, and

electrophysiological properties of such neurons (Kriks et al., 2011). To examine the mechanisms by which α-syn overexpression leads to toxicity and contributes to PD pathogenesis, we obtained lymphocytes from three individual PD patients that carry a triplication in the *SNCA* genomic region (*SNCA*-3X), generated iPSC lines for each of the patients, and utilized these iPSCs to generate human midbrain dopaminergic (DA) neurons. Several clones for each iPSC line were expanded and extensively characterized for pluripotency, residual transgene expression of reprogramming factors, *SNCA*-3X genotype retention, and dopamine neuron differentiation efficiency. The generation and characterization analysis of the PD patient-derived iPSCs and differentiated midbrain DA neurons is shown in section 2.1 of this chapter.

Since the discovery of clinical, genetic, and pathological links between PD and the lysosomal storage disorder Gaucher's disease (GD), recent work has focused on understanding the mechanistic role of GCase in the development of synucleinopathies. Studies on the cellular clearance of physiological and pathological forms of α-syn indicated an important role for the lysosomal system, suggesting that lysosomal dysfunction could lead to α-syn aggregation (Cuervo *et al*., 2004; Lee et al., 2004; Vogiatzi et al., 2008). Since all of the known *GBA1* mutations result in loss of enzymatic function, initial studies were focused on determining if reduction in GCase activity could alter α-syn levels. Later, work from our group and others had shown that reduction of GCase activity, either through shRNA knock-down, conduritol-β-epoxide (CBE) treatment, or endogenously expressed GD-causing mutations in iPSC-derived neurons, resulted in the formation of pathological α-syn similar to that observed in GD and PD brain (Cleeter et al., 2013; Mazzulli *et al*., 2011; Rocha et al., 2015; Rockenstein et al., 2016; Schondorf et al., 2014; Xu et al., 2011). While lysosomal dysfunction and lipid accumulation

may play a role in α-syn accumulation in patients with homozygous mutations in *GBA1*, there is considerable debate regarding whether this same mechanism of action may occur in heterozygote carriers. This is partly due to the fact that some studies have shown that lipid substrate accumulation does not occur in the brains of patients with *GBA1*-PD (Gegg et al., 2012). Additionally, in sporadic PD brain, GCase activity declines with aging and is accompanied by GluCer substrate accumulation (Rocha *et al*., 2015). In long-lived PD patient-derived iPSC neuronal models that were aged for >400 days, we found an age-dependent decline in lysosomal and GCase activity within neurons that harbor two copies of wild-type *GBA1* (Mazzulli *et al*., 2016). Whether aggregation of α-syn itself can result in lysosomal GCase dysfunction has been less thoroughly investigated. Therefore, we used our PD patient-derived neuronal models, which naturally accumulate and form α-syn aggregates through endogenous *SNCA* triplications, to further investigate the relationship between α-syn and GCase. These results are described in section 2.2 of this chapter.

METHODS AND MATERIALS

Reprogramming and culturing of human induced pluripotent stem cells (iPSCs)

B-lymphocytes from healthy controls and PD patients that carry a triplication in the *SNCA* genomic region were obtained from the Coriell NINDS and NIGMS Human Genetic Cell Repositories: GM15845 (Ctrl), GM15010 (3x-1), ND00196 (3x-2), ND00139 (3x-4), ND34391 (Est. 3X). Phenotypic and genotypic data of these subjects is available on https://www.coriell.org. Refer to Table 1 and Table 2 for more details. The B-lymphocytes were reprogrammed into iPSCs by transfection with non-integrating episomal plasmids containing Oct3/4 (Addgene: pCXLE-hOCT3/4-shp53-F), L-Myc (Addgene: pCXLE-hUL), and Sox2 and

Klf4 (Addgene: pCXLE-hSK). All iPSCs were maintained in mTeSR1 media on matrigel-coated plates.

Table 1. Clinical and pathological characterization of Parkinson's disease patient samples.

Patient line	Symptoms	Parkinsonism Diagnosis	Characterization of Mutation	Sex	Age At Sampling	Tissue and Cell Type
3x-1	Onset at age 30; resting tremor, shuffling gait, postural instability, dyskinesias with on/off phenomenon; responsive to anti-parkinsonism therapy	Parkinson's disease	Whole Gene Triplication: 17 genes, including SNCA	Female	38	Blood B-lymphocyte
3x-2	Onset at age 37; bradykinesia, rigidity, responsive to anti-parkinsonism therapy	Parkinson's disease	Whole Gene Triplication: 17 genes, including SNCA	Male	37	Blood B-lymphocyte
3x-4	Onset at age 44; bradykinesia, postural instability, rigidity, gait difficulties, responsive to anti-parkinsonism therapy	Diffuse Lewy Body Disease	Whole Gene Triplication: 17 genes, including SNCA	Female	49	Blood B-lymphocyte
Ctrl	Normal examination with no complaints	None (at risk)	None	Female	59	Blood B-lymphocyte

Table 2. List of human iPSCs generated and / or used in the study.

iPSC line ID	Repository and ID	Diagnosis	Genotype	Genome editing	Reference
3x-1	NIGMS Human Genetic Cell Repository ID #GM15010	Parkinson's Disease	*SNCA* Triplication (17 genes)	*SNCA* correction (3x-1 iso ctrl)	Stojkovska et al., 2021 (under review)
3x-2	NINDS Repository ID #ND00196	Parkinson's Disease	*SNCA* Triplication (17 genes)	*SNCA* correction (3x-2 iso ctrl)	Stojkovska et al., 2021 (under review)
3x-4	NINDS Repository ID #ND00139	Diffuse Lewy Body Disease	*SNCA* Triplication (17 genes)	*SNCA* correction (3x-4 iso ctrl)	Stojkovska et al., 2021 (under review)
Ctrl	NIGMS Human Genetic Cell Repository ID #GM15845	None (at risk)	WT / WT	-	Stojkovska et al., 2021 (under review)
Est. 3X	NINDS Repository ID #ND34391	Parkinson's Disease	*SNCA* Triplication (17 genes)	-	Mazzulli et al., 2016a
Est. Ctrl	-	None	WT / WT	-	Hedrich et al., 2006 Seibler et al., 2011 Mazzulli et al., 2016a
GBA1 N370S / 84GG	NIGMS Human Genetic Cell Repository ID# GM00852	Gaucher's Disease (Type I)	*GBA1* N370S / 84GG	-	Mazzulli et al., 2011; Mazzulli et al., 2016a
GBA1 L444P / L444P	Telethon Genetic Biobank Network	Gaucher's Disease (Type III)	*GBA1* L444P / L444P	-	Schondorf et al., 2014
SNCA A53T	Whitehead Institute Center for Human Stem Cell Research WIBR-hiPS-SNCA A53T, clone 2409	Parkinson's Disease	*SNCA* A53T	A53T correction (A53T iso ctrl)	Soldner et al., 2011 Mazzulli et al., 2016b

Measuring mRNA expression via real-time qPCR

Total RNA was isolated from cells using an RNeasy Mini Prep kit (QIAGEN). cDNA was synthesized by reverse transcriptase PCR (RT-PCR) using the RevertAid First Strand cDNA synthesis kit (Thermo Fisher Scientific). Real-time quantitative PCR (qPCR) was performed on the Applied Biosystems 7500 Fast system using the cDNA and pre-designed TaqMan-primer probes for Nanog and *SNCA* (refer to Table S2). The target mRNA expression was quantified relative to GAPDH using the delta-delta-Ct method, and represented as a fold change.

Pluripotency analysis of reprogrammed iPSC cells via immunofluorescence

Cells were plated on glass coverslips. At the time of the experiment, the cells were fixed in 4% paraformaldehyde (PFA) (Polysciences, Inc.) for 15 minutes (refer to Table S4 for recipe), permeabilized with 0.3% Triton X-100 (Sigma) in PBS for 30 minutes, and blocked with 2% bovine serum albumin (BSA) (Roche) in Triton-PBS for 30 minutes to prevent non-specific antibody binding. Primary antibodies (Sox2, Tra 1-60, Oct4, SSEA4, Nanog; refer to Table S2) were added overnight, followed by incubation with secondary antibodies (Alexa Fluor 488 Goat anti-rabbit IgG and Alexa Fluor 568 Goat anti-mouse IgG; refer to Table S2) for 1 hour. The cells were then washed three times with Triton-PBS and mounted onto microscope slides with DAPI mounting media.

PCR analysis of reprogramming factor transgenes

Forward and reverse PCR primers for each of the reprogramming factor transgenes (Oct3/4, Sox2, Klf4, and L-Myc) were designed so that the PCR product will span both the transgene and the backbone, as indicated in the schematic of Figure 2-2 C. Refer to Table S3 for list of primers.

Copy number analysis of *SNCA* and puromycin

Genomic DNA was extracted from iPSCs using the DNeasy Blood and Tissue Kit (QIAGEN). Real-time quantitative PCR (qPCR) was performed on the Applied Biosystems 7500 Fast system using the genomic DNA and pre-designed TaqMan probe for *SNCA* and a custom probe for puromycin (refer to Table S2). The copy number of each gene was quantified relative to RNAseP.

Fluorescence *in situ* hybridization (FISH) analysis

To confirm the *SNCA* copy number in the reprogrammed iPSCs, fluorescent probes targeting *SNCA* (4q22.1; R: red) and a control region (4p16.3; G: green) were used for fluorescence in situ hybridization analysis. The assay was performed as a service provided by Cell Line Genetics, Inc. (www.clgenetics.com).

Differentiation of iPSCs into midbrain dopaminergic neurons

The iPSCs were differentiated into midbrain dopaminergic neurons using a well-established dual SMAD inhibition protocol (Kriks *et al*., 2011). Briefly, iPSCs were accutased and seeded into 6-well matrigel-coated plates at a density of 0.5-1 x e6 cells per well. iPSCs were fed daily with mTeSR1 media supplemented with Rho-associated kinases (ROCK) inhibitor (Y-27632, EMD Millipore) until individual cells were no longer visible, upon which ROCK inhibitor was removed from the media. The differentiation protocol (refer to Table S1) was initiated at day 0 once the iPSCs reached ~90% confluency, using KSR media (refer to Table S4 for recipe details). On day 10-15, cells were chunked onto 75µg/ml poly-D-lysine (PDL) and 5µg/ml laminin-coated 10cm dishes, and media change using BAGTCD was done every 3 days. On day

25-30, cells were accutased and seeded (i.e., final plated) onto PDL/laminin-coated 24- or 96-well plates depending on the desired experiment, and media change using BAGTCD was done every 3 days until day 40-50. Mature dopaminergic neurons were cultured in neurobasal SM1 media containing SM1 supplement, 1% penicillin / streptomycin, and 1% L-glutamine (refer to Table S4 for recipe). To allow for sufficient α-syn accumulation and aggregation, neurons were aged to 70-90 days for each experiment.

Immunofluorescence analysis of midbrain neuron differentiation efficiency, α-synuclein accumulation, and thioflavin staining

Neurons were fixed in 4% PFA for 15 minutes, permeabilized with 0.1% Triton X-100 in PBS for 30 minutes, and blocked with 2% BSA and 5% normal goat serum (NGS) (Jackson Immuno Research) in Triton-PBS for 30 minutes to prevent non-specific antibody binding. Primary antibodies (anti-α-synuclein LB509, anti-tyrosine hydroxylase (TH), anti-FoxA2, anti-β3-tubulin; refer to Table S2) were added overnight, followed by incubation with secondary antibodies (Alexa Fluor 488 Goat anti-mouse IgG and Alexa Fluor 568 Goat anti-rabbit IgG; refer to Table S2) for 1 hour. The cells were then washed three times with Triton-PBS and mounted onto microscope slides with DAPI mounting media. For thioflavin S (Thio S) co-staining, refer to Stojkovska and Mazzulli, 2021 for protocol details. Briefly, following primary incubation with α-syn, 0.05% Thio S was directly added to cells and incubated for 15 min at RT. Next, cells were washed with a sequence of ethanol steps (twice with 50% ethanol for 20 min each, then once with 80% ethanol for 20 min) and then with Triton-PBS prior to mounting. All images were obtained on a Leica confocal microscope, and image analysis was performed using ImageJ.

Sequential protein extraction and western blot analysis

Cells were harvested in 1X PBS and pelleted by centrifugation at 400xg for 5 minutes. To extract soluble protein, the cell pellets were homogenized in 1% Triton base lysis buffer (refer to Table S4 for recipe) containing protease inhibitor cocktail (PIC) (Roche), phenylmethylsulfonyl fluoride (PMSF) (Sigma), sodium orthovanadate (Na_3VO_4) (Sigma) and sodium fluoride (NaF) (Sigma) (refer to Table S4 for recipe). The Triton extracted lysates were freeze-thawed three times and ultracentrifuged at 100,000xg for 30 minutes at 4°C. To extract insoluble protein, the Triton-insoluble pellets were solubilized with 2% SDS base lysis buffer (refer to Table S4 for recipe) containing PIC via boiling for 10 minutes, followed by sonication and then ultracentrifugation at 100,000xg for 30 minutes at 22°C. The protein concentrations of the Triton and SDS fractions were measured via a BCA protein assay kit (Thermo Fisher Scientific) on a plate reader. Extracted protein lysates were boiled at 100°C for 10 min in Laemmli sample buffer (refer to Table S4), loaded on an SDS-PAGE gel, transferred onto a PVDF membrane (Millipore), and post-fixed in 0.4% PFA (refer to Table S4 for recipe). Membranes were blocked in a 1:1 mixture of 1X TBS and Intercept blocking buffer (Li-Cor Biosciences), followed by overnight incubation with primary antibodies (refer to Table S2) diluted in a 1:1 mixture of 1X TBS-Tween and blocking buffer. The following day, secondary antibodies (refer to Table S2) were added for 1 hour, and the membranes were scanned using a Li-Cor Biosciences infrared imaging system. Quantification of band intensity was done using the ImageStudio software and analysis was performed on Excel and GraphPad Prism.

GCase maturation was measured by quantifying the ratio of post-ER (mature; >62 kDa) to ER (immature; 55-62 kDa) GCase. For quantifications of percent insoluble GCase: first, soluble (Triton fraction) and insoluble (SDS fraction) GCase levels were normalized to

Coomassie gel staining. Then, insoluble GCase was divided by total GCase taken from both Triton and SDS fractions, and the result was shown as a percentage.

Monitoring Protein Trafficking with Endoglycosidase H (Endo H)

To study the subcellular localization and trafficking of GCase between the ER and Golgi, protein lysates were digested with Endoglycosidase H (Endo H) (New England Biolabs). The experimental procedure was performed according to the manufacturer's handbook. Briefly, 10X Glycoprotein Denaturing buffer was added to 40 μg of protein and the reaction was boiled at 100°C for 10 minutes. Following the denaturation, 10X GlycoBuffer 3 and Endo H enzyme were added, and the reaction was incubated at 37°C for 2 hours. Finally, the samples were boiled at 100°C for 10 minutes after the addition of 5X Laemmli buffer and loaded on a 10% SDS-PAGE gel, followed by western blot analysis. A positive digestion results in a downward shift in the molecular size of GCase after it is subjected to SDS-PAGE. Post-ER (70–74 kDa) and ER (55 kDa) forms of GCase were analyzed using the Endo H digested lane and used as a measure of GCase trafficking.

Live-cell lysosomal GCase activity assay

The procedure and analysis method for the activity assay has been previously described in detail (Mazzulli *et al*., 2011; Mazzulli *et al*., 2016). Briefly, cells were plated in 96-well plates. One day prior to the assay, cells were treated with 1mg/ml cascade dextran blue (Life Technologies) for 24 hours. The next day, the cells were first treated with DMSO or 200nM bafilomycin A1 (BafA1) (Santa Cruz) for 1 hour at 37°C, followed by a 1-hour pulse-chase with 100μg/ml artificial fluorescent GCase substrate, 5-(pentafluoro-benzoylamino) fluorescein di-ß-D-

glucopyranoside (PFB-FDGluc) (Life Technologies), at 37°C. The fluorescence signal was measured every 30 minutes for the span of 3-4 hours on a plate reader (Ex=485nm, Em=530nm, for the GCase substrates; Ex=400nm, Em=430nm for cascade dextran blue). For the analysis, the GCase fluorescence signal was normalized to either lysosomal mass by using cascade dextran blue signal or total cell volume by quantifying CellTag 700 staining signal.

Neurofilament toxicity assessment

Following the live-cell lysosomal GCase activity assay, the cells were fixed in 4% PFA in PBS for 15 minutes and stained with an anti-neurofilament marker (refer to Table S2) overnight at 4°C to ensure that changes in lysosomal activity were not due to cell toxicity (refer to Mazzulli *et al*., 2016for details). The next day, IRdye 800CW goat anti-mouse IgG secondary antibody and CellTag 700 stain (refer to Table S2) were added to the wells and incubated for 1 hour, and the plate was scanned on a Li-Cor infrared imaging system. Fluorescence intensity was quantified using the ImageStudio software, and analysis was performed on Excel.

Dual nickase CRISPR/Cas9 strategy and selection of iPSC clones

A pair of guide RNAs (guide RNA 1: 5'-AGCAGCCACAACTCCCTCCTTGG-3'; guide RNA 2: 5'- TGAGAAAACCAAACAGGGTGTGG-3') were designed using the Optimized CRISPR design tool (http://crispr.mit.edu/) and used to direct D10A mutant Cas9 to produce nicks within Exon 2 of the *SNCA* gene. A PITX3-2A-eGFP-PGK-Puro plasmid (Addgene) encoding a puromycin resistance cassette driven by a phosphoglycerate kinase (PGK) promoter was used as a template for homologous recombination (HR) and as a positive selection marker. The gRNAs were cloned into a Cas9-nickase plasmid PX335 (Addgene) and transfected into iPSCs using

Lipofectamine 3000 (Thermo Fisher Scientific) along with a puromycin-containing HR plasmid. Two days following the transfection, iPSCs were cultured in 1μg/ml puromycin containing media for several weeks. To confirm that the puromycin cassette was appropriately inserted in the targeted *SNCA* Exon 2 region, puromycin resistant clones were selected and genomic DNA was extracted and analyzed via PCR (refer to Table S3 for primers). Puromycin copy number analysis and sequencing were also performed on selected clones.

Analysis of off-target effects using the T7EI cleavage assay

Genomic DNA was amplified using primers for each off-target gene (refer to Table S3 for list of primers). The PCR products were then denatured and allowed to re-anneal using a thermal cycler with the following settings: 95°C for 10 minutes, 95-85°C (ramp rate 2°C/sec), and 85-25°C (ramp rate 0.2°C/sec). The hybridized product was then digested with T7 Endonuclease I (T7EI) for 1 hour at 37°C and analyzed on an agarose gel along with a positive control (Genecopoeia).

Statistical analysis

Analyzed data was plotted and tested for statistical significance using the GraphPad Prism software. Statistical significance between two samples was determined using a paired or unpaired t-test with Welch's correction. For more than two samples, significance was determined using a one-way ANOVA with Tukey's post-hoc test. A p-value of <0.05 was considered to be significant ($*p < 0.05$, $**p < 0.01$, $***p < 0.001$, $****p < 0.0001$). For each quantification, the type of error bar used is specified in the figure legends.

RESULTS

2.1 Characterization of *SNCA*-3X Parkinson's disease patient iPSCs and iPSC-derived midbrain dopaminergic neuron models.

Our previous work indicated that α-syn accumulation causes lysosomal dysfunction in PD patient midbrain neurons (Cuddy *et al*., 2019; Mazzulli *et al*., 2011). To further examine the mechanism of this process, we generated several new iPSC lines from B-lymphocytes of a healthy control (Ctrl) and three distinct patients that carry a triplication (3X) in the *SNCA* genomic region that exhibit early onset parkinsonism and dementia (Singleton *et al*., 2003) (Figure 2-1). Initial characterization of the PD patient lymphocytes indicated that the triplication region includes 16 other genes aside from *SNCA* (subject data is available on the Coriell NINDS and NIGMS Human Genetic Cell Repositories) as similarly described in Singleton *et al*., 2003. Using non-integrating episomal plasmids containing the standard reprogramming Yamanaka factors Oct3/4, Sox2, Klf4, and L-Myc (Takahashi and Yamanaka, 2006), we reprogrammed the lymphocytes into induced pluripotent stem cells (iPSCs). For each iPSC line, several clones were created and extensively characterized and the most robust lines (highlighted in red in Figure 2-2 A) were chosen to carry out experiments, which we termed 3x-1 (clone 3; C3), 3x-2 (clone 2; C2), 3x-4, and Ctrl (clone 1; C1).

We assessed the pluripotency of the *SNCA*-3X and healthy control iPSCs by analyzing Nanog mRNA expression (Figure 2-2 A) and immunofluorescence of multiple transcription factors that play a role in pluripotency and maintenance of embryonic stem cells (Figure 2-2 B). We confirmed the absence of transgene expression in each of the iPSCs via PCR and gel analysis to ensure that the reprogrammed iPSCs are maintaining pluripotency via endogenous expression of the Yamanaka factors (Figure 2-2 C). Real-time qPCR (Figure 2-2 D) and fluorescence *in situ*

hybridization (FISH) analysis (Figure 2-2 E) were used to verify that reprogramming did not alter the *SNCA* phenotype and to confirm the doubling of *SNCA* copy number in the *SNCA-3X* iPSCs compared to the healthy control. To generate a relevant human model that more accurately represents PD, we differentiated the iPSCs into midbrain dopaminergic (DA) neurons using a well-established dual SMAD inhibition protocol (Kriks *et al.*, 2011) (Figure 2-1). This protocol generated approximately 70-90% of differentiation efficiency, which was evaluated by immunofluorescence analysis of β3-tubulin and the DA neuron markers FoxA2 and tyrosine hydroxylase (TH) (Figure 2-2 F).

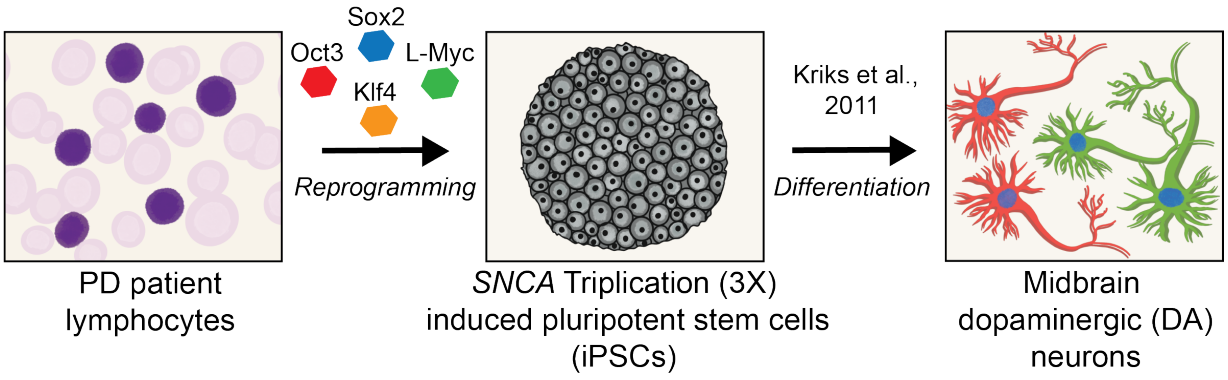

Figure 2-1. Schematic overview of the reprogramming and differentiation of PD patient lines. Lymphocytes obtained from PD patients carrying a triplication in the *SNCA* genomic region were reprogrammed into induced pluripotent stem cells (iPSCs) using standard reprogramming factors: Oct3, Sox2, Klf4, L-Myc. To model PD *in vitro* and gain a better understanding of the disease pathology, iPSCs were differentiated into midbrain dopaminergic (DA) neurons, the PD-relevant cell type, using a well-established dual SMAD inhibition protocol.

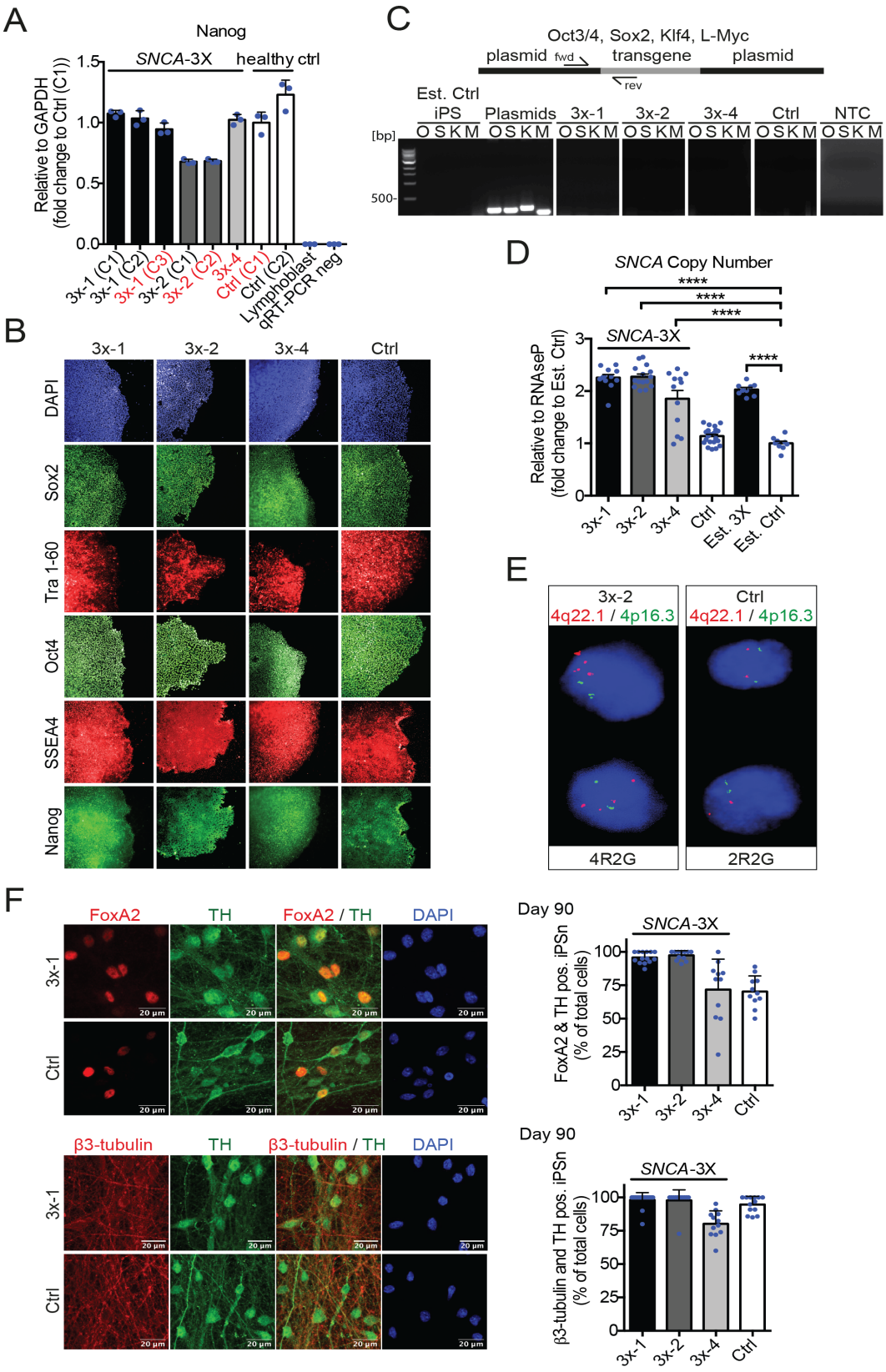
A
Nanog
SNCA-3X
healthy ctrl
Relative to GAPDH (fold change to Ctrl (C1))
1.5
1.0
0.5
0.0
3x-1 (C1)
3x-1 (C2)
3x-1 (C3)
3x-2 (C1)
3x-2 (C2)
3x-4
Ctrl (C1)
Ctrl (C2)
Lymphoblast
qRT-PCR neg
C
Oct3/4, Sox2, Klf4, L-Myc
plasmid
fwd
transgene
rev
plasmid
Est. Ctrl
iPS
Plasmids
3x-1
3x-2
3x-4
Ctrl
NTC
O S K M
[bp]
500-
B
3x-1
3x-2
3x-4
Ctrl
DAPI
Sox2
Tra 1-60
Oct4
SSEA4
Nanog
D
SNCA Copy Number
****
****
****
****
SNCA-3X
Relative to RNAseP (fold change to Est. Ctrl)
3
2
1
0
3x-1
3x-2
3x-4
Ctrl
Est. 3X
Est. Ctrl
E
3x-2
4q22.1 / 4p16.3
Ctrl
4q22.1 / 4p16.3
4R2G
2R2G
F
FoxA2
TH
FoxA2 / TH
DAPI
3x-1
Ctrl
20 µm
β3-tubulin
TH
β3-tubulin / TH
DAPI
3x-1
Ctrl
20 µm
Day 90
SNCA-3X
FoxA2 & TH pos. iPSn (% of total cells)
100
75
50
25
0
3x-1
3x-2
3x-4
Ctrl
Day 90
SNCA-3X
β3-tubulin and TH pos. iPSn (% of total cells)
100
75
50
25
0
3x-1
3x-2
3x-4
Ctrl

Figure 2-2. Characterization of *SNCA*-3X iPSCs and midbrain dopaminergic neurons.

(A) Real-time qPCR analysis of Nanog mRNA expression in *SNCA*-3X and healthy control iPSC clones (n=3 technical replicates per line). Lymphocyte cDNA and a no-template sample (qRT-PCR neg) serve as negative controls. GAPDH serves as a reference gene. Data is shown as mean ± SD.

(B) Immunofluorescence staining of several pluripotency and embryonic stem cell markers in *SNCA*-3X and healthy control (Ctrl) iPSCs. Cell nuclei are stained with DAPI.

(C) PCR analysis of Oct3/4 (O), Sox2 (S), Klf4 (K), and L-Myc (M) plasmid transgenes in *SNCA*-3X and Ctrl iPSCs. A previously established healthy control iPSC line (Est. Ctrl) and a no-template control (NTC) sample serve as negative controls. The plasmids serve as positive controls for each transgene.

(D) *SNCA* copy number analysis of *SNCA*-3X and Ctrl iPSCs (n=3-6 replicates per line from 3 separate experiments). Previously established *SNCA*-3X (Est. 3X) and healthy control (Est. Ctrl) iPSCs are shown as a relative comparison. RNaseP serves as a reference gene. Data is shown as mean ± SEM, ****$p < 0.0001$, using student's unpaired t-test or ANOVA with Tukey's post-hoc test.

(E) Representative fluorescence in-situ hybridization (FISH) analysis of *SNCA*-3X and Ctrl iPSCs. The red signal indicates a probe that spans *SNCA* located in 4q22.1 and the green signal indicates a control probe targeting the 4p16.3 chromosomal region. The result confirms a total of four *SNCA* copies in the PD patient iPSC (4 red, 2 green; 4R2G) indicative of a triplication, while the healthy control contains two copies (2 red, 2 green; 2R2G).

(F) Representative immunofluorescence staining of FoxA2 (red) and tyrosine hydroxylase (TH; green) **(top)** or the neuronal marker β3-tubulin (red) and TH (green) **(bottom)** in day 90 *SNCA*-3X iPSC-derived DA neurons. Cell nuclei are stained with DAPI. Right, quantification of FoxA2+TH **(top)** or β3-tubulin+TH **(bottom)** positive neurons as a percent of total cells for each patient line. Each data point in the scatter plot represents a field of view from different batches of differentiation. Data is shown as mean ± SD. Scale bar, 20μm.

2.2 Defects in GCase maturation and lysosomal function occur specifically through α-syn accumulation.

To determine if the novel lines could recapitulate key features of the PD brain, we matured the PD patient-derived midbrain DA neurons for 90 days, and analyzed for the presence of aggregated α-syn. In addition to the novel iPSC lines, we also incorporated previously established lines in our study (Est. 3X and Est. Ctrl; Table 2) (Mazzulli *et al.*, 2016). Immunofluorescence analysis indicated that patient lines accumulated α-syn within neurites and the cell body that were thioflavin positive, while healthy control neurons displayed lower α-syn

levels and a punctate pattern that is expected for a synaptic protein (Figure 2-3 A, B). Biochemical sequential extraction into soluble and insoluble protein fractions showed significant accumulation of α-syn in both fractions of the *SNCA*-3X DA neurons relative to healthy controls (Figure 2-3 C). We next investigated GCase maturation and lysosomal function. As GCase matures from the ER to the Golgi, it acquires N-linked glycans resulting in an increase in its molecular weight (Bergmann and Grabowski, 1989). Thus, GCase maturity can be assessed by SDS-PAGE / western blot analysis. We found that GCase maturation was reduced in *SNCA*-3X DA neurons indicated by the accumulation of immature, low molecular weight forms of GCase (~55-62 kDa) (Figure 2-4 A). We also observed a decline in GCase activity specifically within lysosomal compartments in living *SNCA*-3X DA neurons compared to the healthy control (Figure 2-4 B). Analysis of neurite degeneration by staining for neurofilament intensity indicated no change between *SNCA*-3X and healthy control DA neurons, suggesting that the decline in GCase activity in patient neurons is not due to cell toxicity (Figure 2-4 C).

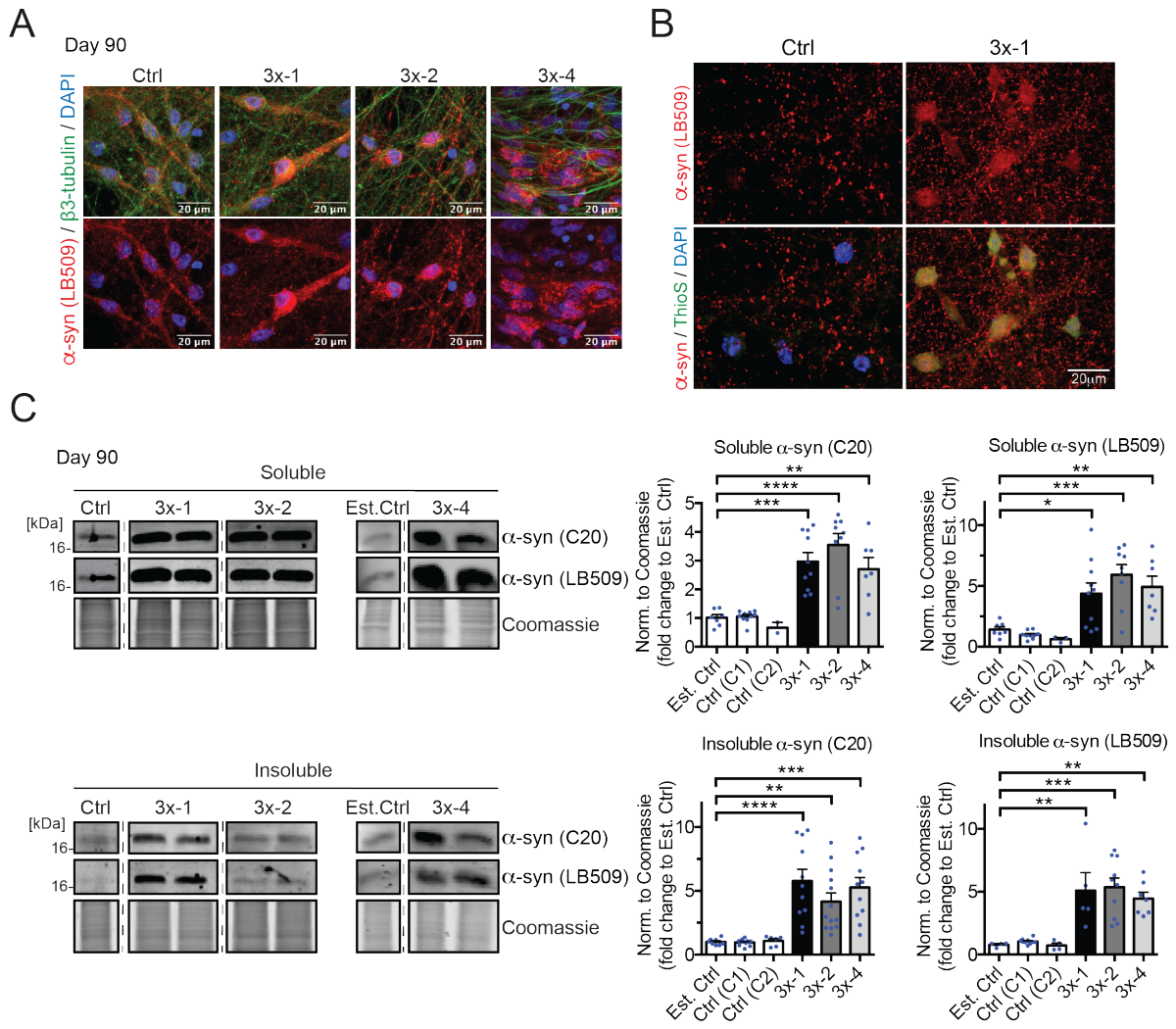

Figure 2-3. α-Syn accumulation and aggregation in *SNCA*-3X midbrain DA neurons.

(A) Immunofluorescence (IF) staining of α-syn (antibody LB509) and β3-tubulin in day 90 Ctrl and *SNCA*-3X DA neurons. Cell nuclei are stained with DAPI. Scale bar, 20µm.

(B) Representative IF co-staining of α-syn (antibody LB509) with thioflavin S (Thio S) in Ctrl and 3x-1 DA neurons. Cell nuclei are stained with DAPI. Scale bar, 20µm.

(C) Sequential protein extraction and western blot analysis of soluble and insoluble α-syn in day 90 Ctrl and *SNCA*-3X DA neurons. Membranes were sequentially probed with C20 and LB509 anti-α-syn antibodies. Irrelevant lanes were cropped out from the blot and are indicated with a dashed line. Right, quantification of soluble and insoluble α-syn levels normalized to Coomassie. Each data point on the scatter plot indicates a biological replicate taken from several culture batches. Data is shown as mean ± SEM, *$p < 0.05$; **$p < 0.01$; ***$p < 0.001$; ****$p < 0.0001$, using ANOVA with Tukey's post-hoc test.

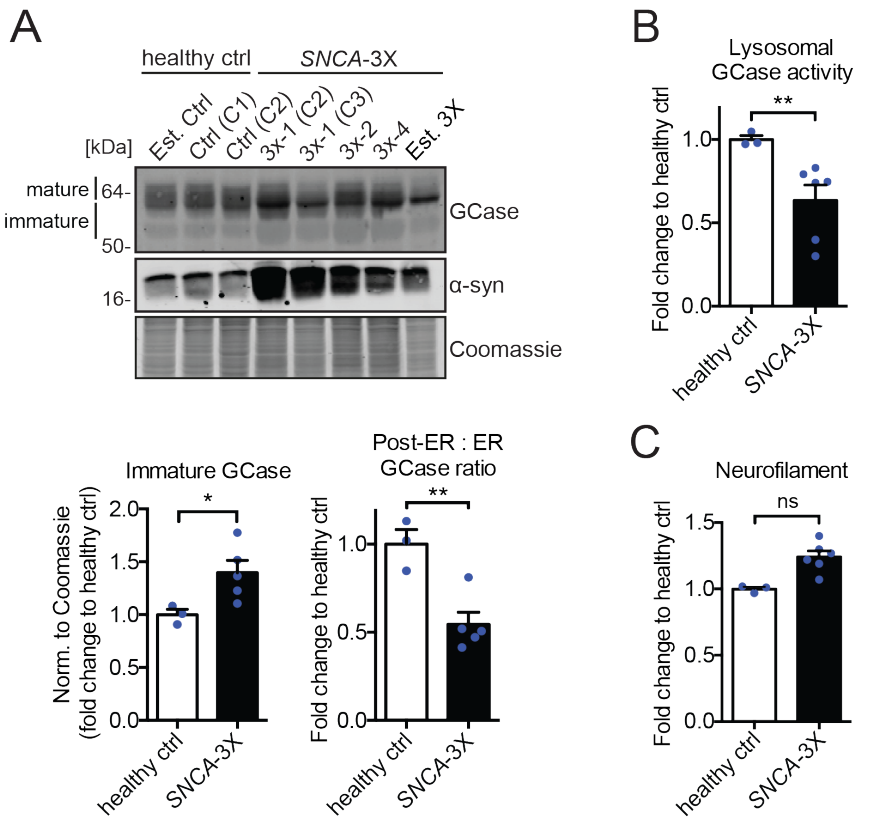

Figure 2-4. *SNCA*-3X midbrain DA neurons exhibit defects in GCase maturation and lysosomal function.

(A) Western blot analysis of immature (~55-62 kDa) and mature (>62 kDa) GCase forms in day 90 healthy control and *SNCA*-3X DA neurons. Previously established lines, Est. 3X and Est. Ctrl are shown as a relative comparison. Blotting for α-syn (antibody C20) was done to confirm its pathological accumulation in neurons. Bottom, immature GCase levels were normalized to the Coomassie stained gel and GCase maturation was calculated by measuring the post-ER (mature) to ER (immature) GCase ratio.

(B, C) Live-cell lysosomal GCase activity and neurofilament analysis of day 90 *SNCA*-3X DA neurons (3x-1, clones C2 and C3, are shown as a representation). Quantification is shown as a fold change to two healthy controls: Ctrl (C1) and Est. Ctrl (n=3 per line).

For all quantifications, values are mean ± SEM, *$p < 0.05$; **$p < 0.01$; ns = not significant, using student's unpaired t-test.

Since the triplication region in the *SNCA*-3X PD patients includes 16 other genes aside from *SNCA*, we aimed to determine if lysosomal dysfunction occurred specifically due to α-syn accumulation and aggregation. Therefore, we created isogenic controls of all three PD patient

iPSC lines by targeted disruption of the *SNCA* gene using previously established CRISPR/Cas9 constructs (Zunke et al., 2018) to reduce the expression of α-syn (Figure 2-5 A). We found that our constructs were efficiently integrated into the *SNCA* gene and chose clones that lacked off-target effects for further studies (Figure 2-5 B, C). At the mRNA level, we found that CRISPR/Cas9 editing caused an approximately 50% decrease in *SNCA* expression in the 3x-1 isogenic control (Figure 2-6 A), corresponding to a 70% decline in soluble α-syn protein that is comparable to α-syn levels in healthy controls (Figure 2-6 B). For the isogenic controls of patients 3x-2 and 3x-4, *SNCA* mRNA expression was reduced by approximately 75% (Figure 2-6 A), and soluble α-syn protein levels were undetectable (Figure 2-6 B). Moreover, no insoluble α-syn was detected in any of the isogenic control lines (Figure 2-6 B). Analysis of DA neuron markers showed that the isogenic controls could differentiate as efficiently as the parental lines, confirming that CRISPR/Cas9 editing or α-syn depletion / knockout has no adverse effects on neurodevelopment *in vitro* (Figure 2-5 D), which has similarly been previously described *in vivo* using α-syn -/- mice (Abeliovich et al., 2000). Analysis of GCase showed that α-syn reduction improved its maturation by reducing the accumulation of immature GCase, while promoting mature GCase (Figure 2-6 C). Digestion with endoglycosidase H (Endo H), an enzyme that only cleaves glycans from immature GCase forms, validated that ER forms of GCase accumulate in *SNCA*-3X DA neurons and that isogenic correction of *SNCA* increases mature forms (Figure 2-6 D). Consistent with this, lysosomal GCase activity was also increased in isogenic controls (Figure 2-6 E). Collectively, these data validate previous findings in novel and robust iPSC-derived synucleinopathy models and indicate that wild-type GCase trafficking and activity are reduced specifically through α-syn accumulation and aggregation.

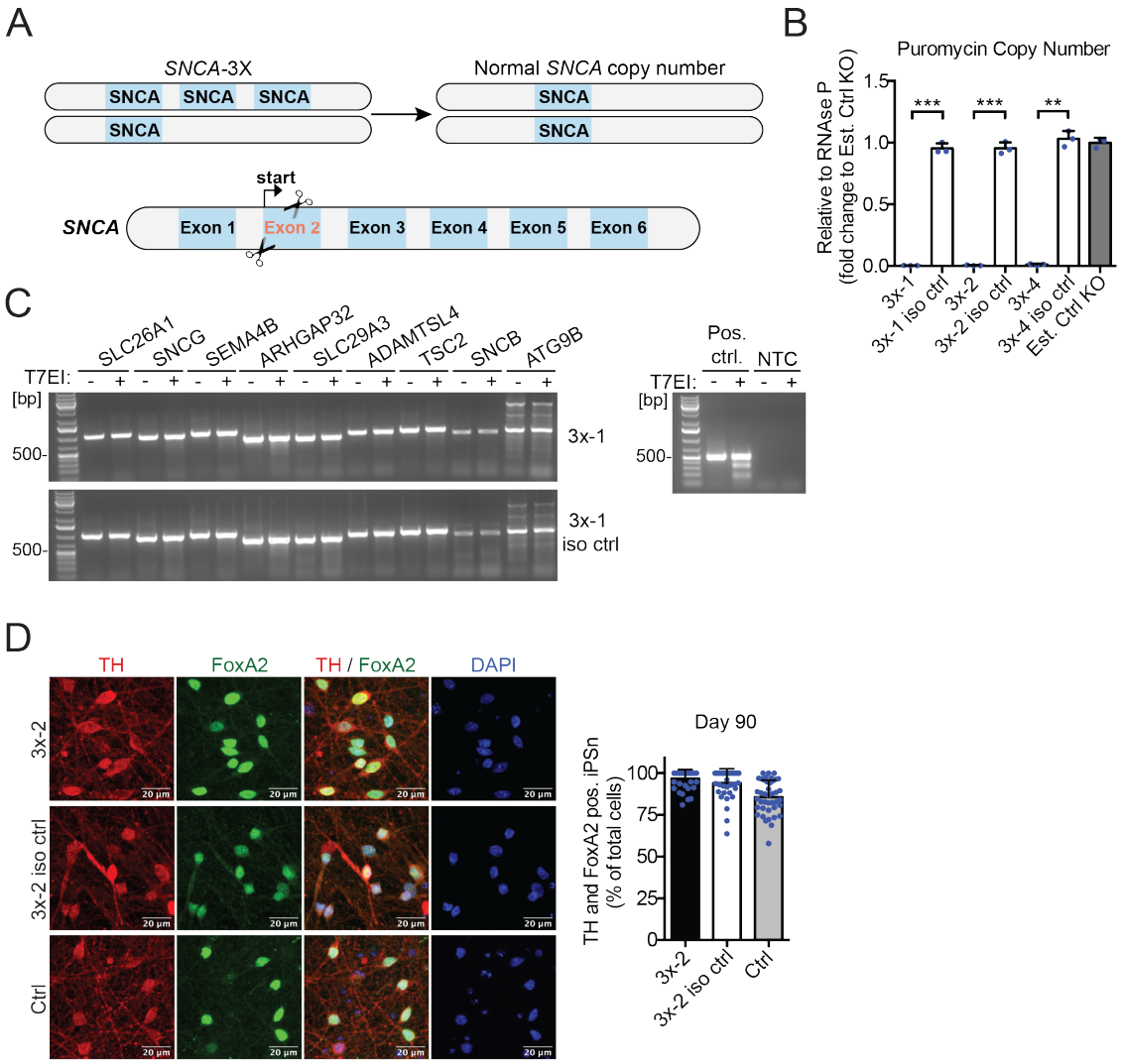

Figure 2-5. Generation and characterization of *SNCA*-3X isogenic control midbrain DA neurons.

(A) Schematic overview of the CRISPR/Cas9 dual nickase strategy used for the generation of *SNCA*-3X isogenic controls. To reduce the levels of α-syn, paired D10A mutant Cas9 nickases and two guide RNAs were used to produce nicks in Exon 2 of *SNCA*. A plasmid encoding a puromycin resistance cassette was used as a template for homology directed repair and as a positive selection marker.

(B) Successful insertion of the puromycin cassette in the isogenic control (iso ctrl) iPSCs for each *SNCA*-3X patient was evaluated by copy number analysis (n=3). RNAseP serves as the reference gene. Quantification is shown as a fold change to a previously established control α-syn knockout (Est. Ctrl KO) iPSC line (Zunke *et al.*, 2018), and statistical analysis was performed between each *SNCA*-3X line and its corresponding isogenic control. Data is shown as mean ± SEM, **p < 0.01; ***p < 0.001, using student's unpaired t-test.

(C) Predicted off-target effects for the selected guide RNAs were tested for mismatches via the T7 Endonuclease I (T7EI) assay, and the PCR products were analyzed by an agarose gel. Representative analysis of 3x-1 and its

corresponding isogenic control are shown. Right, T7EI assay positive control. NTC, no template control.

(D) Representative TH and FoxA2 immunofluorescence staining of day 90 DA neurons (n=3) indicates that midbrain neuron development is unaffected due to CRISPR editing or α-syn depletion. Cell nuclei are stained with DAPI. Right, quantification of FoxA2+TH positive neurons as a percent of total cells. Each data point on the scatter plot indicates a field of view. Data is shown as mean ± SD. Scale bar, 20µm.

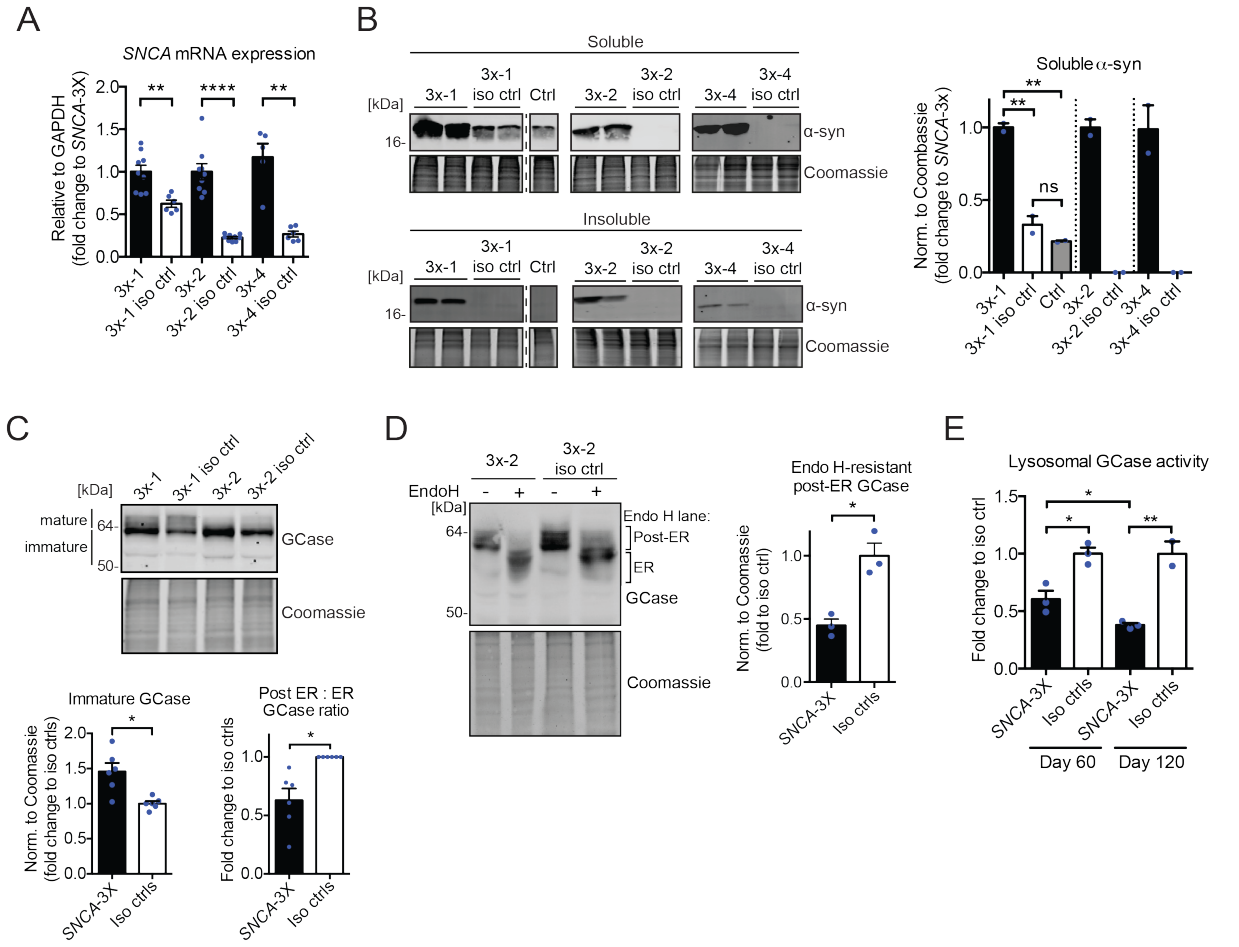

Figure 2-6. α-Syn depletion in *SNCA*-3X isogenic control neurons rescues GCase maturation and lysosomal function.

(A) Real-time qPCR analysis of *SNCA* mRNA expression relative to GAPDH in day 90 DA neurons of each *SNCA*-3X and isogenic control (n=5-9 per line).

(B) Representative western blot analysis of soluble and insoluble α-syn (antibody C20) levels in *SNCA*-3X and isogenic control DA neurons. The healthy control (Ctrl) is included for a relative comparison. The dashed line indicates irrelevant lanes that were cropped out. Right, quantification of soluble α-syn levels in the isogenic control lines normalized to Coomassie, shown as a fold change to each parental *SNCA*-3X line (n=2).

(C) Representative western blot of GCase maturation in day 90 *SNCA*-3X and isogenic control DA neurons. Right,

quantification of immature GCase levels normalized to Coomassie and GCase maturation combined from lines 3x-1, 3x-2, and 3x-4 and their corresponding isogenic controls (n=2 from each line).

(D) Representative western blot of GCase in endoglycosidase H (Endo H) digested lysates of day 120 3x-2 and isogenic control neurons. Right, levels of Endo H-resistant GCase were measured by quantifying mature / post-ER GCase from the Endo H lanes and normalizing to Coomassie (n=3 per line).

(E) Live-cell lysosomal GCase activity in day 60 and day 120 3x-1 and isogenic control DA neurons (n=2-3). Activity is shown as a fold change to the isogenic control at both time points.

For all quantifications, values are mean ± SEM, *p < 0.05; **p < 0.01; ****p < 0.0001; ns = not significant, using student's unpaired (panels A-E) or paired (panel D) t-test.

DISCUSSION

A reduction in GCase activity in both sporadic and *GBA1*-PD brains has been found by several groups (Gegg *et al*., 2012; Murphy et al., 2014; Rocha *et al*., 2015). Analysis of pathologically confirmed idiopathic PD brain harboring wild-type GCase confirmed the reduction of GCase activity in lysosome-enriched fractions, while the activity within ER-derived microsomes was slightly elevated (Mazzulli *et al*., 2011). Alterations in GCase maturity have also been observed in the brains of patients expressing A53T α-syn (Chung *et al*., 2013). During studies on the clearance rate of α-syn, it was serendipitously discovered that the glycosylation patterns of GCase were altered in response to changes in α-syn expression levels (Mazzulli *et al*., 2011). As α-syn levels were reduced, a reduction in the low molecular weight ER-form of GCase occurred concomitantly with an increase in glycosylated high molecular weight forms. Collectively, these data suggest that α-syn does not initially cause an overall reduction in GCase protein in the cell, but instead alters its organelle distribution with specific reduction in lysosomal compartments (Mazzulli *et al*., 2011; Mazzulli *et al*., 2016).

Based on these findings, we hypothesized that the accumulation and aggregation of α-syn could directly cause a decline in wild-type GCase activity. To examine this, we generated iPSC-

derived midbrain dopaminergic (DA) neurons that naturally overexpress wild-type α-syn due to a triplication (3X) in the *SNCA* genomic region. Our iPSC models are derived from three individual PD patients, each of which, importantly, harbors wild-type GCase. We developed and extensively characterized several iPSC clones from each PD patient for pluripotency, residual transgene expression of reprogramming factors, *SNCA*-3X genotype retention, and neural differentiation efficiency (Figure 2-2). We showed that the *SNCA*-3X neurons accumulate and aggregate α-syn (Figure 2-3), recapitulating key pathological features of the PD brain. To determine whether the overexpression of wild-type α-syn affects wild-type GCase activity, we used a lysosomal compartment-specific GCase activity assay, which demonstrated an age-dependent decline in activity in *SNCA*-3X neurons (Figure 2-4 B, Figure 2-6 E). Importantly, we showed that the loss of lysosomal GCase activity occurs specifically due to α-syn, since α-syn depletion in CRISPR/Cas9-generated isogenic controls showed a significant rescue in GCase trafficking and downstream lysosomal function (Figure 2-6). These results are consistent with previous studies showing that α-syn disrupts the early secretory pathway and can block ER-Golgi trafficking (Cooper *et al*., 2006; Gosavi *et al*., 2002). Our studies also validate previous findings in primary neuronal cultures and patient-derived iPSC neurons showing that α-syn overexpression causes the accumulation of an immature GCase form that was sensitive to endoglycosidase H (endoH) and reduces the amount of enzyme that reached the lysosomal compartment (Chung *et al*., 2013; Mazzulli *et al*., 2011; Mazzulli *et al*., 2016). Together, our results indicate that GCase activity can be reduced in the absence of *GBA1* mutations through other factors such as aging and α-syn accumulation, implying that reduced GCase activity may play an important role in both *GBA1*-PD and sporadic PD.

CHAPTER 3

ER proteostasis dysfunction in PD patient-derived midbrain neurons

Preface. The work presented in this chapter of the dissertation has been adapted largely from Stojkovska *et al*., 2021, an original research manuscript titled "Rescue of α-synuclein aggregation in Parkinson's patient neurons by synergistic enhancement of ER proteostasis and protein trafficking" that is currently under peer review.

OVERVIEW

Chronic ER stress is suspected to play a prominent role in PD. The subsequent activation of the unfolded protein response (UPR), as detected by immunoreactivity of UPR markers, has been shown in the substantia nigra of post-mortem PD brains (Credle et al., 2015; Heman-Ackah et al., 2017; Hoozemans et al., 2007). Neurotoxin (6-OHDA and MPP+) primary cell models of PD show an induction of genes involved in ER stress and UPR such as ER chaperones and elements of the ubiquitin proteasome system (UPS) (Holtz and O'Malley, 2003). General markers of UPR activation have also been documented in various synucleinopathy models including α-syn overexpressing yeast (Cooper *et al*., 2006), human mutant *SNCA* A53T transgenic mice (Colla et al., 2012b; Colla et al., 2018), as well as *SNCA* mutation and triplication iPSC-derived cortical neuron models (Chung *et al*., 2013; Heman-Ackah *et al*., 2017). Increased ER stress has also been found in iPSC-derived neuronal models from PD patients carrying *GBA1* mutations (Fernandes et al., 2016). Mutations in *GBA1* lead to destabilization of the GCase protein's structure, resulting in strong UPR induction, expansion / dilation of the ER compartment, and the rapid elimination of the protein through ER associated

degradation (ERAD) (Fernandes *et al*., 2016; Garcia-Sanz et al., 2017; Ron and Horowitz, 2005). However, whether ER stress and UPR activation occurs specifically through α-syn within PD dopaminergic neurons has not been previously investigated.

The ability of mutant α-syn to abnormally localize to the ER compartment has been demonstrated in both cellular and *in vivo* PD models. Ultrastructural analyses of neurons from transgenic mice expressing human wild-type or A53T α-syn have demonstrated that α-syn localizes to or partially within the ER (Colla et al., 2012a; Masliah *et al*., 2000). Since α-syn is primarily a cytosolic protein and does not contain an ER signaling peptide, the abnormal association with the ER poses a potential risk for a disruption in its proper function. Mechanistically, this could occur through the direct interaction of α-syn with ER chaperones. For instance, several studies have used co-immunoprecipitation to show that α-syn pulls down with glucose-regulated proteins GRP78 and GRP94 (Bellucci et al., 2011; Colla *et al*., 2012a), two essential ER chaperones. Whether chaperone functionality is directly affected by α-syn has not been investigated. However, the overexpression of GRP78 has been shown to reduce neurodegeneration in α-syn expressing animal models (Gorbatyuk et al., 2012), further emphasizing the importance of maintaining ER proteostasis in neuronal health. While these studies collectively suggest that ER dysfunction is associated with PD, the mechanistic link between α-syn accumulation, protein misfolding in the ER, and downstream lysosomal dysfunction has not been established.

METHODS AND MATERIALS

Culturing of A53T α-syn and *GBA1* mutant iPSCs and midbrain DA neurons

PD patient iPSCs containing the A53T mutation in *SNCA* were obtained as a gift and were previously described and characterized in Soldner *et al*., 2011. Corresponding A53T isogenic controls were created using zinc-finger nuclease technology. GD patient iPSCs containing the homozygous *GBA1* mutation L444P/L444P were obtained from Telethon Genetic Biobank Network and were previously described and characterized in Schondorf *et al*., 2014. GD patient iPSCs containing the compound heterozygous mutation N370S/84GG were obtained from NIGMS Human Genetic Cell Repository and were previously characterized in Mazzulli *et al*., 2011; Mazzulli *et al*., 2016. Refer to Table 2 for more iPSC details. All iPSCs were maintained in mTeSR1 media on matrigel-coated plates. Differentiation of A53T and *GBA1* mutant iPSCs into midbrain DA neurons was performed the same as *SNCA*-3X iPSCs.

Sequential protein extraction and western blot analysis

Cells were harvested in 1X PBS and pelleted by centrifugation at 400xg for 5 minutes. To extract soluble protein, the cell pellets were homogenized in 1% Triton base lysis buffer (refer to Table S4 for recipe) containing protease inhibitor cocktail (PIC) (Roche), phenylmethylsulfonyl fluoride (PMSF) (Sigma), sodium orthovanadate (Na_3VO_4) (Sigma) and sodium fluoride (NaF) (Sigma) (refer to Table S4 for recipe). The Triton extracted lysates were freeze-thawed three times and ultracentrifuged at 100,000xg for 30 minutes at 4°C. To extract insoluble protein, the Triton-insoluble pellets were solubilized with 2% SDS base lysis buffer (refer to Table S4 for recipe) containing PIC via boiling for 10 minutes, followed by sonication and then ultracentrifugation at 100,000xg for 30 minutes at 22°C. The protein concentrations of the Triton

and SDS fractions were measured via a BCA protein assay kit (Thermo Fisher Scientific) on a plate reader. Extracted protein lysates were boiled at 100°C for 10 min in Laemmli sample buffer (refer to Table S4), loaded on an SDS-PAGE gel, transferred onto a PVDF membrane (Millipore), and post-fixed in 0.4% PFA (refer to Table S4 for recipe). Membranes were blocked in a 1:1 mixture of 1X TBS and Intercept blocking buffer (Li-Cor Biosciences), followed by overnight incubation with primary antibodies (refer to Table S2) diluted in a 1:1 mixture of 1X TBS-Tween and blocking buffer. The following day, secondary antibodies (refer to Table S2) were added for 1 hour, and the membranes were scanned using a Li-Cor Biosciences infrared imaging system. Quantification of band intensity was done using the ImageStudio software and analysis was performed on Excel and GraphPad Prism.

GCase maturation was measured by quantifying the ratio of post-ER (mature; >62 kDa) to ER (immature; 55-62 kDa) GCase.

Insoluble hydrolase analysis of synucleinopathy brain tissues

Sequential protein extraction was performed on post-mortem frontal cortex brain tissues (obtained from the Northwestern University Alzheimer's disease pathology core) obtained from controls, dementia with Lewy bodies (DLB) patients, and patients with DLB co-morbid with Alzheimer's disease (AD). We employed a 5-step extraction protocol using high salt buffer, 1% Triton X-100, 1% Triton + 30% sucrose (Sigma), 1% sarkosyl (Sigma), and sarkosyl-insoluble extracts. Brain tissues were homogenized in high-salt buffer (HSB) (50 mM Tris-HCl pH 7.4, 750 mM NaCl, 10 mM NaF, 5 mM EDTA) with protease and protein phosphatase inhibitors, incubated on ice for 20 minutes and centrifuged at 100,000 x g for 30 minutes at 4°C. The pellets were then re-extracted with HSB, followed by sequential extractions with 1% Triton X-100-

containing HSB and 1% Triton X-100-containing HSB with 30% sucrose. The pellets were then resuspended and homogenized in 1% sarkosyl-containing HSB, rotated at 4°C overnight and centrifuged at 100,000 x g for 30 min. The resulting sarkosyl-insoluble pellets were washed once with PBS and resuspended in PBS by brief sonication. This suspension was termed the 'sarkosyl-insoluble fraction', which was analyzed by western blot.

Insoluble GCase analysis of ER microsome-enriched idiopathic PD brain tissues

ER microsomes were enriched using subcellular fractionation. Post-mortem cingulate cortex brain tissues obtained from idiopathic PD (iPD) patients were lysed and homogenized in 0.25M sucrose buffer containing 10mM HEPES (pH 7.4) and 0.01M EDTA and centrifuged at 6,800 x g for 5 minutes at 4°C to remove nuclei and unbroken cells. The extraction was repeated on the resulting pellet. The final supernatants were combined and further centrifuged at 17,000 x g for 10 minutes at 4°C to remove mitochondria. Further centrifugation of the resulting supernatant at 100,000 x g for 1 hour removes the cytosolic components, leaving the ER microsome components in the final pellet. Sequential extraction of soluble and insoluble protein from this final pellet was performed using 1% Triton and 2% SDS lysis buffer, respectively. Insoluble fractions were analyzed via western blot.

***GBA1* mutation genotyping of human brain samples**

Genomic DNA was extracted from 50mg human brain tissue (frontal / temporal cortex) using the PureLink genomic DNA kit (Invitrogen). To amplify the *GBA1* gene, 25ng genomic DNA was used as a template for PCR using the following forward and reverse primers, respectively: 5'-TGTGTGCAAGGTCCAGGATCAG-3' and 5'-ACCACCTAGAGGGGAAAGTG-3'. The PCR

products were run on a 1% agarose gel to confirm amplification of the *GBA1* gene and to rule out accidental amplification of the *GBA1* pseudogene (*GBAP*). Sequencing of the most common *GBA1* mutations (L444P, N370S, E326K) was performed using primers listed in Table S3, and analysis was done using the Snapgene software.

Transmission Electron Microscopy (TEM) analysis

Neurons were fixed in 2.5% glutaraldehyde (Electron Microscopy Sciences) in PBS for 30 minutes, and then washed six times with PBS for 5 minutes. Cells were post-fixed with 1% osmium tetroxide (OsO_4) (Electron Microscopy Sciences) in PBS for 1 hour, and then washed three times with water. Next, cells were dehydrated with ethanol (twice with 50% ethanol for 5 minutes, then twice with 70% ethanol for 10 minutes) and stained with 1% uranyl acetate (Electron Microscopy Sciences) in 70% ethanol for 45 minutes. Cells were further dehydrated with ethanol (once with 70% ethanol, then twice with 90% ethanol for 10 minutes, then three times with 100% ethanol for 10 minutes). To evaporate the ethanol, 100% ethanol was mixed at a 1:1 ratio with an LX112 resin mix containing LX112 (Ladd Research Industries), DDSA (Electron Microscopy Sciences), and NMA (Electron Microscopy Sciences), and added to the cells for 1 hour with the lid off. Next, LX112 resin mix alone was added to the cells for 1 hour. Finally, cells were embedded by combining LX112 resin mix with DMP-30 (Electron Microscopy Sciences) and allowing the resin to solidify overnight at 60°C. Samples were then thin sectioned (~70nm width) on a UC7 ultramicrotome, as a service provided by the Northwestern University Center for Advanced Microscopy and viewed on a FEI Tecnai Spirit G2 transmission electron microscope (TEM). For each cell that was imaged via EM, all clearly defined ER regions were analyzed for both length and area using the 'Measure' function in

ImageJ. The length and ER area (in micrometers) of each individual ER profile were plotted on a graph using GraphPad Prism.

mRNA expression analysis of ER chaperones and stress signals

Total RNA was isolated from cells using an RNeasy Mini Prep kit (QIAGEN). cDNA was synthesized by reverse transcriptase PCR (RT-PCR) using the RevertAid First Strand cDNA synthesis kit (Thermo Fisher Scientific). Real-time qPCR was performed on the Applied Biosystems 7500 Fast system using the cDNA and pre-designed TaqMan-primer probes for GRP78, CANX, XBP1-S, or EDEM (refer to Table S2). The target mRNA expression was quantified relative to β-actin using the delta-delta-Ct method and represented as a fold change.

Human H4 neuroglioma cell culture

Human H4 neuroglioma cells were stably transfected to overexpress wild-type (WT) α-syn under the control of a tetracycline-inducible promoter via a Tet-off system. α-Syn expression was turned off by the addition of 1μg/ml doxycycline (DOX) (Sigma), a tetracycline analog, for a minimum of 3 days. Cells were cultured in Optimem media with 5% heat-inactivated fetal bovine serum (FBS), 0.2 mg/ml geneticin, 0.2 mg/ml hygromycin B, and 1% penicillin / streptomycin (Thermo Fisher Scientific) (refer to Table S4 for recipe details).

ER stress induction of H4 cells or iPSC neurons

To induce ER stress and activate the UPR, H4 cells or iPSC neurons were treated with 30nM thapsigargin (Tg) (Sigma) or 50ng/ml brefeldin A (BFA) for 24 hours prior to harvesting, and

analysis of mRNA and/or protein expression of known ER stress markers (GRP78, GRP94, CANX, p-eIF2α) was performed.

Semi-quantitative RT-PCR analysis of XBP1 mRNA

Using cDNA as the template, human XBP1 mRNA was detected using PCR primers (forward: TTACGAGAGAAAACTCATGGCC; reverse: GGGTCCAAGTTGTCCAGAATGC) specific for both spliced (S; product size 263 bp) and unspliced (U; product size 289) isoforms (Samali et al., 2010). The PCR product was analyzed on an agarose gel along with a brefeldin A (BFA) positive control.

Proteasomal inhibition of iPSC neurons

iPSC neurons were treated with 50nM or 1μM epoxomicin (Epox) (Fisher) for 24 hours to inhibit the proteasome. Analysis of GCase levels following treatment was performed via western blot analysis. Successful proteasomal inhibition was confirmed by blotting for ubiquitin.

Proximity Ligation Assay (PLA)

H4 cells or iPSC neurons plated on coverglass were fixed with 4% PFA for 20 minutes at RT. The cells were then washed three times with PBS, permeabilized with 0.3% Triton X-100 in PBS for 1 hour at 4°C, and then blocked with 2% BSA (Roche) and 5% NGS (Jackson Immuno Research) in Triton-PBS for 30 minutes at RT. Interaction between α-syn and ER chaperones was determined via the Duolink *In situ* Red Starter Kit Mouse/Rabbit (Sigma). Cells were incubated with primary antibodies (anti-α-synuclein syn211, anti-α-synuclein C20, anti-CANX, anti-GRP94; refer to Table S2) overnight followed by a 1 hour, 37°C incubation with the PLA

probes (secondary antibodies labeled with distinct oligonucleotides) provided in the kit. If the PLA probes are in proximity, the addition of ligase and DNA polymerase results in rolling circle amplification. For the ligation step, cells were washed twice with 1X wash buffer A (provided in the PLA kit) for 5 minutes each, and incubated with ligase (1:40 dilution) for 30 minutes at 37°C. For the amplification step, cells were washed twice with 1X wash buffer A for 2 minutes each, and incubated with polymerase diluted (1:80) in an amplification buffer containing fluorescently labeled complementary nucleotide probes for 100 minutes at 37°C. After the incubation, the cells were washed twice with 1X wash buffer B (provided in the PLA kit) for 10 minutes each followed by a quick wash with 0.01X wash buffer B. Finally, the cover glass was mounted onto microscope slides with DAPI mounting media. All images were obtained on a Leica confocal microscope, with PLA excitation at 488nm. Counting of PLA particles was automated using ImageJ using the 'Measure' function. To determine the level of interaction, the number of PLA particles were normalized to the number of nuclei within an acquired field of view.

ER microsome-enrichment of iPSC-derived neurons

ER microsomes were crudely enriched using subcellular fractionation. *SNCA*-3X and healthy and isogenic control iPSC-derived neurons were gently homogenized in sucrose HEPES buffer (SHB) (refer to Table S4 for recipe details). The homogenate was centrifuged at 6,800 x g for 5 minutes at 4°C to remove nuclei and unbroken cells. Following removal of the supernatant (S1), the extraction was repeated using SHB buffer and the second supernatant (S2) was combined with S1. The combined supernatants (S1+S2) were further centrifuged at 17,000 x g for 10 minutes at 4°C to remove mitochondria. Further centrifugation of the resulting supernatant (S3)

at 100,000 x g for 1 hour at 4°C removes the cytosolic components (supernatant S4), leaving the ER microsomes in the third and final pellet, termed P3. The P3 pellet was extracted in 1% Triton lysis buffer and analyzed by western blot.

Super-resolution structured illumination microscopy (SIM)

iPSC neurons were plated on coverglass, fixed in 4% PFA for 15 minutes, permeabilized with 0.1% Triton X-100 in PBS for 30 minutes, and blocked with 2% BSA and 5% NGS in Triton-PBS for 30 minutes. Primary antibodies (anti-α-synuclein syn211, anti-PDIA6; refer to Table S2) were added overnight, followed by incubation with secondary antibodies (Alexa Fluor 488 Goat anti-mouse IgG and Alexa Fluor 568 Goat anti-rabbit IgG; refer to Table S2) for 2 hours. The cells were then washed three times with Triton-PBS and mounted onto microscope slides with DAPI mounting media. Imaging was performed using an oil immersion 100X objective lens on a Nikon structured illumination microscope (N-SIM) at the Northwestern University Center for Advanced Microscopy. Images were captured and slices were reconstructed using the Nikon NIS Elements program.

Statistical analysis

Analyzed data was plotted and tested for statistical significance using the GraphPad Prism software. Statistical significance between two samples was determined using a paired or unpaired t-test with Welch's correction. For more than two samples, significance was determined using a one-way ANOVA with Tukey's post-hoc test. A p-value of <0.05 was considered to be significant ($*p < 0.05$, $**p < 0.01$, $***p < 0.001$, $****p < 0.0001$). For each quantification, the type of error bar used is specified in the figure legends.

RESULTS

3.1 Defects in GCase maturation induce its aggregation in the ER of patient midbrain neurons and synucleinopathy brains.

The accumulation of immature proteins in the ER can overwhelm the folding machinery, leading to protein misfolding (Marquardt and Helenius, 1992). While aggregation of immature lysosomal hydrolases has not been previously documented or linked to any pathological process, we hypothesized that α-syn-induced trafficking disruptions may have become severe enough to cause GCase instability, misfolding and aggregation. To test this, lysates from *SNCA*-3X DA neurons were sequentially extracted and analyzed by western blot. We found elevated levels of immature GCase in Triton X-100-insoluble fractions compared to isogenic controls (Figure 3-1 A). This was confirmed in a distinct synucleinopathy patient model expressing A53T α-syn that previously demonstrated disrupted protein trafficking of GCase (Cuddy *et al*., 2019) (Figure 3-1 B).

To determine if GCase misfolds and aggregates *in vivo*, we compared the levels of GCase in 1% sarkosyl-insoluble fractions from brains of patients with either Dementia with Lewy bodies (DLB), or DLB with co-existing Alzheimer's disease (AD) pathology. In age-matched healthy control brains, we detected mild amounts of insoluble GCase that migrated at 55 kDa likely representing the non-glycosylated immature protein, as well as insoluble GCase fragments that migrated between 42 and 48 kDa (Figure 3-1 C). Despite the fact that we observed some variability between control brains, comparison with age and post-mortem interval (PMI)-matched synucleinopathy brain showed a 1.8-fold elevation of insoluble GCase in DLB brain, and a more dramatic increase of nearly 4-fold in DLB+AD brain (Figure 3-1 C, Table 3). To determine if aggregated GCase occurs in the ER *in vivo*, we isolated microsomes from PD brain

and performed a sequential extraction. We found a significant elevation of insoluble GCase in PD brain compared to controls (Figure 3-1 D, Table 4). To determine if this effect is specific for GCase, we analyzed the solubility of two other hydrolases, including cathepsin D and hexosaminidase B. We found that insoluble immature forms of cathepsin D accumulated in DLB brain, but hexosaminidase B was only found in the soluble fraction with no change seen between control and disease (Figure 3-2, Table 5). Together, these data indicate that α-syn induced perturbations in hydrolase maturation lead to the accumulation of aggregated, insoluble hydrolases in the ER.

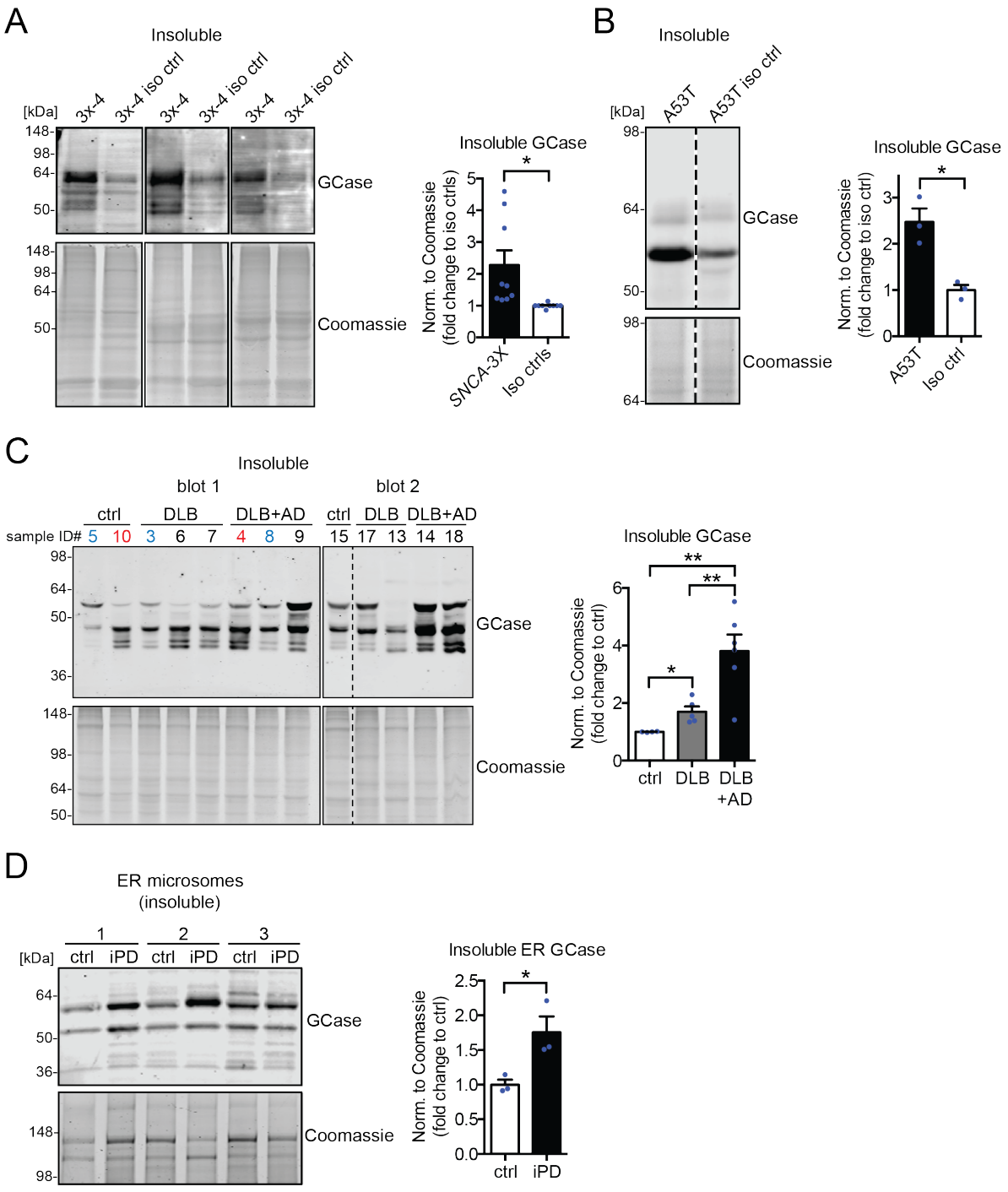

Figure 3-1. Accumulation of insoluble immature GCase in *SNCA*-3X midbrain DA neurons and human synucleinopathy brains.

(A) Day 90 *SNCA*-3X DA neurons were sequentially extracted and the Triton X-100-insoluble fractions were analyzed by western blot for GCase. Three replicates of line 3x-4 are shown as a representative example. Right, quantification of insoluble GCase normalized to Coomassie combined from lines 3x-1, 3x-2, and 3x-4 (n=3-4 from

each line, n=10 total).

(B) PD patient line expressing A53T α-syn and isogenic control were analyzed as in A.

(C) GCase western blot analysis of 1% sarkosyl insoluble extracts from the frontal cortex in controls or synucleinopathy patient brains (DLB, dementia with Lewy bodies; DLB + AD, DLB with Alzheimer's disease (AD) pathology). Right, quantification of insoluble GCase normalized to Coomassie and grouped by similar post-mortem intervals (PMI) (blue, PMI = <10 hrs; black, PMI < 20hrs; red, PMI < 30 hrs).

(D) ER microsome fractions from the cingulate cortex of 3 controls and 3 PD brains were sequentially extracted and Triton X-100-insoluble lysates were analyzed by western blot for GCase. Right, quantification of insoluble GCase from microsome fractions, normalized to Coomassie.

In panels B and C, the dashed line represents irrelevant lanes that were cropped out from the same blot. See Table 3 and Table 4 for clinical and pathological data and raw GCase quantifications from the patient brain samples. For all quantifications, values are the mean ± SEM, *$p < 0.05$; **$p < 0.01$, using student's unpaired t-test (panels A-D) or ANOVA with Tukey's post-hoc test (panel C).

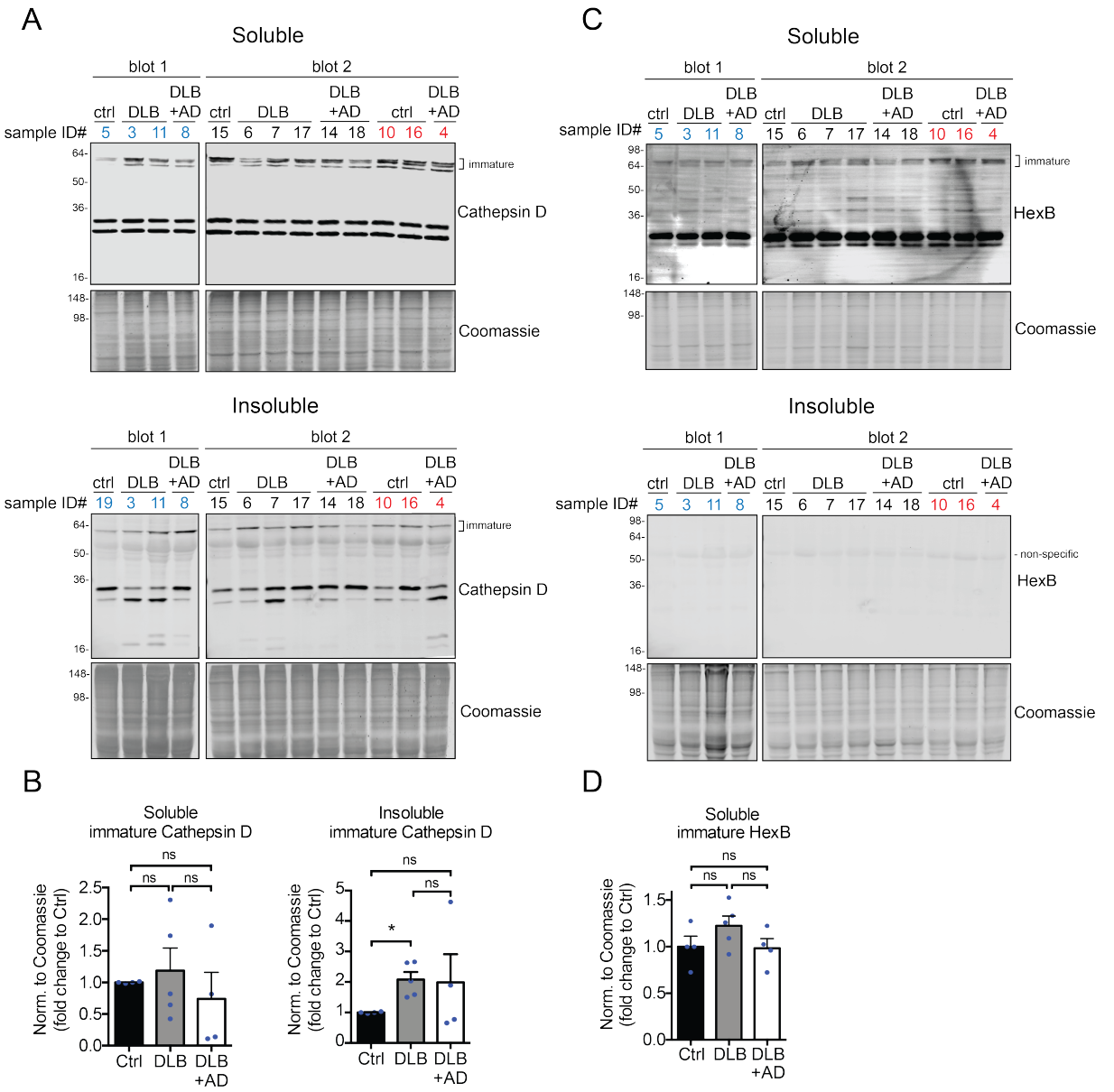

Figure 3-2. Specificity of insoluble lysosomal hydrolase accumulation in human synucleinopathy brains.

Sequential extraction and western blot analysis for **(A)** cathepsin D and **(C)** hexosaminidase B (Hex B) was performed as in Figure 3-1. See Table 5 for clinical and pathological patient data and the cathepsin D quantifications of the brain samples.

(B) Quantification of soluble and insoluble immature forms of cathepsin D, normalized to Coomassie (n=4-5).

(D) Quantification of soluble immature forms of Hex B, normalized to Coomassie (n=4-5). Only soluble forms of the hydrolase were detected.

For all quantifications, data represents mean ± SEM, *p<0.05; ns = not significant, using ANOVA with Tukey's post-hoc test.

Table 3. Clinical, pathological, and raw western blot data from human brain analysis of insoluble GCase.

PMI group	Pathological Diagnosis	Sample #	Presense of *GBA1* mut	Brain Region	Sex	PMI (hrs)	Age	Blot #	Insol. GCase - raw intensity	Coomassie - raw intensity	Normalized GCase	Fold to ctrl / PMI group
PMI < 10 hrs	CTRL (AD-normal aging; Braak stage III)	5	N	Frontal Cortex	F	6	89	1	13600	34800	0.39	1
	DLB	3	N	Frontal Cortex	M	4	68	1	20600	25600	0.8	2.06
	DLB	11	no sample	Frontal Cortex	F	6	75	not shown	22500	24222	0.93	2.38
	DLB + AD	8	N	Frontal Cortex	N	9	78	1	29100	23000	1.27	3.24
PMI < 20 hrs	CTRL (AD-normal aging; Braak stage I)	15	N	Frontal Cortex	M	13	95	2	30400	27300	1.11	1
	DLB	6	no sample	Frontal Cortex	M	15	72	1	43800	24200	1.81	1.63
	DLB	7	N	Frontal Cortex	M	19	83	1	38300	25300	1.51	1.36
	DLB	17	N	Frontal Cortex	F	unknown	85	2	40400	25800	1.57	1.41
	DLB	13	Y (L444P/wt)	Frontal Cortex	F	15	81	2	25000	15600	1.6	1.44
	DLB + AD	9	N	Frontal Cortex	M	12	77	1	93300	20200	4.62	4.15
	DLB + AD	14	N	Frontal Cortex	M	13	74	2	118000	18900	6.24	5.61
	DLB + AD	18	N	Frontal Cortex	M	14	51	2	117000	22000	5.32	4.78
PMI < 30 hrs	CTRL (AD-pathology; Braak stage III)	10	N	Frontal Cortex	F	30	85	1	28800	22700	1.27	1.01
	CTRL (AD-normal aging; Braak stage II)	16	no sample	Frontal Cortex	M	27	88	not shown	34500	28000	1.23	0.99
	DLB + AD	4	Y (N370S/wt)	Frontal Cortex	M	23	57	1	69700	25300	2.75	2.2

Notes: The numbers in the shaded column were plotted in Figure 3-1 C. DLBD diagnosis includes high Lewy bod pathology with low / moderate AD pathology (ADNC low; normal aging Braak stages I-III). DLBD + AD includes high Lewy body pathology with high AD pathology (ADNC high; Ab score= =A3; neurofibrillary tangle score=B3; neuritic plaque score=C3).

Table 4. Clinical, pathological, and raw western blot data from human brain ER microsome fractionation analysis.

Pathological Diagnosis	Gel label	Brain Region	Sex	PMI (hrs)	Age	Insol. GCase - raw intensity	Coomassie - raw intensity	Normalized GCase	Fold to ctrl
CTRL	Ctrl 1	Cingulate Cortex	M	unknown	85	390	8690	0.0448792	0.94
CTRL	Ctrl 2	Cingulate Cortex	F	unknown	79	644	14800	0.0435135	0.91
CTRL	Ctrl 3	Cingulate Cortex	F	19	91	965	17700	0.0545198	1.14
PD	iPD 1	Cingulate Cortex	M	unknown	80	1120	15200	0.0736842	1.55
PD	iPD 2	Cingulate Cortex	M	24	73	1190	11300	0.1053097	2.21
PD	iPD 3	Cingulate Cortex	M	24	66	971	13500	0.0719259	1.51

Notes: The numbers in the shaded column were plotted in Figure 3-1 D.

Table 5. Clinical, pathological, and raw western blot data from human brain analysis of insoluble Cathepsin D.

PMI group	Pathological Diagnosis	Sample #	Insoluble Cathepsin D - raw intensity	Coomassie - raw intensity	Normalized Cathepsin D	Fold to ctrl / PMI group
PMI < 10 hrs	CTRL (AD-normal aging; Braak stage III)	19	408000	35500000	0.0115	1.00
	DLB	3	694000	38100000	0.0182	1.58
	DLB	11	1300000	55700000	0.0233	2.03
	DLB + AD	8	1930000	36300000	0.0532	4.63
PMI < 20 hrs	CTRL (AD-normal aging; Braak stage I)	15	262000	22300000	0.0117	1.00
	DLB	6	684000	21900000	0.0312	2.66
	DLB	7	414000	23500000	0.0176	1.50
	DLB	17	745000	24100000	0.0309	2.63
	DLB + AD	14	396000	17800000	0.0222	1.89
	DLB + AD	18	187000	20600000	0.0091	0.77
PMI < 30 hrs	CTRL (AD-pathology; Braak stage III)	10	402000	17700000	0.0227	1.03
	CTRL (AD-normal aging; Braak stage II)	16	487000	22800000	0.0214	0.97
	DLB + AD	4	336000	23200000	0.0145	0.66

Notes: The numbers in the shaded column were plotted in Figure 3-2 B.

3.2 ER fragmentation in *SNCA*-3X DA neurons that accumulate immature wild-type GCase.

When misfolded proteins accumulate in the ER, the UPR normally acts to increase protein folding capacity by expansion of the ER compartment and upregulation of ER chaperones to accommodate the added protein load (Fujiwara et al., 1988; Schuck et al., 2009; Walter and Ron, 2011). We hypothesized that reduced GCase maturation and accumulation of immature, aggregated GCase in the ER would induce ER stress. To assess ER stress induction in *SNCA*-3X DA neurons, we first examined the ER morphology by transmission electron microscopy (TEM). Despite the accumulation of immature GCase, *SNCA*-3X DA neurons did

not exhibit ER expansion but instead showed a decrease in total ER area relative to isogenic controls (Figure 3-3 A), with shorter, fragmented ER tubules (Figure 3-3 A). In contrast, Gaucher's disease (GD) neurons, which express and retain mutant GCase in the ER, demonstrated a severely dilated ER, consistent with an activation of the UPR as previously noted (Ron and Horowitz, 2005) (Figure 3-3 A). This was confirmed by quantifying the area of each clearly identifiable ER segment in neurons. These data indicate that the ER fails to accommodate the accumulation of misfolded wild-type GCase by ER expansion, suggesting that *SNCA*-3X DA neurons may lack the ability to initiate a UPR response.

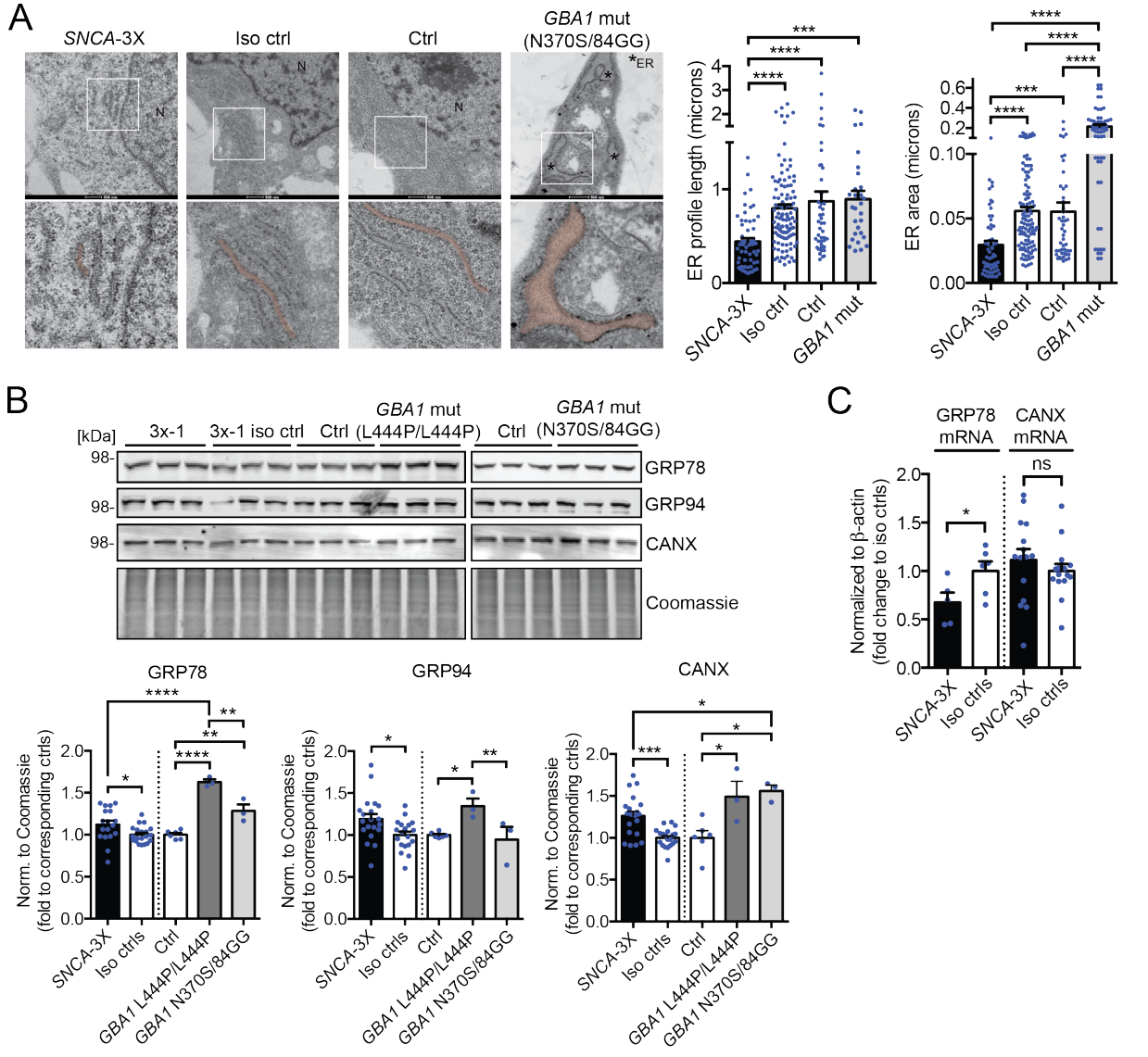

Figure 3-3. Alterations in ER morphology and baseline characterization of the ER stress response in *SNCA*-3X midbrain DA neurons.

(A) Representative ER ultrastructure of day 65 *SNCA*-3X (3x-2), mutant *GBA1* (N370S/84GG), and control DA neurons. Examples of ER segments are highlighted in red. The white boxes indicate the zoomed-in regions of the images underneath. N=nucleus, * = ER (endoplasmic reticulum). Scale bar, 500 nm. Right, quantifications of length and area of each clearly identifiable ER segment in each line (n=3-9 cells per line; each data point on the scatter plot indicates a measured ER segment).

(B) Baseline expression of ER stress markers in day 90 *SNCA*-3X (lines 3x-1, 3x-2, 3x-4), mutant *GBA1* (N370S/84GG and L444P/L444P), and corresponding isogenic and healthy control DA neurons (n=2-5 for each line). Levels of *SNCA*-3X and mutant *GBA1* neuron ER stress markers were normalized to Coomassie and are

shown as a fold change to the isogenic or healthy controls, respectively. Each data point in the scatter plot indicates a biological replicate taken from several experiments.

(C) GRP78 and CANX mRNA expressions in *SNCA*-3X and isogenic controls were measured via real-time qPCR and quantified relative to β-actin. Data for GRP78 mRNA was combined from 3x-1 and 3x-2 and corresponding isogenic controls (n=2-3 per line). Data for CANX mRNA was combined from 3x-1, 3x-2, and 3x-4 and corresponding isogenic controls (n=3-7 per line).

For all quantifications, values are mean ± SEM, *p < 0.05; **p < 0.01; ***p < 0.001; ****p < 0.0001; ns = not significant, using student's unpaired t-test (panels B, C) or ANOVA with Tukey's post-hoc test (panels A, B).

3.3 *SNCA*-3X DA neurons exhibit mild elevation of ER stress-related chaperones in the absence of UPR activation.

We next examined the levels of ER chaperones known to be involved in GCase folding or upregulated during ER stress, including the glucose-regulated proteins GRP78 and GRP94 and calnexin (CANX), by western blot (Kozutsumi et al., 1988; Tan *et al*., 2014). GRP78 and GRP94 preferentially bind to misfolded or aggregated proteins with exposed hydrophobic patches (Marquardt and Helenius, 1992; Melnick et al., 1994), while CANX normally binds to monoglucosylated N-glycan branches of non-aggregated folding intermediates (Ou *et al*., 1993) and retains them in the ER until properly folded (Rajagopalan et al., 1994). Compared to isogenic control lines, we observed mild elevations in all three chaperones that ranged from 10-25% (Figure 3-3 B). Moreover, the mRNA of GRP78 and CANX were not elevated in *SNCA*-3X DA neurons, indicating the absence of a UPR-induced transcriptional response (Figure 3-3 C). In comparison, GD-derived DA neurons carrying either the N370S/84GG or L444P/L444P mutation in GCase showed a more dramatic increase (~25-60%) in GRP78 and CANX relative to the healthy control**,** while GRP94 levels were elevated by ~25% only in the *GBA1* L444P / L444P mutant (Figure 3-3 B). The increased levels of GRP78, GRP94, and CANX in GD neurons compared to *SNCA*-3X DA neurons are likely due to the destabilizing effect of the

GCase mutations and are consistent with previous findings (Ron and Horowitz, 2005).

The dramatic ER fragmentation phenotype and accumulation of aggregated immature GCase prompted us to examine UPR signaling pathways in *SNCA*-3X DA neurons in more detail. During UPR, activation of the IRE1 pathway increases splicing of XBP1 mRNA, resulting in a functionally active transcription factor XBP1-S that upregulates expression of ER chaperones and ERAD machinery (Calfon et al., 2002; Yoshida et al., 2001) (Figure 1-2). Therefore, we measured XBP1-S and the expression of downstream transcriptional targets in *SNCA*-3X DA neurons. Using two independent assays, semi-quantitative RT-PCR and real-time qPCR, we surprisingly did not observe an increase of XBP1-S in *SNCA*-3X DA neurons compared to controls (Figure 3-4 A, B). However, we found that the *SNCA*-3X DA neurons were capable of activating the UPR by treating with different ER stress inducers. Thapsigargin (Tg) and brefeldin A (BFA) are both well-established compounds that cause ER stress and activate the UPR through distinct mechanisms (Booth and Koch, 1989; Helms and Rothman, 1992; Price et al., 1992). In *SNCA*-3X and control DA neurons, these ER stressors successfully induced a dramatic upregulation of XBP1-S mRNA (Figure 3-6 A) and significantly increased mRNA / protein levels of ER chaperones including GRP78, GRP94, and CANX (Figure 3-5 B, D) to a similar degree. These results were confirmed in another model of wild-type α-syn overexpression, human H4 neuroglioma cells that contain *SNCA* under the control of a tetracycline-inducible promoter (Figure 3-5 A, C). This indicates that α-syn accumulation does not affect the ability of *SNCA*-3X patient DA neurons to sense or transduce UPR signals under stressful conditions.

Next, we determined whether the PERK pathway of the UPR is activate in *SNCA*-3X DA neurons by measuring eIF2α, a eukaryotic initiation factor which upon phosphorylation by

PERK leads to global translational attenuation (Harding et al., 1999). We did not observe baseline elevation of phospho-eIF2α in patient neurons (Figure 3-6 B), indicating that the PERK pathway is not active. However, treatment with Tg increased phospho-eIF2α to a similar degree in both isogenic controls and *SNCA*-3X DA neurons (Figure 3-6 B). Collectively, these results suggest that the PD neurons fail to sense perturbations in ER proteostasis induced by α-syn, despite dramatic ER fragmentation and accumulation of aggregated immature GCase.

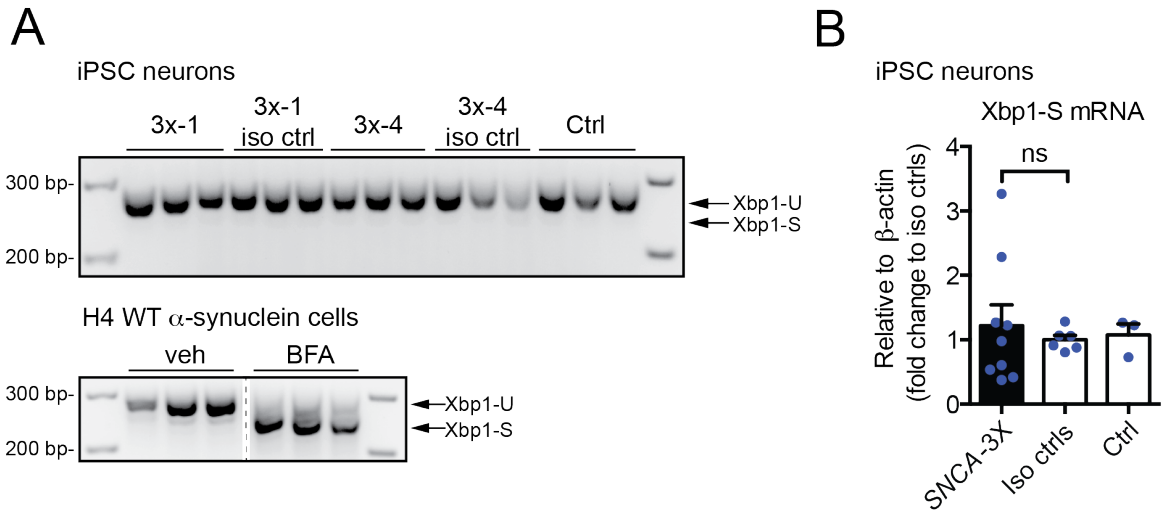

Figure 3-4. *SNCA*-3X midbrain DA neurons do not show baseline UPR activation despite α-syn and GCase accumulation.

(A) Semi-quantitative PCR agarose gel analysis of unspliced (U) and spliced (S) XBP1 mRNA in day 90 *SNCA*-3X and control DA neurons **(top)** and H4 WT α-syn overexpressing cells **(bottom)**. Treatment with brefeldin A (BFA) was done as a positive control. The dashed line indicates irrelevant lanes that were cropped out.

(B) XBP1-S mRNA expression in *SNCA*-3X and control DA neurons was measured by real-time qPCR and is shown relative to β-actin. Baseline XBP1-S mRNA is combined from day 90 3x-1, 3x-2, and 3x-4 and the isogenic controls of 3x-1 and 3x-4 (n=3 per line). Data is shown as mean± SEM; ns = not significant, using student's unpaired t-test.

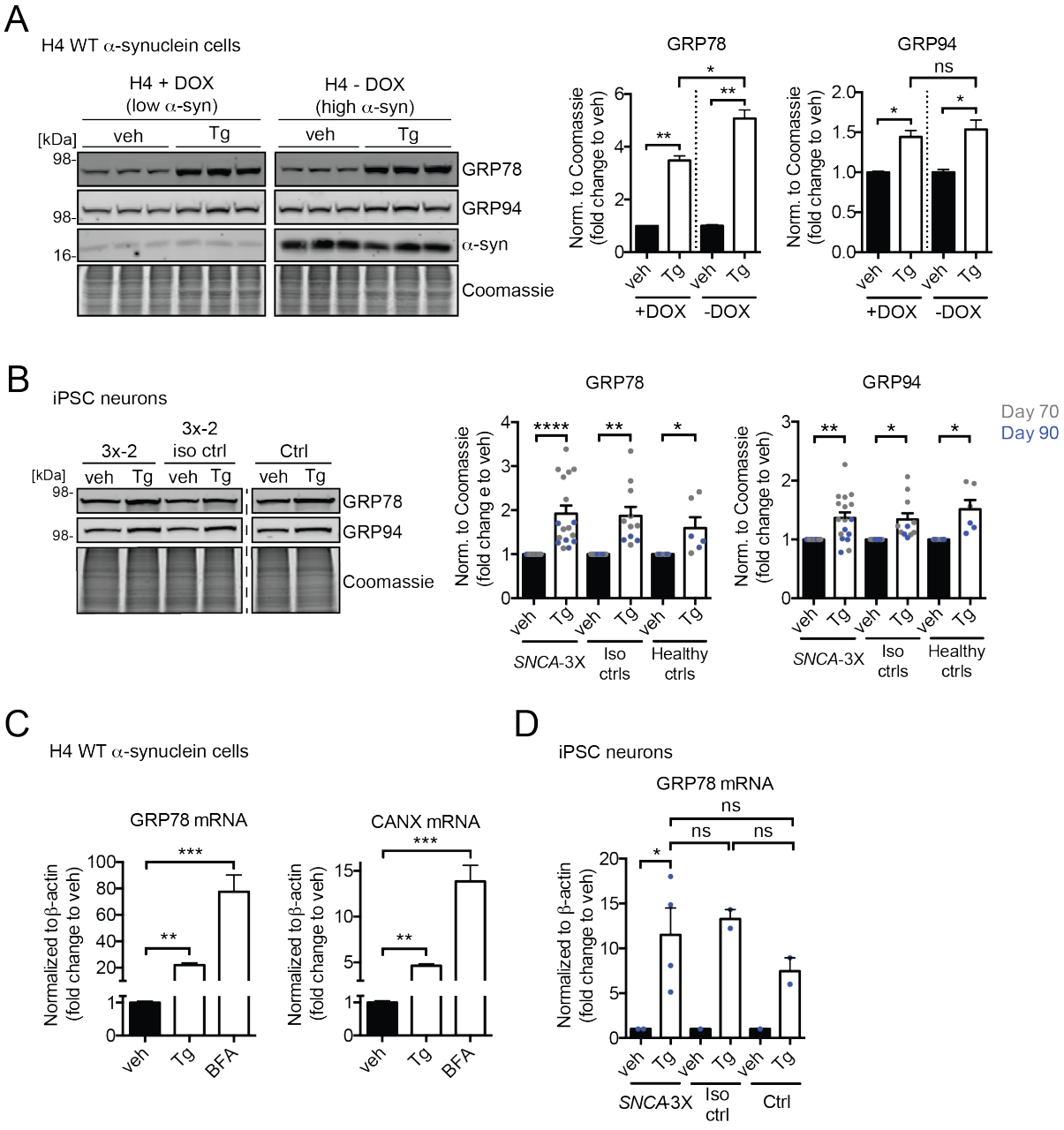

Figure 3-5. *SNCA*-3X midbrain DA neurons and cell lines that accumulate α-syn upregulate ER chaperones in response to ER stress induction.

To induce ER stress and activate the UPR, cells were treated with vehicle (veh) or 30nM thapsigargin (Tg) for 24 hours.

(A) H4 WT α-syn overexpressing cells were first treated with 1μg/ml doxycycline (DOX) for 3 days to turn off α-syn expression, followed by treatment with veh or Tg. Right, GRP78 and GRP94 quantifications were normalized to Coomassie (n=3).

(B) *SNCA*-3X and isogenic and healthy control DA neurons were treated with veh or Tg and analyzed for induction

of ER stress markers at day 70 and 90. Irrelevant lanes were cropped out from the blot and are indicated with a dashed line. Right, GRP78 and GRP94 levels were normalized to Coomassie, and are shown as a fold change to the vehicle for each set of lines. Analysis is of several lines of *SNCA*-3X: 3x-1, 3x-2, 3x-4, Est. 3x; isogenic controls: 3x-1 iso ctrl, 3x-2 iso ctrl, Est. 3x iso ctrl; healthy controls: Ctrl, Est. Ctrl. Each data point in the scatter plot indicates a biological replicate taken from several experiments.

(C, D) H4 WT α-syn overexpressing cells (n=4) and day 90 *SNCA*-3X and control DA neurons were treated for 24 hours with ER stress inducers (30nM Tg or 50ng/ml brefeldin A (BFA)). mRNA expression of GRP78 and CANX was quantified relative to β-actin. In panel D, analysis is combined from lines 3x-2 and 3x-4, and the isogenic control is from 3x-4.

For all quantifications, values are mean ± SEM, *p < 0.05; **p < 0.01; ***p < 0.001; ****p < 0.0001; ns = not significant, using student's unpaired (panels A, B, D) or paired (panel A, D) t-test or ANOVA with Tukey's post-hoc test (panel C).

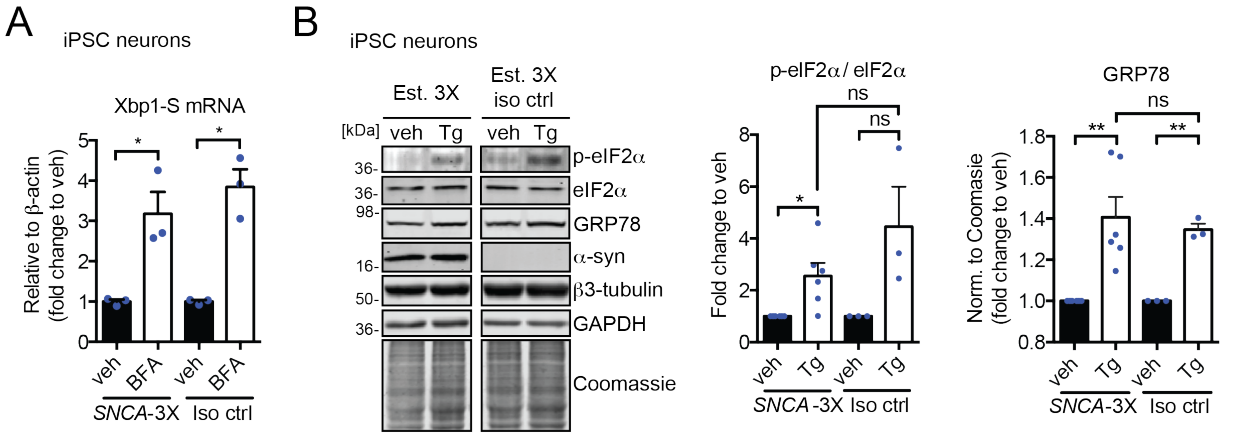

Figure 3-6. *SNCA*-3X midbrain DA neurons activate IRE1 and PERK UPR signaling in response to ER stress induction.

(A) Day 110 *SNCA*-3X (3x-2) and isogenic control DA neurons were treated with 50ng/ml BFA for 24 hours to induce ER stress. XBP1-S mRNA expression was measured by real-time qPCR and is shown relative to β-actin (n=3 per line).

(B) Representative western blot showing activation of the PERK arm of the UPR in day 90 *SNCA*-3X (Est. 3X) and isogenic control DA neurons treated with 30nM Tg for 24 hours. Right, quantifications of the ratio of phosphorylated to total eIF2α and of GRP78 expression normalized to Coomassie. Analysis is combined from 3x-1 and Est. 3X, and the isogenic control is from Est. 3X (n=3 per line).

For all quantifications, values are mean ± SEM, *p < 0.05; **p < 0.01; ns = not significant, using student's unpaired (panel A, B) or paired (panel B) t-test.

Proteins that are retained and accumulate in the ER are normally recognized by quality control machinery and eliminated by ERAD. For retained glycoproteins including lysosomal hydrolases, this process is mediated by EDEM1 (ER degradation-enhancing α-mannosidase-like protein 1). EDEM1 is a lectin-containing adapter protein that removes misfolded glycoproteins from the CANX folding cycle and delivers them to the cytosol for degradation through the UPS (Smith et al., 2011). EDEM1 expression is upregulated by ER stress through the IRE1 pathway of the UPR, helping to rebalance ER proteostasis (Lee et al., 2003). To determine if ERAD is altered in patient-derived *SNCA*-3X DA neurons, we measured the expression levels of EDEM1. Compared to the isogenic controls, we found no change in EDEM1 mRNA or protein levels (Figure 3-7 A-C). Since variability was observed in the levels of EDEM1 between culture samples of *SNCA*-3X lines, we correlated EDEM1 and α-syn protein levels in patient neurons and found a significant negative relationship (Figure 3-7 D). This negative correlation suggests samples with abundant α-syn pathology have reduced EDEM1 levels and therefore compromised ability to remove retained proteins from the CANX folding cycle.

Consistent with a lack of ERAD enhancement, we found no change in the levels of immature wild-type GCase upon proteasomal inhibition of *SNCA*-3X DA neurons (Figure 3-8 A). In contrast, GD neurons showed a dramatic upregulation of EDEM1 compared to both healthy controls and *SNCA*-3X lines (Figure 3-7 B, C), and significant elevation of GCase protein upon proteasomal inhibition (Figure 3-8 B). Overall, these data indicate that despite retaining immature GCase in the ER, the EDEM1 / ERAD pathway is not active in *SNCA*-3X DA neurons. In contrast, ERAD is elevated in GD patient DA neurons and leads to elimination of mutant GCase, consistent with previous findings in other cell models (Ron and Horowitz, 2005).

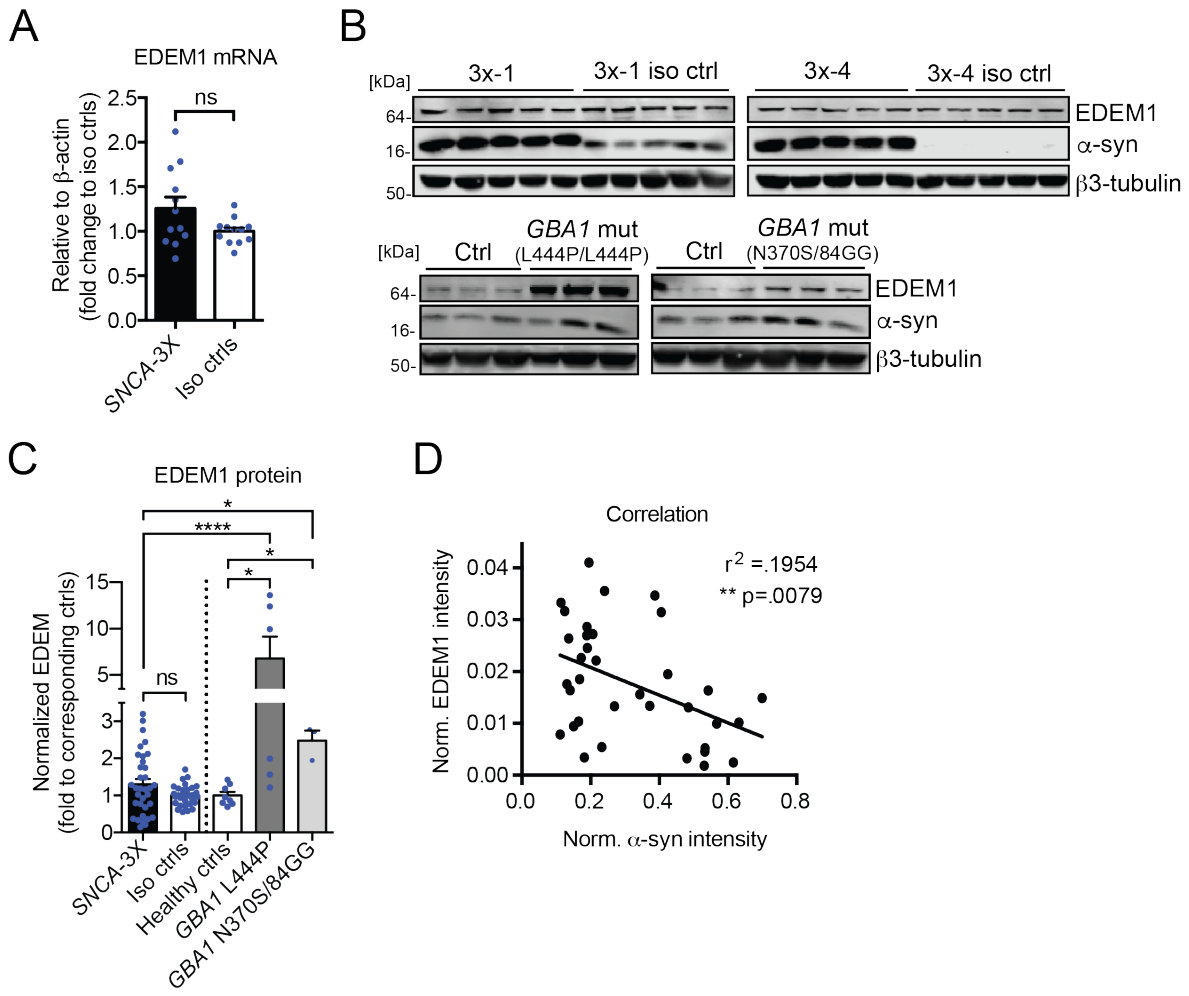

Figure 3-7. Lack of activation of EDEM1, an ER-associated degradation regulator, in *SNCA*-3X midbrain DA neurons.

(A) EDEM1 mRNA expression relative to β-actin in day 90 *SNCA*-3X and isogenic control DA neurons. Analysis is combined from lines 3x-1, 3x-2, and 3x-4 and the corresponding isogenic (n=4 per line).

(B) Representative western blot for EDEM1 in day 90 *SNCA*-3X and *GBA1* mutant DA neurons that accumulate α-syn.

(C) Quantification of EDEM1 expression in *SNCA*-3X and *GBA1* mutant DA neurons shown as a fold change to the isogenic and healthy controls, respectively. Analysis is combined from 3x-1, 3x-2, 3x-4, and Est. 3X (n=5-13 per line) and the corresponding isogenic controls (n=5-12 per line), as well Ctrl and Est. Ctrl for the healthy controls (n=2-6 per line).

(D) Correlation between EDEM1 and α-syn levels from *SNCA*-3X patient DA neurons indicated in panel C. Each data point in the scatter plot indicates a biological replicate of a patient sample.

For all quantifications, values are mean ± SEM, *p < 0.05; **p < 0.01; ***p < 0.001; ****p < 0.0001; ns = not significant, using student's unpaired (panels A and C) t-test or ANOVA with Tukey's post-hoc test (panel C).

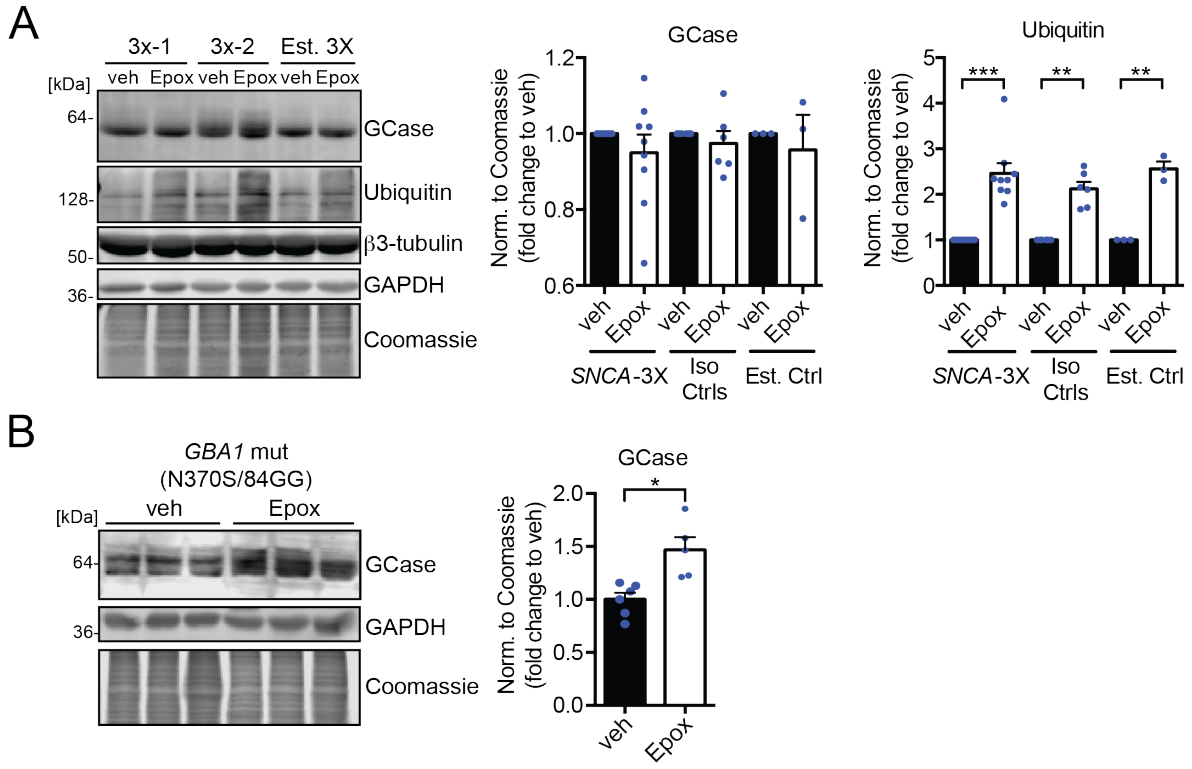

Figure 3-8. Proteasome inhibition of *SNCA*-3X and *GBA1* mutant midbrain DA neurons.

(A) Day 90 *SNCA*-3X and control DA neurons were treated with 50nM epoxomicin (Epox) for 24 hours to inhibit proteasomal degradation, and GCase and ubiquitin levels were analyzed via western blot. Right, quantification of GCase and ubiquitin levels normalized to Coomassie. Analysis is combined from 3x-1, 3x-2, and Est. 3X, and isogenic controls are from 3x-2 and Est. 3X (n=3 per line).

(B) GCase expression in *GBA1* mutant DA neurons treated with 1μM Epox. Right, quantification of GCase levels normalized to Coomassie (n=5-6).

For all quantifications, values are mean ± SEM, *p < 0.05; **p < 0.01; ***p < 0.001; ****p < 0.0001; ns = not significant, using student's unpaired (panels A, B) or paired t-test (panel A).

3.4 α-Synuclein accumulates at the ER and is in close proximity to ER chaperones in *SNCA*-3X DA neurons.

Although α-syn is known to be a synaptic protein under physiological conditions, our immunofluorescence analysis indicated its accumulation at the cell body in *SNCA*-3X DA neurons (Figure 2-3 A, B), consistent with previously characterized PD patient lines (Cuddy *et*

al., 2019; Mazzulli *et al*., 2016). Further, studies using transgenic α-syn overexpression models indicated that pathological α-syn can abnormally localize to the ER compartment (Bellucci *et al*., 2011; Colla *et al*., 2012a; Colla *et al*., 2012b; Colla *et al*., 2018; Guardia-Laguarta et al., 2014; Masliah *et al*., 2000; Paillusson et al., 2017). To determine if α-syn associates with the ER in our PD patient models, we used super-resolution structured illumination microscopy (SIM). Imaging analysis revealed increased colocalization of α-syn with the established ER marker protein disulfide isomerase (PDI) in *SNCA*-3X DA neurons compared to healthy controls that express normal α-syn levels (Figure 3-9 A). Furthermore, enrichment of ER microsomes from *SNCA*-3X DA neurons indicated that more α-syn is found in these fractions compared to control DA neurons (Figure 3-9 B), confirming previous findings that α-syn can abnormally localize to the ER compartment.

To probe at the potential molecular mechanism by which α-syn could disrupt ER proteostasis, we analyzed its proximity to ER chaperones including CANX and GRP94 by an *in situ* proximity ligation assay (PLA). PLA negative controls indicated a minimal background signal, suggesting specificity of the antibodies under these conditions (Figure 3-10 A). Analysis in α-syn overexpressing cell lines and *SNCA*-3X patient DA neurons showed that α-syn localizes to and interacts with both CANX and GRP94 (Figure 3-10 B, C). These results suggest that α-syn may disrupt ER proteostasis and GCase trafficking through aberrant association and sequestration of ER chaperones, thereby allowing wild-type GCase to become retained, misfolded, and eventually aggregated in the ER.

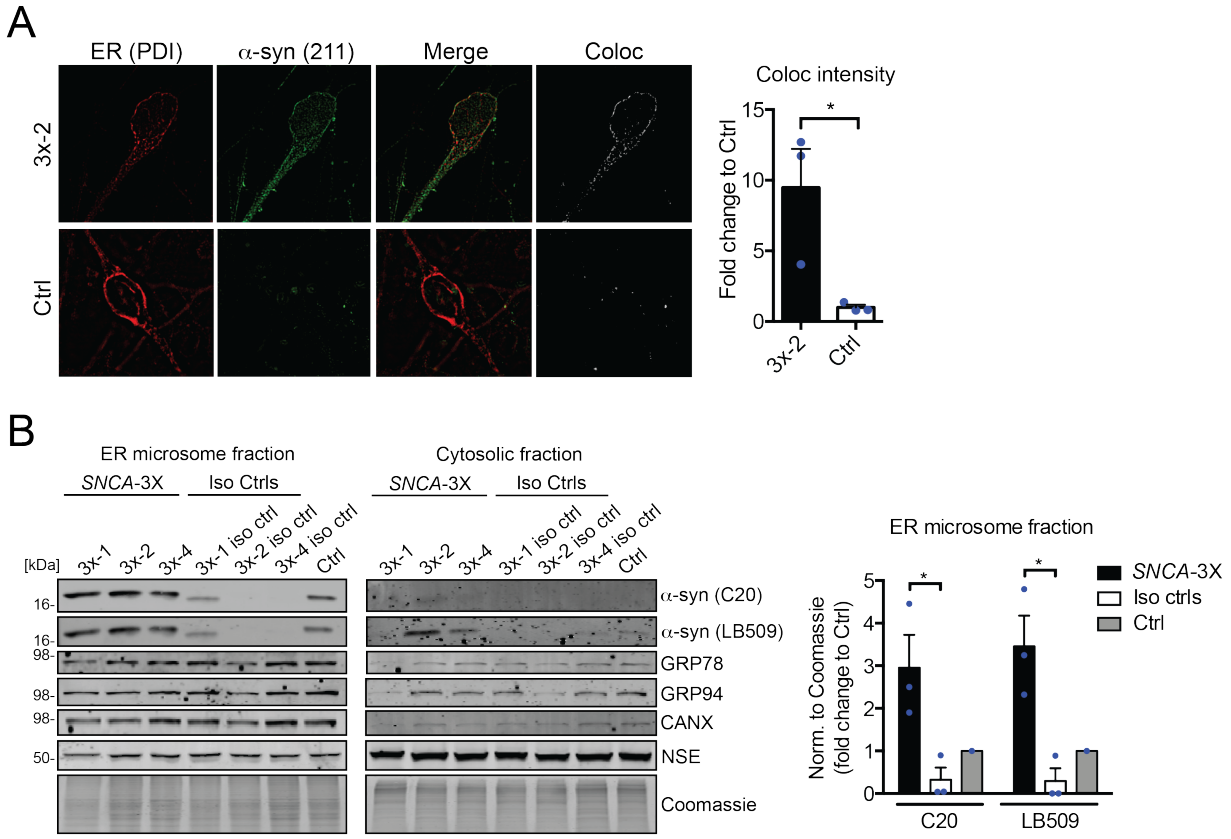

Figure 3-9. Aberrant localization of α-syn to the ER in *SNCA*-3X midbrain DA neurons.

(A) Super-resolution SIM analysis of protein disulfide isomerase (PDI) and colocalization with α-syn (antibody 211). Quantification of the colocalization in 3x-2 neurons compared to healthy control neurons that express normal levels of α-syn is shown on the right (n=3).

(B) Subcellular fractionation of day 120 DA neurons and western blot analysis of α-syn (antibodies C20 and LB509) demonstrates its accumulation within ER microsome fractions in *SNCA*-3X neurons compared to controls. ER (GRP78, GRP94, CANX) and cytosolic (NSE) markers were analyzed to assess enrichment of the ER. Right, quantification of C20 and LB509 α-syn levels in ER microsome fractions of *SNCA*-3X and isogenic and healthy control neurons (n=3, except n=1 for Ctrl).

For all quantifications, data is shown as mean ± SEM, *p<0.05, using student's unpaired t-test.

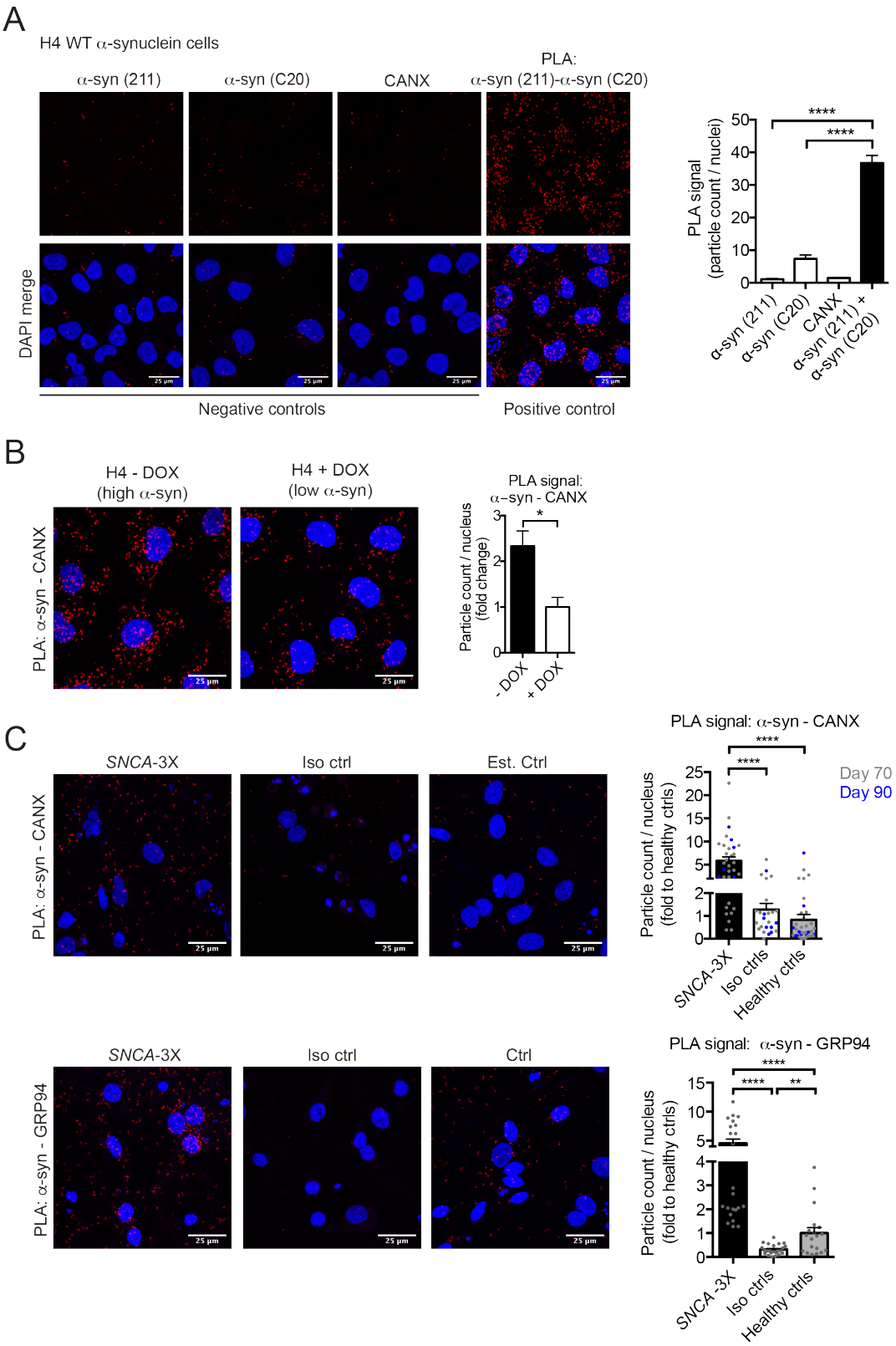
A
H4 WT α-synuclein cells
α-syn (211)
α-syn (C20)
CANX
PLA:
α-syn (211)-α-syn (C20)
DAPI merge
Negative controls
Positive control
PLA signal
(particle count / nuclei)
****
****
α-syn (211)
α-syn (C20)
CANX
α-syn (211) +
α-syn (C20)
B
H4 - DOX
(high α-syn)
H4 + DOX
(low α-syn)
PLA: α-syn - CANX
PLA signal:
α–syn - CANX
Particle count / nucleus
(fold change)
*
- DOX
+ DOX
C
SNCA-3X
Iso ctrl
Est. Ctrl
PLA: α-syn - CANX
PLA signal: α-syn - CANX
Particle count / nucleus
(fold to healthy ctrls)
Day 70
Day 90
SNCA-3X
Iso ctrls
Healthy ctrls
SNCA-3X
Iso ctrl
Ctrl
PLA: α-syn - GRP94
PLA signal: α-syn - GRP94
**
SNCA-3X
Iso ctrls
Healthy ctrls

Figure 3-10. Accumulation of α-syn leads to its increased association with ER chaperones.

(A) The PLA background signal was determined by staining with a single primary antibody (α-syn (211), α-syn (C20), or CANX). α-Syn aggregate formation under high α-syn overexpression was used as a positive control, as indicated by a positive α-syn (211)-α-syn (C20) PLA signal. PLA signal was calculated as the number of red particles normalized to the number of nuclei within an acquired field of view (n=3-7). Scale bar, 25μm.

(B) H4 WT α-syn overexpressing cells were treated with 1μg/μl DOX for 3 days to turn off α-syn expression. Increased association of α-syn with CANX was determined by a proximity ligation assay (PLA). Cell nuclei are stained with DAPI. Right, PLA signal was calculated as the number of red particles normalized to the number of nuclei within an acquired field of view (n=5) and is shown as a fold change to the +DOX condition. Scale bar, 25μm.

(C) PLA analysis of Day 70 *SNCA*-3X and control DA neurons shows increased association of α-syn with CANX **(top)** and GRP94 **(bottom)**. Cell nuclei are stained with DAPI. Right, PLA signal was quantified as in A, and each data point on the scatter plot represents the PLA signal from an acquired field of view from n=3-4 biological replicates per line. Scale bar, 25μm.

For all quantifications, values are mean ± SEM, *$p < 0.05$; **$p < 0.01$; ****$p < 0.0001$, using student's unpaired t-test (panel B) or ANOVA with Tukey's post-hoc test (panel A, C).

DISCUSSION

Recent advances in genetics and pathology have highlighted perturbations in the proteostasis network that center on lysosomal degradation and trafficking pathways in both PD and DLB. Using novel PD models that naturally accumulate α-syn through endogenous mutations, we examined changes in the proteostasis pathway that occur during the initial stages of α-syn pathology when insoluble aggregates start to accumulate, but prior to neurotoxicity. Our studies indicated that a critical pathogenic cascade is triggered upon α-syn accumulation at the ER, leading to its fragmentation, compromised folding capacity, and GCase dysfunction (Figures 3-1, 3-2, 3-3). Other studies using transgenic overexpression models of α-syn have documented the association of α-syn with ER components (Colla *et al*., 2012a), and are consistent with our findings in PD patient neurons that naturally develop α-syn pathology. Although normally a

cytosolic protein enriched in synapses, pathogenic α-syn accumulates in both neurites and at the cell body in PD neurons (Figure 2-3). Our data indicates that the mislocalization of α-syn promotes its association and possible interaction with ER chaperones that are important for maintaining GCase folding (Figures 3-9, 3-10). Since α-syn translation does not occur on ER ribosomes, this aberrant association must occur downstream of its synthesis and accumulation. This association may overwhelm the proteostasis capacity of the ER, leading to ER dysfunction. In addition, α-syn can perturb protein trafficking at the Golgi, which likely slows the export of cargo from the ER, resulting in the accumulation of immature proteins. Overall, our data highlight the negative pleiotropic effects of α-syn on multiple branches of the proteostasis pathway.

A surprising consequence of α-syn-induced trafficking disruption was the aggregation of immature GCase into insoluble species. While several destabilizing point mutations of lysosomal hydrolases can cause multiple lysosomal storage diseases (LSDs) (Zunke and Mazzulli, 2019), we document a unique example where lysosomal dysfunction occurs through the misfolding and aggregation of wild-type immature GCase. Other lysosomal diseases that are caused by specific genetic mutations in trafficking machinery including I-Cell disease, or LIMP2 depletion that occurs in acute myoclonus renal failure (AMRF), do not show accumulation of immature hydrolases but instead are characterized by aberrant secretion into the media (Reczek et al., 2007; Wiesmann et al., 1971b). Therefore, the aggregation of immature hydrolases induced by α-syn appears to be unique to synucleinopathies. The lack of ERAD activity in *SNCA*-3X DA cultures (Figures 3-7, 3-8) likely contributes to the aberrant accumulation and destabilization of GCase in the ER. GCase may also be particularly susceptible to aggregation as a membrane-

associated enzyme, since aberrant exposure of hydrophobic patches during prolonged folding cycles in the ER may promote its self-association into insoluble aggregates. However, in addition to GCase, we also found the accumulation of immature, insoluble cathepsin D but not hexosaminidase B (Figure 3-2). This indicates that while not all hydrolases are susceptible to aggregation, the effect is not specific for GCase. One other study has shown that a rare point mutation in β-hexosaminidase that causes Tay-sachs disease results in the accumulation of an insoluble enzyme precursor, preventing its trafficking to the lysosome (Proia and Neufeld, 1982). It will be of interest in future studies to examine the factors that induce aggregation of GCase, cathepsin D, and other hydrolases in proteinopathies beyond PD and DLB.

Unexpectedly, we did not observe activation of the UPR (Figures 3-3, 3-4, 3-5, 3-6), which normally serves to circumvent the accumulation of proteins by expanding ER volume and upregulating folding machinery. Other synucleinopathy models generated by transgenic α-syn overexpression or patient-derived iPSC cortical models exhibited signs of UPR activation (Colla *et al*., 2012a; Heman-Ackah *et al*., 2017). It is possible that in other models, the cells were examined at a different pathological stage. This is an important consideration since it appears that in some studies, ER stress markers are elevated during the latest stages of the pathological cascade, indicated by elevated UPR markers in post-mortem brain (Credle *et al*., 2015; Heman-Ackah *et al*., 2017; Hoozemans *et al*., 2007). However, UPR activation does not appear to be selective for synucleinopathies, as many other neurodegenerative diseases exhibit similar features, suggesting the phenomenon may be a general characteristic for late-stage, age-related diseases (Wang and Kaufman, 2016). Our studies were purposely done at early stages of α-syn pathology, between day 60 and 90 in our midbrain models (Cuddy *et al*., 2019; Mazzulli *et al*., 2016), in order to capture phenotypic events that occur prior to lysosomal dysfunction and

neurodegeneration. Our findings suggest that α-syn perturbs proteostasis at the ER while simultaneously concealing the cell's ability to sense these perturbations. The finding of insoluble GCase aggregation in the ER, along with severe ER fragmentation, indicates that ER perturbations have reached a critical disease threshold. Under periods of ER stress, one of the goals of the UPR is to decrease the overall ER protein load by halting global protein synthesis. However, our recent work showed that GCase mRNA is actually elevated in PD midbrain neurons that accumulate α-syn, further suggesting communication problems between the ER and the nucleus (Cuddy *et al*., 2019). Despite the fact that UPR signaling did not appear to be initiated, we found that patient neurons were capable of responding to ER stress inducers such as Tg and BFA just as well as the controls (Figures 3-5, 3-6). This indicates that while ER perturbations are unrecognized in PD neurons, the UPR sensors remain functional and retain their ability to trigger signaling to the nucleus to stimulate chaperone expression and XBP1-S. The mechanisms for how α-syn masks ER dysfunction remain to be determined, but may involve aberrant interactions with proteins involved in the initial ER stress triggers including GRP78.

Recent work has shown that the UPR can be harnessed to provide protection in neurodegenerative diseases (Grandjean et al., 2020; Vidal et al., 2021). Since our data indicates that the UPR is still capable of activation, it is possible that enhancers of the UPR will provide benefit in synucleinopathies. Such strategies could restore ER proteostasis by stimulating XBP1-S-mediated ER compartment expansion and elevation of chaperones, providing a more conducive environment for GCase folding while preventing the growth of GCase aggregates. These methods would have to avoid maladaptive UPR signaling pathways that promote apoptosis from prolonged stimulation (Wang and Kaufman, 2016).

CHAPTER 4

Synergistic enhancement of ER chaperone function and protein trafficking rescues lysosomal function and reduces α-syn in *SNCA*-3X DA neurons.

Preface. The work presented in this chapter of the dissertation has been adapted largely from Stojkovska *et al*., 2021, an original research manuscript titled "Rescue of α-synuclein aggregation in Parkinson's patient neurons by synergistic enhancement of ER proteostasis and protein trafficking" that is currently under peer review.

OVERVIEW

The aberrant association of α-syn with ER chaperones and aggregation of immature GCase suggests that ER chaperone function may be overwhelmed in *SNCA*-3X patient neurons. Furthermore, previous studies have shown that accumulation of the GCase substrate, glucosylceramide (GluCer), which occurs in both *SNCA*-3X and A53T α-syn iPSC-midbrain cultures (Cuddy *et al*., 2019; Mazzulli *et al*., 2016), reduces ER calcium *in vitro* and *in vivo* (Korkotian et al., 1999; Liou et al., 2016; Pelled et al., 2005). This, in turn, compromises the function of calcium-dependent chaperones such as CANX. Disrupted calcium homeostasis has also been independently observed in several PD models (Apicco et al., 2021; Caraveo et al., 2014), and is consistent with fragmentation of the ER in *SNCA*-3X DA neurons (Figure 3-3) (Ha et al., 2020; Koch et al., 1988). Therefore, we next determined if enhancing ER chaperone function by increasing ER calcium can rescue wild-type GCase proteostasis and its downstream lysosomal activity.

METHODS AND MATERIALS

Treatment of H4 cells or iPSC neurons with small molecules

H4 cells or iPSC neurons were treated with vehicle or either 25μM diltiazem (DILT) (Sigma), 40μM dantrolene (DANT) (Sigma), or 1μM DHBP (Sigma), and media was changed every other day for the duration of the experiment. For the combination compound experiments, H4 cells or iPSC neurons were treated with vehicle, 25μM DILT, 5nM farnesyl transferase inhibitor (FTI) (Link Medicine), or DILT+FTI combination, and media was changed every other day for the duration of the experiment. For the combination of genetic manipulation and compound treatment (e.g., RyR3 KD + FTI, DILT + ykt6-CS), cells were infected and treatment was begun at the same time, with media change every other day for the duration of the experiment.

Sequential protein extraction and western blot analysis

Cells were harvested in 1X PBS and pelleted by centrifugation at 400xg for 5 minutes. To extract soluble protein, the cell pellets were homogenized in 1% Triton base lysis buffer (refer to Table S4 for recipe) containing PIC (Roche), PMSF (Sigma), Na_3VO_4 (Sigma) and NaF (Sigma) (refer to Table S4 for recipe). The Triton extracted lysates were freeze-thawed three times and ultracentrifuged at 100,000xg for 30 minutes at 4°C. To extract insoluble protein, the Triton-insoluble pellets were solubilized with 2% SDS base lysis buffer (refer to Table S4 for recipe) containing PIC via boiling for 10 minutes, followed by sonication and then ultracentrifugation at 100,000xg for 30 minutes at 22°C. The protein concentrations of the Triton and SDS fractions were measured via a BCA protein assay kit (Thermo Fisher Scientific) on a plate reader. Extracted protein lysates were boiled at 100°C for 10 min in Laemmli sample buffer (refer to Table S4), loaded on an SDS-PAGE gel, transferred onto a PVDF membrane (Millipore), and

post-fixed in 0.4% PFA (refer to Table S4 for recipe). Membranes were blocked in a 1:1 mixture of 1X TBS and Intercept blocking buffer (Li-Cor Biosciences), followed by overnight incubation with primary antibodies (refer to Table S2) diluted in a 1:1 mixture of 1X TBS-Tween and blocking buffer. The following day, secondary antibodies (refer to Table S2) were added for 1 hour, and the membranes were scanned using a Li-Cor Biosciences infrared imaging system. Quantification of band intensity was done using the ImageStudio software and analysis was performed on Excel and GraphPad Prism.

GCase maturation was measured by quantifying the ratio of post-ER (mature; >62 kDa) to ER (immature; 55-62 kDa) GCase. For quantifications of percent insoluble GCase: first, soluble (Triton fraction) and insoluble (SDS fraction) GCase levels were normalized to Coomassie gel staining. Then, insoluble GCase was divided by total GCase taken from both Triton and SDS fractions, and the result was shown as a percentage.

In vitro whole-cell lysate GCase activity assay

The procedure and analysis method for the activity assay has been previously described in detail (Mazzulli *et al*., 2011). Briefly, 1% BSA and 5µg Triton-soluble protein lysate treated with or without conduritol-β-epoxide (CBE, an inhibitor specific for lysosomal GCase) (Millipore) were added to GCase activity assay buffer containing sodium taurocholate in a 96-well black bottom plate. The samples were incubated with 5mM fluorescent GCase substrate 4-methylumbelliferyl β-glucopyranoside (4-MU-Gluc) (Chem-Impex) for 30 minutes at 37°C, and the reaction was stopped using equi-volume of 1M glycine, pH 12.5. The fluorescence signal was measured on a plate reader (Ex=365nm, Em=445). Relative fluorescence units from CBE treated lysates were subtracted from non-CBE treated lysates to obtain the activity of GCase.

Live-cell lysosomal GCase activity assay

The procedure and analysis method for the activity assay has been previously described in detail (Mazzulli *et al*., 2011; Mazzulli *et al*., 2016). Briefly, cells were plated in 96-well plates. One day prior to the assay, cells were treated with 1mg/ml cascade dextran blue (Life Technologies) for 24 hours. The next day, the cells were first treated with DMSO or 200nM bafilomycin A1 (BafA1) (Santa Cruz) for 1 hour at 37°C, followed by a 1-hour pulse-chase with 100μg/ml artificial fluorescent GCase substrate, 5-(pentafluoro-benzoylamino) fluorescein di-ß-D-glucopyranoside (PFB-FDGluc) (Life Technologies), at 37°C. The fluorescence signal was measured every 30 minutes for the span of 3-4 hours on a plate reader (Ex=485nm, Em=530nm, for the GCase substrates; Ex=400nm, Em=430nm for cascade dextran blue). For the analysis, the GCase fluorescence signal was normalized to either lysosomal mass by using cascade dextran blue signal or total cell volume by quantifying CellTag 700 staining signal.

Assessment of calnexin activity by Concanavalin-A pulldown

H4 WT α-syn overexpressing cells were treated with vehicle or 25μM Diltiazem (Sigma) for 4 days, harvested, and extracted in 0.3% CHAPS lysis buffer (refer to Table S4 for recipe details). For pulldown of total N-linked glycosylated proteins, 1500 μg lysate was mixed with 20 μg/ml biotinylated Concanavalin (Con-A) (Vector Laboratories) and the reaction mixture was incubated overnight at 4°C under gentle rotation. To recover Con-A bound proteins, 25 μL neutrAvidin agarose beads (Thermo Fisher Scientific) were added to the reaction mix and samples were incubated at 4°C for 1 hour. The beads were collected by centrifugation at 2500 x g for 2 min, followed by three washes with lysis buffer. N-glycosylated proteins were eluted by boiling the samples at 95°C for 10 min in 2X Laemmli sample buffer. Samples were analyzed by

western blot for calnexin (CANX), GCase, and total N-glycosylated proteins by Coomassie brilliant blue staining. Calnexin activity was indirectly assessed by quantifying CANX levels in Con-A pulled down samples.

Ryanodine receptor RyR3 knock-down using shRNA constructs

MISSION shRNA sequences targeting human RyR3 were obtained from Sigma and tested for efficiency in HEK293T cells by real-time qPCR analysis using RyR3 TaqMan probes. Clone ID #TRCN0000053349 was found to achieve the most efficient knock-down and was therefore used in subsequent experiments. This lentiviral plasmid was packaged into lentiviral particles and the virus was used to infect H4 cells or iPSC neurons.

Lentiviral preparation and transduction of H4 cells and iPSC neurons

Lentiviral plasmids containing 1) scrambled or RyR3 shRNA and 2) vector or ykt6-CS were packaged into lentiviral particles by transfecting HEK293FT cells with X-tremeGENE transfection reagent (Roche). The virus was collected and concentrated using Lenti-X concentrator (Clontech) and tittered with a HIV1-p24 antigen ELISA kit (Zeptometrix). H4 cells and iPSC neurons were infected at a multiplicity of infection (MOI) of 3 or 5 and were harvested after 5 days or 2 weeks following infection, respectively.

Statistical analysis

Analyzed data was plotted and tested for statistical significance using the GraphPad Prism software. Statistical significance between two samples was determined using a paired or unpaired t-test with Welch's correction. For more than two samples, significance was determined

using a one-way ANOVA with Tukey's post-hoc test. A p-value of <0.05 was considered to be significant (*p < 0.05, **p < 0.01, ***p < 0.001, ****p < 0.0001). For each quantification, the type of error bar used is specified in the figure legends.

RESULTS

Previous culture studies showed that elevating ER proteostasis by enhancing ER calcium levels can be achieved by blocking ryanodine receptors (RyRs) that mediate calcium efflux from the ER, thereby increasing CANX function (Mu et al., 2008; Ong et al., 2010) (Figure 4-1). We selected the RyR inhibitor diltiazem (DILT) (Figure 4-1) since it is non-toxic and is an FDA-approved drug for the treatment of high blood pressure and angina. DILT treatment is an established method to enhance CANX function and has been shown to improve the folding, trafficking, and function of mutant GCase in GD patient fibroblasts (Ong *et al*., 2010; Sun et al., 2009).

Initial dose response studies of DILT indicated that cultures could tolerate a maximum dose of 25μM without toxicity (not shown). To first validate that DILT could enhance chaperone function in our α-syn overexpression models, we assessed CANX functionality by measuring its binding activity to N-glycosylated proteins using the lectin concanavalin A (Con-A). Compared to vehicle treatment, CANX binding activity was significantly increased in DILT treated cells, as indicated by increased CANX and GCase pulldown with Con-A (Figure 4-2 A). To determine whether GCase folding can be enhanced by increasing chaperone function, we first assessed GCase maturation in H4 WT α-syn overexpressing cells treated with 25μM DILT. DILT treatment successfully decreased immature / ER forms of GCase and increased GCase maturation (Figure 4-2 B). DILT also elevated GCase protein levels and maturation in healthy

control DA neurons, indicating that enhancement of the folding pathway can be achieved in neurons without α-syn pathology or ER perturbations (Figure 4-2 C). In *SNCA*-3X patient DA neurons, DILT abrogated the build-up of insoluble GCase while concomitantly elevating soluble forms of the enzyme starting at 2 weeks and continuing to 8 weeks of treatment (Figure 4-2 D). Although DILT mainly increased immature forms of GCase, we observed a slight elevation in post-ER forms, indicating a mild improvement in maturation in *SNCA*-3X DA neurons (Figure 4-2 E)**.** GCase activity was elevated in whole-cell lysates that include both of its ER and post-ER forms, indicating that DILT enhanced properly folded, functional GCase (Figure 4-2 F, left). Despite this, the *in situ* assay that measures GCase activity within lysosomes of living neurons indicated no change in activity (Figure 4-2 F, right). Consistently, we found that α-syn levels were also not changed, indicating that DILT treatment alone could not sufficiently induce lysosomal α-syn degradation in neurons, even after a prolonged incubation of 8 weeks (Figure 4-2 G). Taken together, these results suggest that enhancing ER proteostasis with DILT can promote functional, soluble forms of GCase, but cannot improve lysosomal function in a sufficient manner to reduce α-syn.

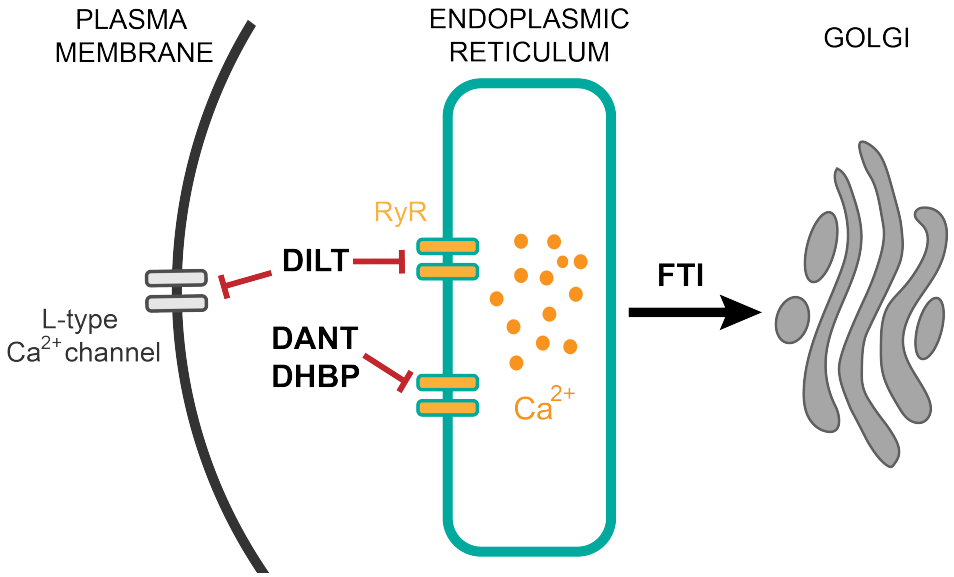

Figure 4-1. Targets of compounds used to enhance ER proteostasis and protein trafficking.

To pharmacologically enhance ER proteostasis, we used three individual small molecules, diltiazem (DILT), dantrolene (DANT), and DHBP, that bind to and inhibit ryanodine receptors (RyRs) located on the ER membrane. These compounds are known to increase ER calcium levels, thereby improving ER chaperone function and overall ER proteostasis. Although all three compounds are specific RyR inhibitors, DILT additionally inhibits L-type calcium channels on the plasma membrane, which are involved in regulating intracellular calcium levels via the mechanism of calcium-induced calcium release (CICR). To pharmacologically enhance ER-Golgi trafficking of proteins, we used the farnesyl transferase inhibitor (FTI) LNK-754, known to target and enhance the SNARE protein ykt6 and therefore enhance ER-Golgi vesicle fusion.

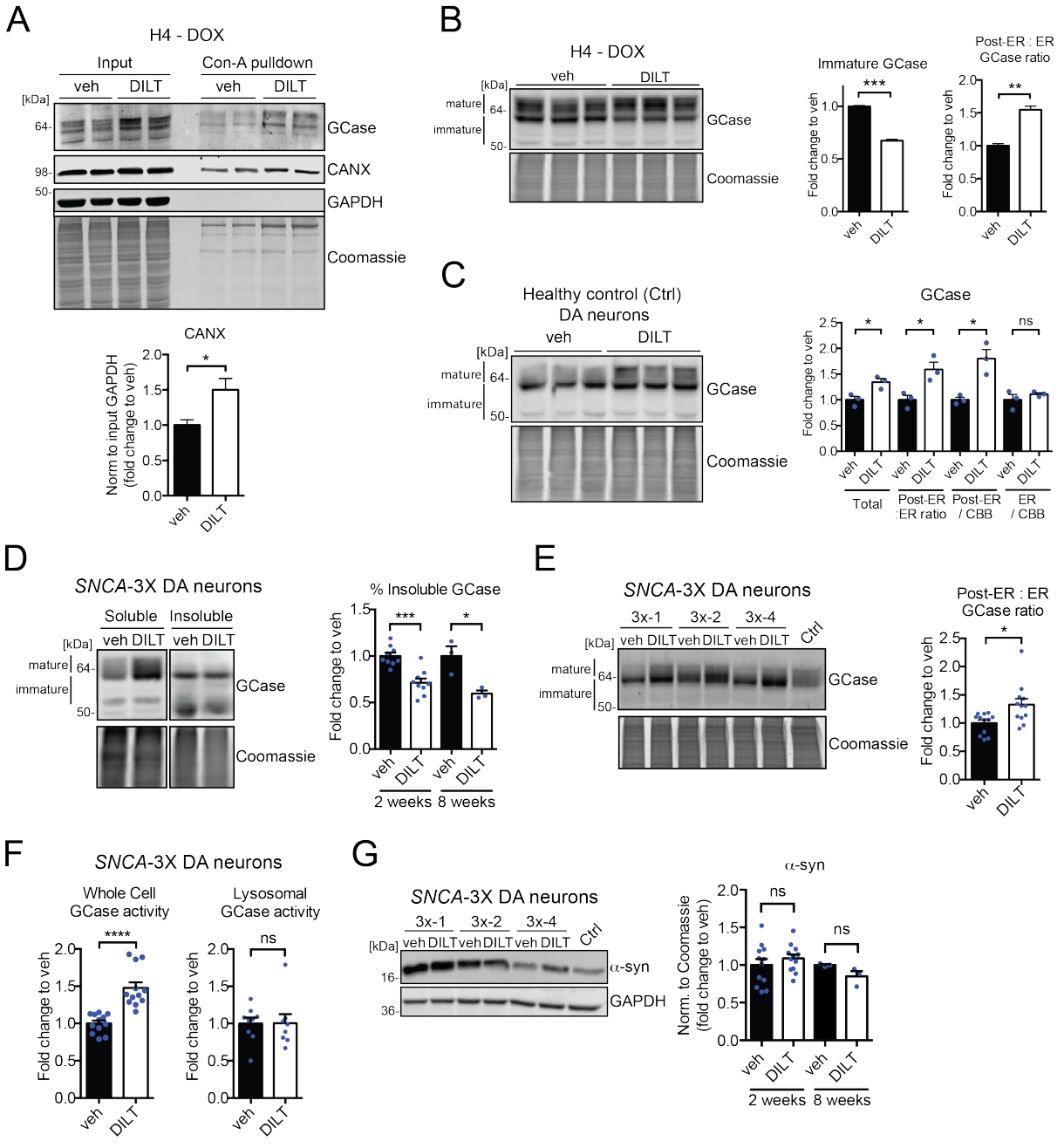

Figure 4-2. Enhancing ER chaperone function by chemically targeting RyRs with diltiazem improves GCase proteostasis.

To determine whether enhancing ER function can improve GCase proteostasis in H4 WT α-syn overexpressing cells and *SNCA*-3X DA neurons, cells were treated with vehicle (veh) or 25μM diltiazem (DILT), a ryanodine receptor inhibitor.

(A) H4 WT α-syn overexpressing cells were treated for 5 days with veh or DILT and N-glycosylated proteins were pulled down using concanavalin A (Con-A). Binding of CANX to Con-A was assessed by western blot and used as

a measure of CANX function. GCase and GAPDH serve as positive and negative controls for the pulldown, respectively. Bottom, quantification of CANX levels in the Con-A pulldown in DILT treated cells, normalized to GAPDH from the input (n=3-4).

(B) Western blot analysis and quantification of immature GCase (normalized to Coomassie) and GCase maturation in DILT treated H4 WT α-syn overexpressing cells (n=3).

(C) Day 120 healthy control (Ctrl) DA neurons were treated with 25μM DILT for 2 weeks and GCase was analyzed by western blot. Right, quantifications of total GCase, post-ER, and ER forms of GCase were normalized to Coomassie (n=3). The post-ER to ER GCase ratio (maturation) is also shown (n=3).

(D) *SNCA*-3X DA neurons were treated for 2 or 8 weeks, sequentially extracted, and analyzed for levels of soluble and insoluble GCase. Western blot of day 90 3x-1 DA neurons treated for 8 weeks is shown as a representation. Right, percentage of insoluble GCase was quantified for the 2-week (combined from day 90 3x-1 (n=6) and 3x-2 (n=3) neurons) and 8-week (day 120 3x-1 neurons only (n=3)) treatment length.

(E) GCase maturation of day 90 *SNCA*-3X DA neurons treated with DILT for 2 weeks was analyzed by western blot. Coomassie is shown as a loading control. Right, quantification of GCase maturation is combined from lines 3x-1 (clones C2 and C3), 3x-2, and 3x-4 (n=3 per line).

(F) Left, whole-cell GCase activity of *SNCA*-3X lysates from panel E. Right, live-cell lysosomal GCase activity in day 90 *SNCA*-3X DA neurons treated with DILT for 2 weeks. **(G)** Western blot analysis was used to determine whether enhancing GCase proteostasis by improving ER function influences α-syn levels. The blot from panel E was reprobed for α-syn and is shown. GAPDH is shown as a loading control. Right, quantification of α-syn levels normalized to Coomassie at 2 and 8 weeks of DILT treatment. For the 2-week treatment, data is combined from lines 3x-1 (clones C2 and C3), 3x-2, and 3x-4 (n=3 per line); 8-week treatment is of day 120 3x-1 neurons only (n=3).

For all quantifications, values are mean ± SEM, *p < 0.05; **p<0.01; ***p < 0.001; ****p < 0.0001; ns = not significant, using student's unpaired t-test.

To confirm that enhancing ER proteostasis and wild-type GCase levels can be improved by RyR inhibition, we treated H4 WT α-syn overexpressing cell lines and *SNCA*-3X DA neurons with two additional distinct and specific RyR inhibitors, dantrolene (DANT) and 1,1′-diheptyl-4,4′-bipyridinium (DHBP) (Fruen et al., 1997; Kang et al., 1994) (Figure 4-1). DANT and DHBP treatment elevated GCase maturation and solubility levels, although not as robustly as DILT (Figure 4-3). When higher concentrations or longer incubation periods were attempted, we

observed cell toxicity, consistent with previous findings (Ong *et al*., 2010; Wang et al., 2011). Finally, we directly tested the effect of RyR inhibition on GCase solubility by knocking down RyR with shRNA constructs. We specifically knocked down RyR3 since RyR3 is expressed widely throughout the brain (Giannini et al., 1995) and previous studies indicated that RyR3 depletion could rescue the severe mutant (L444P) form of GCase in patient cells (Ong *et al*., 2010). Real-time qPCR analysis indicated approximately 40-60% knock-down (KD) of RyR3 in cell lines and patient neurons (Figure 4-4 A, C), resulting in increased solubility of GCase in both cell lines and patient neurons (Figure 4-4 B, D). The rescue effect of RyR3 KD was identical to that of DILT treatment (Figure 4-4 B), suggesting that the solubilizing activity of DILT can be attributed to inhibition of RyR3 rather than off-target effects. Further, DILT had no effect on GCase solubility in RyR3 KD cells (Figure 4-4 B), once again indicating that DILT acts through RyR3 receptors on the ER. Analysis of GCase maturation in RyR3 KD cells showed a mild improvement in cell lines that was similar to DILT treatment (Figure 4-4 B), and no change in *SNCA*-3X DA neurons (Figure 4-4 D). DILT caused a mild elevation of GCase maturation in RyR3 KD cell lines, a result that likely occurred from the inhibition of other RyR isoforms (Figure 4-4 B). Together, these data show that RyR inhibition with three distinct compounds and shRNA can improve GCase proteostasis in the ER, but has little effect on increasing GCase trafficking in cells that accumulate α-syn.

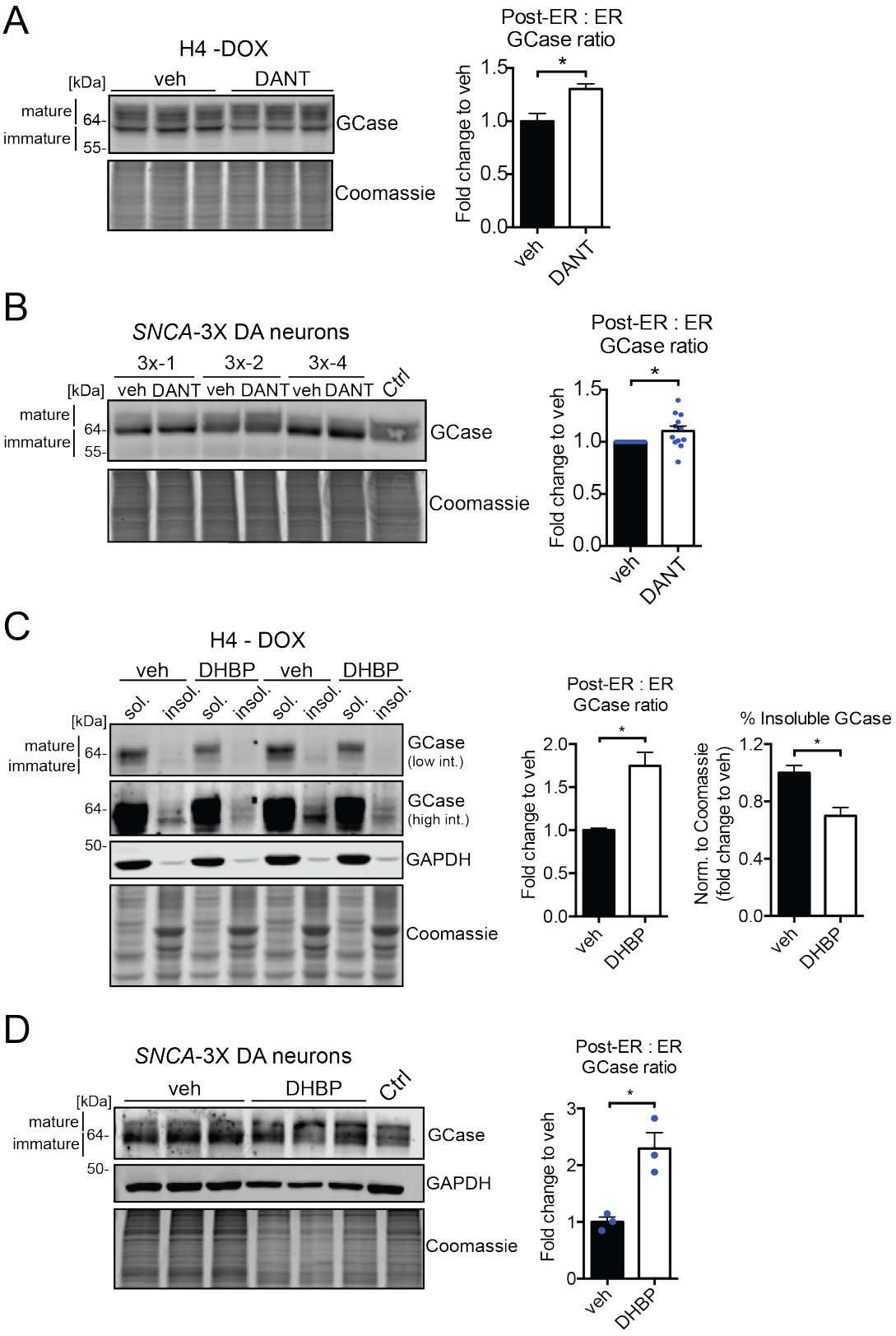
A
H4 -DOX
[kDa]
veh
DANT
mature
immature
64-
55-
GCase
Coomassie
Post-ER : ER
GCase ratio
Fold change to veh
1.5
1.0
0.5
0.0
*
veh
DANT
B
SNCA-3X DA neurons
3x-1
3x-2
3x-4
[kDa]
veh DANT veh DANT veh DANT Ctrl
mature
immature
64-
55-
GCase
Coomassie
Post-ER : ER
GCase ratio
Fold change to veh
1.5
1.0
0.5
0.0
*
veh
DANT
C
H4 - DOX
veh
DHBP
veh
DHBP
sol.
insol.
sol.
insol.
sol.
insol.
sol.
insol.
[kDa]
mature
immature
64-
GCase
(low int.)
64-
GCase
(high int.)
50-
GAPDH
Coomassie
Post-ER : ER
GCase ratio
Fold change to veh
2.0
1.5
1.0
0.5
0.0
*
veh
DHBP
% Insoluble GCase
Norm. to Coomassie
(fold change to veh)
1.2
0.8
0.4
0.0
*
veh
DHBP
D
SNCA-3X DA neurons
veh
DHBP
Ctrl
[kDa]
mature
immature
64-
50-
GCase
GAPDH
Coomassie
Post-ER : ER
GCase ratio
Fold change to veh
3
2
1
0
*
veh
DHBP

Figure 4-3. Enhancing ER chaperone function by chemically targeting RyRs with dantrolene or DHBP improves GCase proteostasis.

To further validate that enhancing ER function can improve GCase proteostasis in H4 WT α-syn overexpressing cells and *SNCA*-3X DA neurons, cells were treated with vehicle and 40μM dantrolene (DANT) or 1μM 1,1'-diheptyl-4,4'-bipyridinium dibromide (DHBP), two additional ryanodine receptor inhibitors.

(A, C) H4 cells were treated for 5 days with DANT or DHBP and GCase maturation / solubility was determined by western blot. GAPDH and Coomassie gel staining are shown as extraction and loading controls, respectively. Quantifications of GCase maturation and / or solubility with the treatment are shown on the right (n=3).

(B, D) GCase maturation of day 90 *SNCA*-3X DA neurons treated with DANT or DHBP for 2 weeks was analyzed by western blot. GAPDH and Coomassie gel staining are shown as extraction and loading controls, respectively. Quantifications of GCase maturation with the treatment are shown on the right. Data from panel B is from 3x-2 (n=3). Data from panel D is combined from lines 3x-1 (clones C2 and C3), 3x-2, and 3x-4 (n=3 per line).

For all quantifications, values are mean ± SEM, $*p < 0.05$, using student's unpaired t-test.

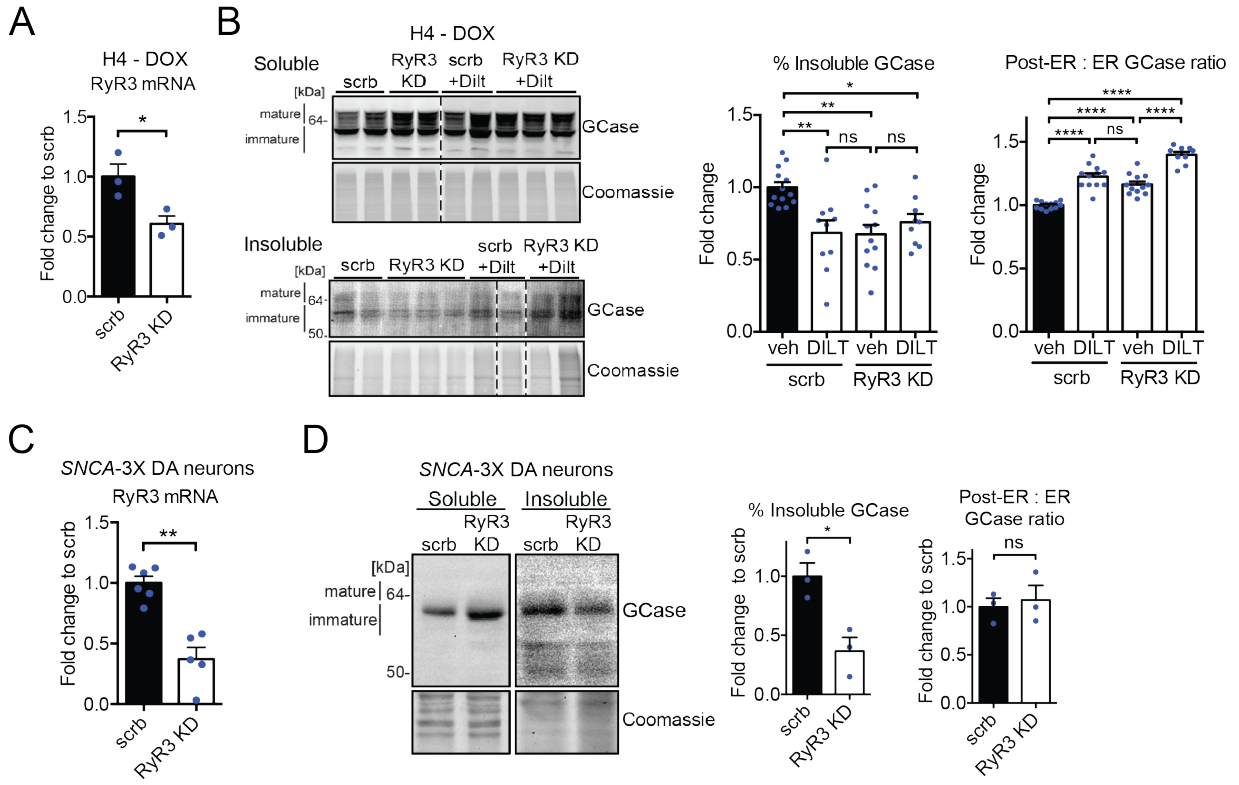

Figure 4-4. Enhancing ER chaperone function by genetically targeting RyRs improves GCase proteostasis.

To genetically validate that RyR inhibition is sufficient in improving GCase proteostasis, H4 WT α-syn overexpressing cells and *SNCA*-3X DA neurons were lentivirally infected with scrambled (scrb) or RyR3 shRNA for 5 days or 2 weeks, respectively.

(A) RyR3 knock-down (KD) efficiency in H4 cells was measured by real-time qPCR analysis of RyR3 mRNA (n=3).

(B) Western blot analysis of soluble (top blot) and insoluble (bottom blot) GCase after RyR3 KD (MOI = 5) in H4 cells. Addition of DILT following scrb or RyR3 KD was used to determine the specificity of the compound. Coomassie is shown as a loading control. Irrelevant lanes were cropped out from the blots and are indicated with a dashed line. Right, quantifications of percent insoluble GCase normalized to Coomassie and GCase maturation in H4 cells after DILT treatment in scrb or RyR3 KD cells (n=9-13).

(C) RyR3 KD efficiency in DA neurons was measured by real-time qPCR analysis of RyR3 mRNA (n=5-6; combined from two individual experiments).

(D) Scrb or RyR3 KD (MOI = 3) *SNCA*-3X DA neurons were sequentially extracted and analyzed for soluble and insoluble GCase. Western blot of day 90 3x-1 neurons is shown as a representation. Right, percentage of insoluble GCase and GCase maturation in RyR3 KD neurons (n=3).

For all quantifications, values are mean ± SEM, *p < 0.05; **p < 0.01; ****p < 0.0001; ns = not significant, using student's unpaired t-test (panels A, C, D) or ANOVA with Tukey's post-hoc test (panel B).

The failure to rescue lysosomal GCase activity by RyR inhibition, despite the elevation of properly folded, soluble ER GCase, suggests that factors downstream of the ER may inhibit hydrolase trafficking. Our previous work showed that α-syn inhibits GCase trafficking by preventing ER-Golgi vesicle fusion through impeding the function of the SNARE protein ykt6 (Cuddy *et al*., 2019). Further, farnesyltransferase inhibitors (FTIs) can restore ykt6 activity, thereby improving GCase trafficking and lysosomal activity in PD neurons (Cuddy *et al*., 2019). Therefore, we next determined whether enhancing ER-to-Golgi vesicle fusion, together with ER proteostasis, could cooperate to rescue GCase activity and reduce pathological α-syn levels. We found that treatment with FTI (LNK-754) and DILT resulted in a significant increase of GCase maturation compared to each compound alone in both H4 WT α-syn overexpressing cells and *SNCA*-3X DA neurons (Figure 4-5 A; Figure 4-6 A). This effect was not additive but synergistic, since the percent increase caused by FTI + DILT was greater than the sum of the enhancement by each individual compound alone (Figure 4-6 B). This is consistent with fact that each compound targets a distinct portion of the proteostasis pathway. To determine if improved folding and trafficking of GCase out of the ER could restore ER morphology, we measured ER profile lengths and ER area using EM in treated patient DA neurons. We found that FTI + DILT treatment substantially increased both ER length and area, consistent with increased GCase solubility and function (Figure 4-6 C). FTI + DILT treatment also elevated functional, soluble forms of GCase in both whole-cell lysates and live-cell *in situ* lysosomal assays (Figure 4-5 B; Figure 4-6 D). Importantly, the GCase activity enhancement was sufficient to synergistically reduce both soluble and insoluble α-syn in both H4 WT α-syn overexpressing cells and *SNCA*-3X DA neurons (Figure 4-5 C; Figure 4-6 E-G). Finally, we confirmed these results by genetic manipulations, by either combining RyR3 KD with FTI, or DILT with expression of ykt6-CS

that cannot be farnesylated (Cuddy *et al*., 2019). These combinations could effectively enhance GCase trafficking and reduce α-syn better than either treatment alone (Figure 4-8) in both cell lines and patient neurons. Our data suggests that simultaneous enhancement of two critical proteostasis branches, ER proteostasis and downstream trafficking pathways, provides a more effective rescue of GCase function compared to either treatment alone, resulting in a reduction of pathological α-syn in patient neurons.

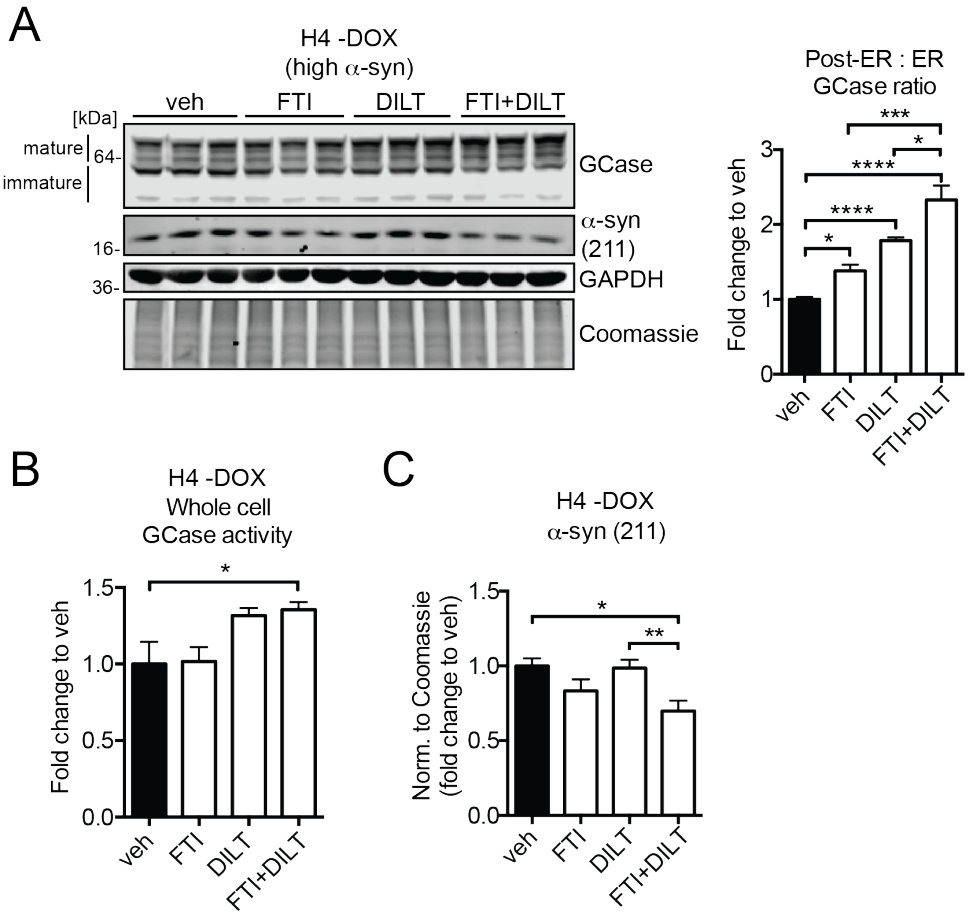

Figure 4-5. Combining ER proteostasis and trafficking enhancers synergistically improves GCase function and reduces α-syn in H4 WT α-syn overexpressing cells.

To synergistically enhance ER proteostasis and ER-Golgi protein trafficking, H4 WT α-syn overexpressing cells were treated for 5 days with vehicle, 5nM farnesyl transferase inhibitor (FTI), 25μM DILT, or an FTI+DILT

combination.

(A) H4 cells were analyzed for GCase maturation and α-syn levels via western blot. GAPDH and Coomassie are shown as loading controls. Right, quantification of GCase maturation (n=3 per condition, combined from 3 individual experiments for n=9 total).

(B) Whole-cell GCase activity in treated H4 cells (n=5 per condition).

(C) Analysis of α-syn (antibody 211) levels normalized to Coomassie from the blot in panel A.

For all quantifications, values are mean ± SEM, *p < 0.05; **p < 0.01; ***p < 0.001; ****p < 0.0001, using ANOVA with Tukey's post-hoc test.

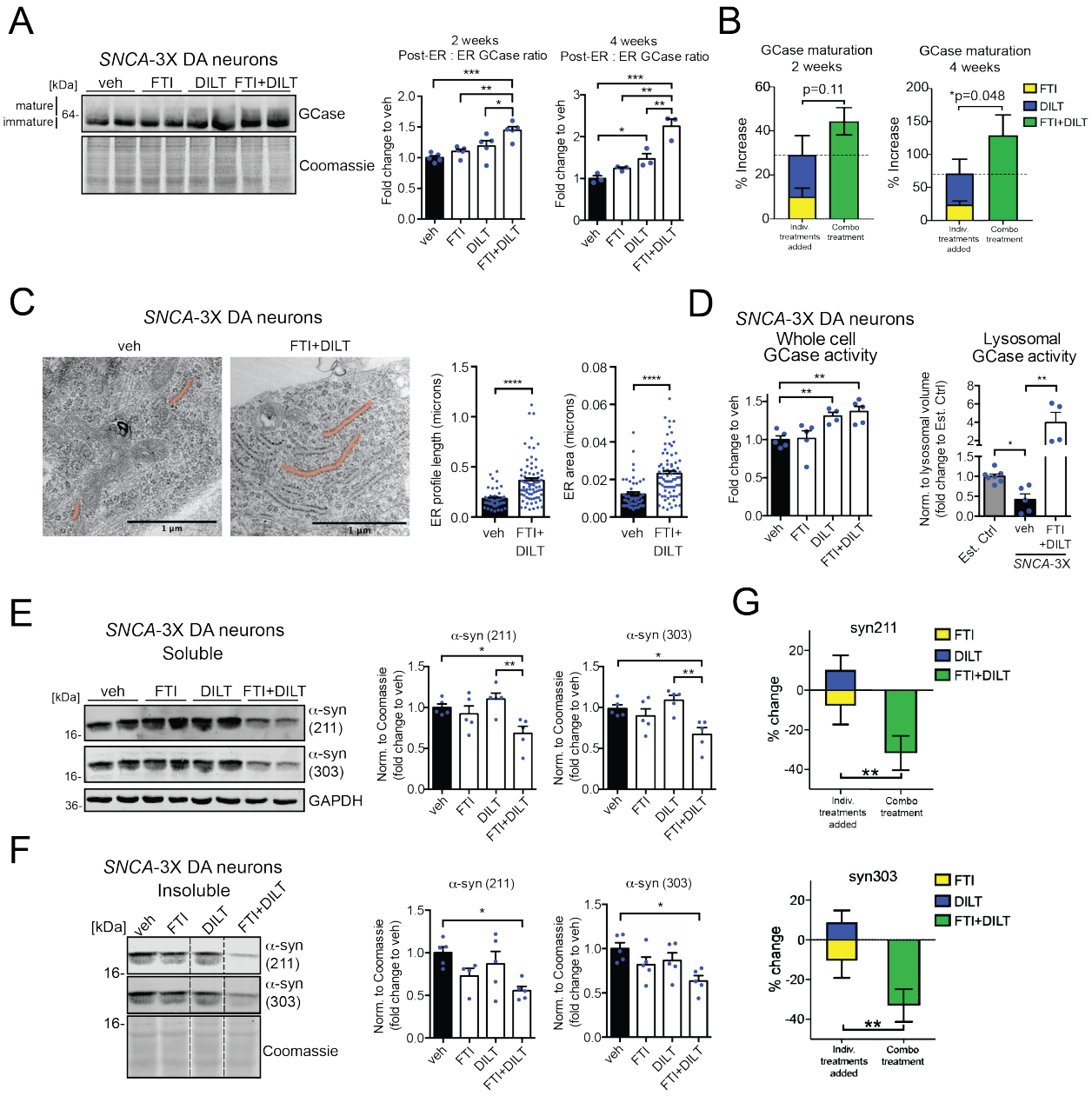

Figure 4-6. Synergistic enhancement of lysosomal GCase by simultaneous improvement of ER proteostasis and trafficking restores ER morphology and reduces α-syn in *SNCA*-3X DA neurons.

To synergistically enhance ER proteostasis and ER-Golgi protein trafficking, *SNCA*-3X DA neurons were treated with vehicle, 5nM FTI, 25μM DILT, or an FTI+DILT combination.

(A) GCase maturation of day 90 3x-1 DA neurons treated with FTI+DILT for 2 weeks was analyzed by western blot. Coomassie is shown as a loading control. Right, quantification of GCase maturation for the 2-week treatment is combined from day 90 3x-1 (n=2) and 3x-2 (n=3) neurons; quantification for the 4-week treatment is from day 120 3x-1 neurons only (n=3).

(B) Analysis of the effect on GCase maturation due to each individual compound and the combination treatment.

(C) Day 90 3x-2 DA neurons were treated with FTI+DILT for 2 weeks and ER morphology was assessed by TEM imaging. Examples of ER segments are highlighted in red. Scale bar, 1μm. Right, quantification of the length and area of each clearly identifiable ER segment (n=3 cells for vehicle condition, n=9 cells for FTI+DILT condition; each data point on the scatter plot indicates a measured ER segment).

(D) Left, whole-cell GCase activity of treated 3x-1 and 3x-2 lysates from panel A (n=5). Right, live-cell lysosomal GCase activity of veh or FTI+DILT treated 3x-2 DA neurons (n=4-5). GCase activity in healthy control neurons (Est. Ctrl) is shown as a comparison (n=7).

(E) The blot from panel A was sequentially probed with 211 and 303 anti-α-syn antibodies. GAPDH is shown as a loading control. Right, quantification of total and pathological α-syn levels normalized to Coomassie in day 90 3x-1 (n=2) and 3x-2 (n=3) neurons treated with FTI+DILT for 2 weeks.

(F) Day 90, 3x-2 DA neurons treated with FTI+DILT for 2 weeks were sequentially extracted, and the Triton X-100-insoluble fractions were analyzed by western blot for α-syn. Membranes were sequentially probed with syn211 and syn303 anti-α-syn antibodies. Irrelevant lanes were cropped out from the blot and are indicated with a dashed line. Right, quantification of total and pathological α-syn levels normalized to Coomassie.

(G) The effect of each individual compound and the combination treatment on α-syn levels (antibodies 211 and 303) in *SNCA*-3X DA neurons was analyzed as in panel B.

For all quantifications, values are mean ± SEM, *$p < 0.05$; **$p < 0.01$; ***$p < 0.001$; ****$p < 0.0001$, using student's unpaired t-test (panels B, C, D, G) and ANOVA with Tukey's post-hoc test (panels A, D, E, F).

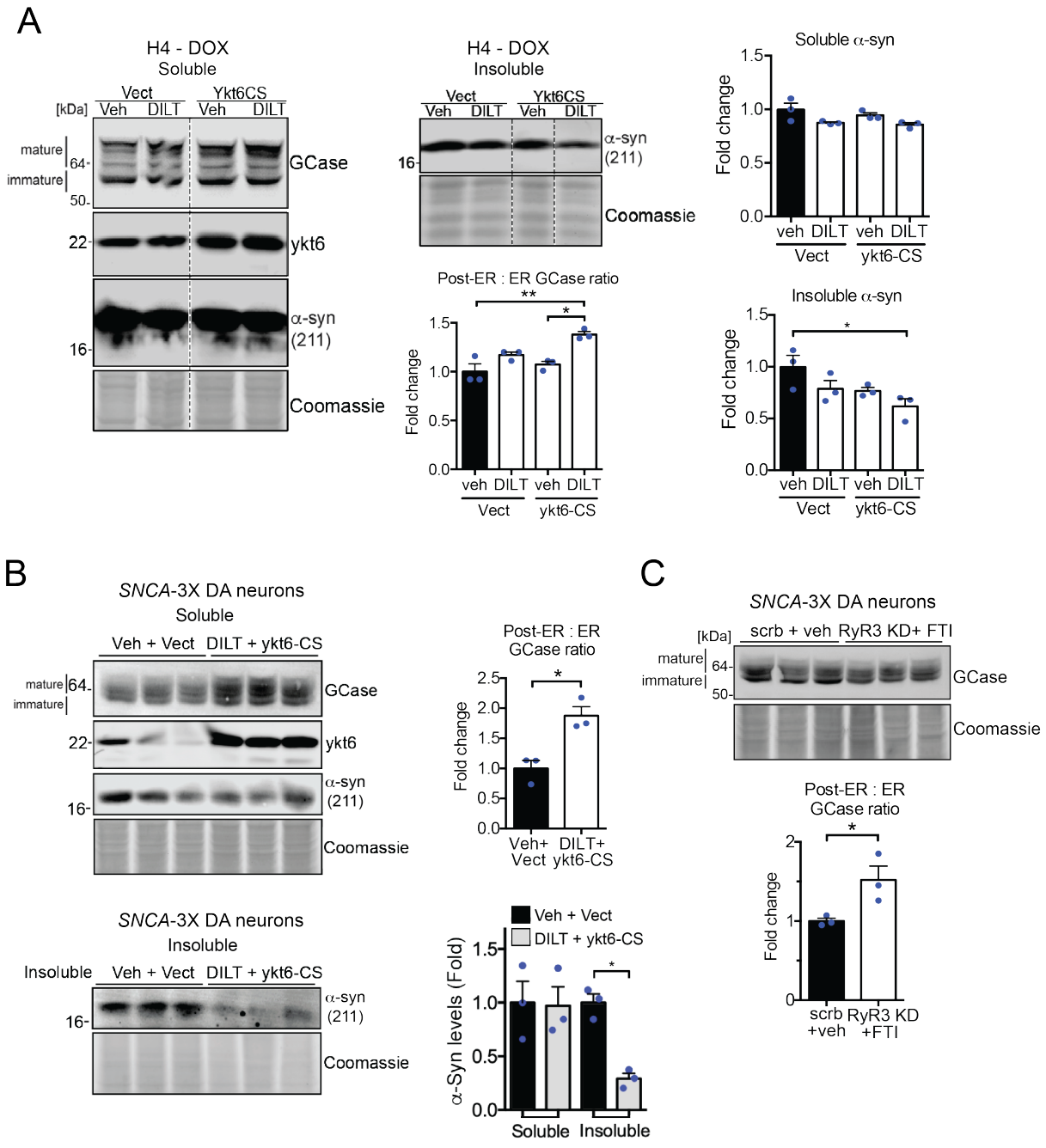

Figure 4-7. Combined enhancement of ER proteostasis with trafficking by genetic manipulations improves GCase proteostasis and reduces α-syn.

(A) H4 WT α-syn overexpressing cells were lentivirally infected with vector (vect) or ykt6-CS and treated with DILT in combination (MOI = 3, 5-day treatment). Sequential extraction and western blot analysis of GCase and soluble and insoluble α-syn was performed. Blotting for ykt6 was done to confirm successful overexpression. Coomassie is shown as a loading control. Analysis of GCase maturation and soluble and insoluble α-syn levels are shown (n=3).

(B) Western blot analysis of GCase and soluble and insoluble α-syn in 3x-1 DA neurons overexpressing ykt6-CS in combination with DILT treatment (MOI = 3, 2-week treatment). Blotting for ykt6 was done to confirm successful overexpression. Coomassie is shown as a loading control. Right, quantifications of GCase maturation and soluble and insoluble α-syn levels.

(C) GCase maturation in RyR3 KD 3x-1 DA neurons in combination with 5nM FTI treatment was analyzed by western blot (MOI=3, 2-week treatment). Coomassie is shown as a loading control. Bottom, quantification of GCase maturation (n=3).

For all quantifications, values are mean ± SEM, *$p < 0.05$; **$p<0.01$, using student's unpaired t-test (panels B, C) or ANOVA with Tukey's post-hoc test (panel A).

DISCUSSION

The unique finding that insoluble GCase accumulates in PD patient neurons prompted us to examine the effect enhancing its solubility on lysosomal function. Our data indicates that enhancing ER proteostasis with diltiazem (DILT), dantrolene (DANT), or DHBP, three established methods of enhancing ER folding capacity (Ong *et al*., 2010), can promote GCase folding and solubility (Figures 4-2, 4-3). However, the downstream therapeutic effects of enhancing this pathway alone were marginal. We observed only mild elevations in GCase maturation, and no change in lysosomal activity or α-syn levels in patient neurons. This marginal rescue was due to the previously established effects of α-syn inhibiting protein trafficking downstream of the ER (Cooper *et al*., 2006; Cuddy *et al*., 2019; Gitler *et al*., 2008). Our previous work showed that enhancement of protein trafficking can be achieved with a clinically-validated FTI that activates lysosomes by enhancing the ER-Golgi SNARE protein ykt6 (Cuddy *et al*., 2019). Interestingly, FTIs have been shown to activate lysosomes and reduce pathology in other neurodegenerative disease models characterized by tau accumulation (Hernandez et al., 2019). We show that enhancing ER proteostasis and simultaneously targeting downstream trafficking pathways can effectively improve GCase maturation and reduce pathological α-syn (Figures 4-5,

4-6, 4-7). Enhancement of the lysosomal pathway, and proteostasis in general, holds promise as a disease-modifying therapeutic strategy for synucleinopathies as well as other protein aggregation diseases. Our study provides a novel method for simultaneously targeting multiple branches of the proteostasis pathway, including folding, trafficking and degradation, to restore balance in PD patient neurons. Therapeutic enhancement of multiple proteostasis pathways may provide optimal benefit in PD, given the pleiotropic deleterious effects of α-syn accumulation in multiple subcellular locations. Furthermore, combining two distinct treatments that target distinct cellular pathways may enable administration of lower doses of each drug, which would limit compound toxicity if these treatments should progress to the clinic.

CHAPTER 5

Summary and Discussion

5.1 Importance of understanding the molecular etiology of Parkinson's disease

Parkinson's disease (PD) was first medically described in 1817 by James Parkinson, who noted many of the symptoms that are used to clinically diagnose patients today: resting tremor, shuffling gait, muscular rigidity, and a propensity to bend the trunk forward (Parkinson, 2002). Early treatments for PD were based on empirical observations, with anticholinergic drugs being used as early as the nineteenth century. Since the discovery of dopaminergic deficits in PD, treatment options changed to dopamine replacement therapy. The development of levodopa (L-DOPA) in the late 1960s represents one of the biggest breakthroughs in the medical field. This drug, which is capable of crossing the blood-brain-barrier, is broken down into dopamine in the brain and is primarily used to alleviate some of the symptoms of PD. As of today, no treatment exists against PD development or progression. Additionally, diagnosis of PD tends to occur once symptoms have already appeared, by which point it is estimated that 70-80% of the dopaminergic neurons in the brain have been lost (El-Agnaf et al., 2006). Currently, no definitive diagnostic test exists for PD and significant efforts have been made to find reliable molecular biomarkers. Therefore, understanding the mechanisms that lead to the development and progression of this debilitating disease are crucial for the development of potential biomarkers and therapies that are capable of treating not only the symptoms but also to stop or possibly reverse the disease.

Current experimental models for PD are predominantly genetic or neurotoxin-based, and many human cell lines and animal models involve artificial genetic manipulation strategies

which do not fully represent human pathology. Furthermore, perhaps one of the largest caveats of studying a neurodegenerative disease is the time factor. PD is a progressive condition and is considered to be a disease of the aging. Therefore, no current model can fully and accurately recapitulate what happens in the aging human nervous system during PD. The development of stem cell technology and human induced pluripotent stem cells (iPSCs) has permitted the generation of neuronal cells from individual patients, allowing the study of disease-specific phenotypes and cellular vulnerabilities that underlie disease. Furthermore, since the majority of PD cases are sporadic in nature, iPSC technology offers the opportunity to study such cases, which is crucial for the understanding of cellular pathogenic phenotypes that are relevant to the majority of PD patients. However, as with any model that exists in a dish, a major disadvantage of using iPSC models is that they cannot fully recapitulate the complex interactions that occur between different cell types during neurodegeneration.

In this dissertation, we utilized PD patient-derived iPSC midbrain dopaminergic neuron models to gain mechanistic insights into the development of PD. Since α-syn plays a large role in the pathogenesis of PD, we chose to utilize samples from PD patients that harbor a genetic triplication (3X) in the *SNCA* genomic region. The *SNCA*-3X leads to natural overexpression of the wild-type α-syn protein. However, the molecular mechanisms by which the overabundance of the wild-type protein leads to a pathological condition are not fully understood.

5.2 Connecting α-syn pathology to lysosomal dysfunction

The regulation of protein expression, folding, transport, and clearance, also known as proteostasis, is critical for proper cellular function and health. Disruption of any of these steps, which may occur due to genetic factors or the natural aging process, poses a challenge for the

cell machinery responsible for maintaining proteostasis. Therefore, gaining a mechanistic understanding in how proteostasis is mismanaged due to the overabundance of a critical protein can open new avenues for therapeutic targets that may be beneficial for PD and other neurodegenerative diseases characterized by protein accumulation and aggregation.

A53T and other familial-linked *SNCA* point mutations that result in the accelerated oligomerization or fibrillization of α-syn (Conway *et al*., 1998; Ghosh *et al*., 2013; Greenbaum *et al*., 2005; Rutherford *et al*., 2014) are well known to lead to familial Parkinson's disease (PD) (Polymeropoulos *et al*., 1997). However, the discovery of familial PD patients with duplications (2X) or triplications (3X) in *SNCA* strengthens the detrimental role that wild-type α-syn plays in disease pathogenesis. The finding that wild-type α-syn overexpression in *SNCA*-2X / 3X leads to the accumulation of the protein into insoluble Lewy inclusions suggests that the balance between synthesis and degradation of α-syn is disrupted in the PD brain. The molecular mechanism by which this proteostasis dysfunction occurs remains unsolved in the PD field.

There is converging evidence that the autophagy-lysosomal pathway plays an important role in the clearance of both physiological and pathological forms of α-syn (Cuervo *et al*., 2004; Lee *et al*., 2004; Vogiatzi *et al*., 2008), suggesting that there is a close relationship between lysosomal dysfunction and α-syn-induced toxicity. Perhaps the most critical evidence for lysosomal dysfunction in PD came from the discovery that loss-of-function mutations in *GBA1*, a gene that encodes the lysosomal hydrolase β-glucocerebrosidase (GCase), represent the greatest genetic risk factor for the development of PD. Although the loss of GCase function plays an important role in Gaucher's disease (GD) and *GBA1*-PD, studies have shown that sporadic PD brains exhibit a decline in wild-type GCase activity that is associated with aging (Gegg *et al*.,

2012; Murphy *et al*., 2014; Rocha *et al*., 2015), suggesting a broader role for GCase dysfunction in PD.

In this study, we generated novel iPSC-derived midbrain DA neuron models (Figure 2-2) from PD patients that harbor wild-type *SNCA* triplications. To allow for the α-syn phenotype to develop, we aged these neurons in culture for 60-90 days. Several major advantages of this type of model are that it is human patient-derived, it utilizes the cells that are vulnerable and specific to disease pathology, and that it involves the natural development of α-syn pathology without artificial genetic or chemical manipulation as traditionally used in mouse models of PD. Although iPSC-derived DA neurons are a beneficial tool to study the initial stages of α-syn aggregate formation prior to cell death, it is important to recognize that the several months of aging of these neurons is not equivalent to the decades long aging of the human PD brain.

The combination of genetic susceptibility and aging *in vitro* allows the opportunity for disease-specific phenotypes to emerge. Here, we show that aged *SNCA*-3X DA neurons accumulate α-syn and form insoluble α-syn aggregates within the cell body as well as neurites (Figure 2-3). Additionally, *SNCA*-3X DA neurons, which harbor wild-type GCase, exhibit an age-dependent decline in lysosomal GCase function (Figure 2-4). Taken together, these findings indicate that our models recapitulate several important features of the PD brain. In agreement with numerous previous findings (Cooper *et al.*, 2006; Gitler *et al.*, 2008; Gosavi *et al.*, 2002; Mazzulli *et al.*, 2011; Mazzulli *et al.*, 2016; Thayanidhi *et al.*, 2010), we found that loss of lysosomal GCase function occurs through α-syn impeding the maturation of GCase through the ER-Golgi portion of the secretory pathway, thereby redistributing GCase away from lysosomal compartments (Figure 2-4). To determine the specificity of α-syn to lysosomal dysfunction, we

generated and characterized novel isogenic control *SNCA*-3X iPSC-derived DA neurons that were depleted of α-syn (Figure 2-5) and found that the specific reduction in α-syn is sufficient to improve the maturation and lysosomal activity of GCase (Figure 2-6). Collectively, these findings offer further insights into the mechanistic link between α-syn accumulation and the functional loss of wild-type GCase.

Recent evidence suggests that a reduction in GCase activity accelerates the progression and symptoms of PD (Suzuki et al., 2015). However, aging is still considered to be the most critical risk factor for synucleinopathies. In addition to this, the finding that GCase activity gradually declines with aging in healthy subject control brains strongly suggests that progressive lysosomal dysfunction occurs with the natural aging process (Rocha *et al*., 2015). Therefore, it would be important for future studies to further investigate how subtle and chronic perturbations in the proteostasis machinery can generate cellular pathology in the context of both healthy and synucleinopathy brains.

5.3 Identification of an unexpected ER proteostasis phenotype due to wild-type α-syn pathology

It is well established that in GD, both N370S and L444P mutant forms of GCase get retained in the ER and activate the UPR and ERAD (Bendikov-Bar et al., 2011; Maor et al., 2013; Ron and Horowitz, 2005). Interestingly, GD severity has been correlated with the levels of misfolded GCase in the ER (Ron and Horowitz, 2005). Previous studies have also shown that the accumulation of GCase's substrate GluCer can cause ER dilation (Farfel-Becker et al., 2014; Korkotian *et al*., 1999), a well-characterized morphological alteration due to ER dysfunction. In addition, GluCer accumulation is thought to cause the loss of calcium from ER stores, possibly

contributing to ER proteostasis dysfunction (Korkotian and Segal, 1999; Lloyd-Evans et al., 2003; Pelled *et al*., 2005). Here, we show that in contrast to the ER morphological changes seen with mutant GCase, PD patient midbrain neurons that harbor wild-type GCase and accumulate the hydrolase in the ER exhibit shorter ER length profiles and overall a less elaborate and interconnected ER network (Figure 3-3). Such morphological features have previously been documented in cells undergoing ER stress, possibly due to fragmentation of the ER compartment (Ha *et al*., 2020). Recent findings suggest that the ER can be remodeled by a process called ER-phagy, a process that degrades the ER using autophagic machinery, and that this process is upregulated under ER stress (Dikic, 2018; Grumati et al., 2018; Hubner and Dikic, 2020). Whether the ER morphological changes we observed in *SNCA*-3X DA neurons occur due to alterations in ER-phagy will be of importance for future studies.

In addition to mechanisms that involve loss of GCase function, our results demonstrate that a gain-in-toxic function of GCase may be a potential mechanism for cellular toxicity. Unlike in GD models, where the ER accumulation of immature mutant GCase leads to its rapid degradation by ERAD / UPS, we made the interesting observation that the ER accumulation of immature wild-type GCase in *SNCA*-3X neurons leads to the formation of insoluble GCase aggregates (Figure 3-1; Figure 5-1). Moreover, we found that this aggregation phenotype is not specific to GCase but rather includes other lysosomal enzymes such as Cathepsin D (Figure 3-2). We confirmed these findings in human DLB and PD brains (Figure 3-1; Figure 3-2). The accumulation of lysosomal hydrolases into insoluble aggregates has not been previously documented in neurodegenerative diseases. For instance, it is well known that in fibroblasts containing mutations in LIMP2, the receptor that is involved in trafficking GCase to lysosomes, wild-type GCase does not accumulate nor aggregate but instead is secreted into the media

(Reczek *et al*., 2007). Additionally, the abnormal trafficking of lysosomal enzymes in the severe lysosomal storage disorder Inclusion-Cell disease, also leads to their secretion into the media rather than their aggregation (Wiesmann et al., 1971a). Therefore, our study is the first to show that the lysosomal hydrolase aggregation phenotype is unique to synucleinopathies. It will be of interest to examine the factors that induce aggregation of GCase, cathepsin D, and other hydrolases in proteinopathies beyond PD and DLB that are characterized by lysosomal dysfunction. We hypothesized that the aggregation phenotype likely occurs due to defects in ERAD or its machinery which is exacerbated by α-syn overexpression (Figure 3-7; Figure 3-8; Figure 5-1), but the precise mechanistic role by which α-syn could lead to these defects remains to be determined by future studies. This may illuminate novel therapeutic opportunities centered on enhancing lysosomal function by targeting protein folding / degradation in the ER, promoting soluble enzymes that can be delivered to the lysosome.

Chronic ER accumulation of proteins can overwhelm the proteostasis machinery and result in ER stress and activation of the unfolded protein response (UPR). For instance, the upregulation of ER-resident chaperones is indicative of ER stress induction as the cell attempts to restore ER proteostasis. However, severe or chronic ER stress can lead to a signaling switch favoring cell death rather than survival. Therefore, proper protein folding and quality control in the ER is vital and is particularly important for post-mitotic cells such as neurons. The presence of ER stress in PD has been well documented in various cellular, *in vivo*, and brain models (Chung *et al*., 2013; Colla *et al*., 2012a; Hoozemans *et al*., 2007), and increased levels of the chaperones GRP78 and CANX have been previously documented in *GBA1*-PD iPSC-derived midbrain neurons and drosophila models (Fernandes *et al*., 2016; Garcia-Sanz *et al*., 2017; Sanchez-Martinez et al., 2016). We confirmed these findings in our *GBA1* mutant DA neuron

models by showing increased levels of GRP78, GRP94 and CANX expression relative to healthy control neurons (Figure 3-3). To our surprise, we found that ER chaperones were only mildly elevated by α-syn overexpression in *SNCA*-3X DA neurons, and that this elevation was not due to induction of any of the UPR pathways (Figure 3-3; Figure 3-4). These findings were unexpected given that we observed the accumulation and aggregation of immature GCase in the ER. Furthermore, it is well established that the increased load on the ER posed by the accumulation of immature or misfolded proteins leads to expansion of the ER through UPR signaling pathways. In line with our negative UPR results, we found that the ER is fragmented and that its overall area is decreased (Figure 3-3). It is important to note that although activation of canonical UPR signaling has been previously detected in various cellular PD models, ours is the first to study the UPR in PD patient-specific midbrain dopaminergic neurons. Additionally, while UPR induction is present in post-mortem PD brains and indicates the importance of ER stress in PD, one must consider whether the simple post-mortem aspect contributes to this induction. Consequently, it is of importance that we examined UPR signaling during phases of α-syn pathology but preceding neurotoxicity.

Next, we conjectured that *SNCA*-3X neurons are not capable of activating the UPR. To test this, we pharmacologically activated the UPR by treating neurons using two well-established ER stressors, thapsigargin (Tg) or brefeldin A (BFA). We observed similar levels of induced ER stress-related proteins and successful activation of the PERK and IRE1 UPR arms between Tg / BFA treated *SNCA*-3X and isogenic and healthy controls DA neurons (Figure 3-5; Figure 3-6), indicating that *SNCA*-3X neurons can successfully sense stressful conditions and activate the UPR. Broadly, our results indicate that the ER deals with wild-type and mutant GCase by utilizing different mechanisms, however further investigation of the factors that regulate these

mechanisms will be necessary. The UPR is a highly sensitive system, and it is likely that the ER is able to successfully detect mutant GCase due to its rapid accumulation and high propensity to misfold. On the other hand, the steady build-up of wild-type GCase in the ER due to α-syn accumulation appears to evade the UPR's detection, perhaps due to disruptions caused by α-syn. A similar scenario exists with the glycoprotein alpha-1-antitrypsin (AT), mutations in which cause liver disease and emphysema. Severe mutations in AT lead to its ER accumulation and rapid degradation by ERAD due to activation of the UPR. However, less severe AT mutants cause the protein to accumulate and aggregate in the ER compartment without activation of the UPR (Hidvegi et al., 2005). Together with our results, these findings strongly suggest that the machinery that is responsible for UPR activation may be able to distinguish the physical characteristics (e.g., monomers versus polymers) of ER accumulated proteins.

One important question that arises from our studies is whether α-syn itself can directly cause perturbations of the ER compartment. Ultrastructural analysis of neurons from A53T mutant α-syn mice shows the severe dilation of the ER cisternae (Colla *et al*., 2012a), suggesting that α-syn itself can alter the ER morphology possibly through abnormally localizing to the ER compartment (Bellucci *et al*., 2011; Colla *et al*., 2012a; Colla *et al*., 2018). Co-immunoprecipitation studies indicate the ability of α-syn to interact with ER chaperones including GRP78 and GRP94 (Bellucci *et al*., 2011; Colla *et al*., 2012a), providing an explanation for how α-syn might disrupt the morphology and consequently proper function of the ER. Our results further add to these previous studies, by confirming that α-syn accumulation leads to its aberrant localization to the ER and increases its interaction with CANX and GRP94 in *SNCA*-3X DA neurons (Figure 3-9; Figure 3-10), thus sequestering them from their proper

function. It may be postulated that simply the elevated levels of α-syn increase the probability of its interaction with ER chaperones. However, the selective interaction of α-syn with ykt6 but not with other ER-Golgi trafficking components (e.g., Rab1a, sec22b, syntaxin 5, bet1) (Cuddy *et al*., 2019; Mazzulli *et al*., 2016) makes this possibility less likely.

5.4 Repurposing drugs for new targets in disease

The unusual discovery that α-syn accumulation leads to wild-type GCase misfolding and aggregation in the ER presents novel therapeutic opportunities focused on restoring proper GCase folding and solubility. A majority of studies have focused on enhancing mutant GCase proteostasis, primarily at the early portion of the secretory pathway such as the ER. For instance, proteasome inhibitors can function as ER proteostasis regulators through inhibition of GCase degradation via ERAD as well as through enhancing expression of endogenous chaperones (Mu *et al*., 2008). Other proteostasis regulators, such as compounds that increase ER calcium levels (e.g., diltiazem, dantrolene, or DHBP) enhance the activity of calcium-dependent chaperones and have shown positive rescue effects in models of mutant GCase (Liou *et al*., 2016; Ong *et al*., 2010). Studies using diltiazem, an FDA-approved drug for the treatment of high blood pressure, have shown that the interaction between GCase and CANX is ER calcium dependent (Ong *et al*., 2010), suggesting that such compounds may be beneficial for repurposing in the context of PD and wild-type GCase accumulation. We tested this hypothesis in two models of α-syn overexpression, inducible H4 neuroglioma cells and PD patient neurons. Treating cells with diltiazem, dantrolene, or DHBP enhanced ER chaperone activity, sufficiently restored GCase solubility and folding, and subsequently partially enhanced GCase maturation (Figure 4-2; Figure 4-3; Figure 5-1). However, we found that ER proteostasis / chaperone enhancement was

not able to fully restore lysosomal GCase activity (Figure 4-2), which we hypothesized occurred due to α-syn's impediment of downstream trafficking to the Golgi. Combining diltiazem with FTI, a clinically-validated small molecule that enhances ER-Golgi trafficking, lead to a robust increase in GCase maturation and lysosomal GCase function that was sufficient to reduce pathological α-syn levels (Figure 4-5; Figure 4-6; Figure 5-1). Collectively, our studies indicate the importance of targeting the ER in α-syn / GCase pathology since it addresses the root of the problem. Furthermore, based on our studies involving UPR defects, it is also possible that further development of ER proteostasis regulators that exploit and enhance the UPR machinery may be beneficial for synucleinopathies regardless of the *GBA1* phenotype. Additionally, such proteostasis regulators may also be viable strategies for other lysosomal storage diseases characterized by loss-of-function mutations. The combination enhancement of ER proteostasis and trafficking suggests that simultaneous targeting of multiple portions of the proteostasis pathway results in greater therapeutic benefit (Figure 5-1). Collectively, our results present a novel therapeutic strategy for PD and other age-related neurodegenerative diseases characterized by a proteostasis imbalance.

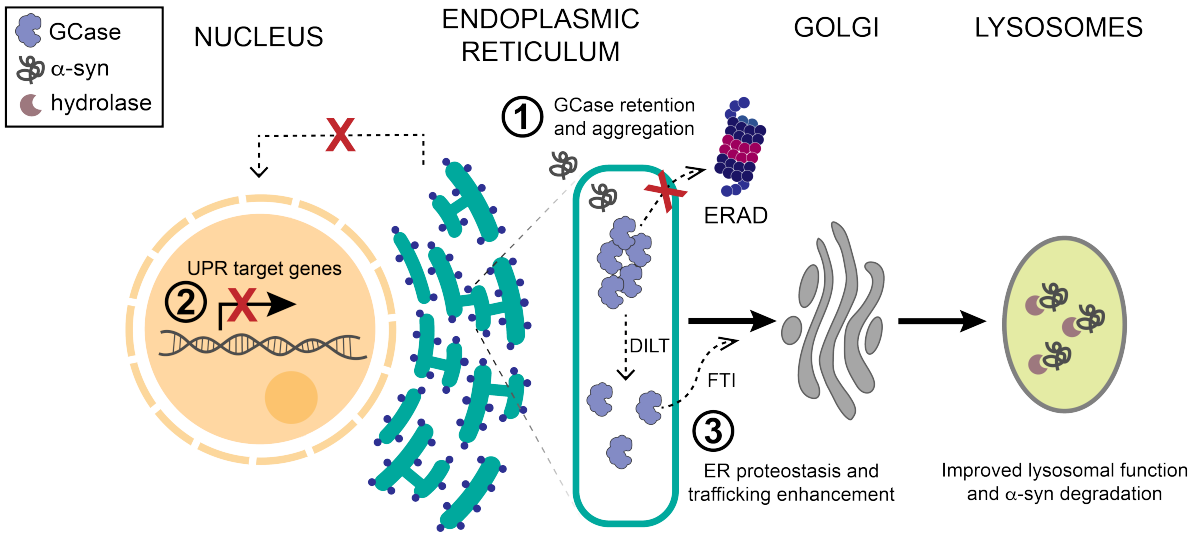

Figure 5-1. Schematic overview of proteostasis dysfunction and rescue in PD patient neurons that accumulate wild-type α-synuclein. A pathogenic cascade is triggered upon α-synuclein (α-syn) accumulation at the ER, leading to ER fragmentation, failure of UPR activation, and accumulation and aggregation of immature β-glucocerebrosidase (GCase) **(1, 2)**. Enhancing ER folding capacity promotes the formation of soluble, properly folded GCase, while combined treatment with protein trafficking enhancers rescues lysosomal function and reduces pathological α-syn **(3)**.

5.5 Additional molecular mechanisms of α-syn toxicity

Although the pathogenesis of PD undoubtedly involves defects in protein trafficking and lysosomal dysfunction, studies implicate a multitude of additional pathways in PD pathology including mitochondrial dysfunction and oxidative stress, autophagic dysfunction and disrupted calcium homeostasis.

Mitochondria play pivotal roles in preserving proper cellular function. These organelles generate adenosine triphosphate (ATP) through the electron transport chain (ETC), which is a source of energy that is fundamental for the support of many biochemical functions within cells. Mitochondria also maintain their integrity through their own quality control system that includes

mitochondrial chaperones important for protein folding and proteolytic enzymes important for protein degradation. Furthermore, the bioenergetic capacity and maintenance of mitochondrial proteostasis are both highly dependent on the fusion and fission dynamics of mitochondria. Therefore, it is not surprising that disruptions in mitochondrial integrity or function are implicated in neurodegeneration.

Many of the genes responsible for the onset of familial forms of PD, such as *PINK1*, Parkin, and DJ-1, play a role in mitochondrial integrity and function. For instance, *PINK1* and Parkin play important roles in initiating mitophagy, a process that involves the autophagic clearance of damaged mitochondria via lysosomes (Narendra et al., 2008; Youle and Narendra, 2011). Loss-of-function mutations in *PINK1*/Parkin are well-known to lead to defects in mitochondrial morphology and ATP production and increased sensitivity to reactive oxygen species (ROS), which form as a by-product of the respiratory chain (Gautier et al., 2008; Wood-Kaczmar et al., 2008). Wild-type DJ-1 is a sensor for ROS (Mitsumoto and Nakagawa, 2001; Taira et al., 2004) and PD-related loss-of-function mutations in the protein increase oxidative stress (Hao et al., 2010; Kim et al., 2005), collectively contributing to neurotoxicity. Interestingly, there is also evidence that mutations in *GBA1* contribute to mitochondrial dysfunction. For instance, a decline in GCase activity due to mutations leads to impaired mitochondrial respiration and ATP production as well as morphological disruptions of the organelle (Cleeter *et al.*, 2013; Osellame et al., 2013; Xu et al., 2014). These findings strongly support the notion that lysosomal function is important for proper mitochondrial function and highlight the important role of organellar crosstalk in sustaining cellular health and homeostasis.

There is a large amount of evidence from *in vivo* and *in vitro* PD models that highlights the effect of α-syn aggregation on mitochondrial morphology and function. For instance, the

overexpression of WT or A53T mutant α-syn has been shown to cause mitochondrial fragmentation (Butler et al., 2012; Guardia-Laguarta *et al.*, 2014; Nakamura et al., 2011; Pozo Devoto et al., 2017; Xie and Chung, 2012; Zambon et al., 2019), while α-synuclein depletion can restore mitochondrial length (Kamp et al., 2010; Pozo Devoto *et al.*, 2017). These results are similar to our observations of ER fragmentation in *SNCA*-3X DA neurons and suggest that α-syn can influence organelle size and integrity. The exact process by which α-syn may do this is yet to be understood, but the biophysical properties of membranes and α-syn's ability to bind lipids (Middleton and Rhoades, 2010) are plausible mechanisms.

The proper control of ATP production is perhaps even more important for dopaminergic neurons, as they are some of the most energy-requiring cells in the human body due to their extensive synaptic connections. PD patient brains exhibit functional abnormalities in complex I and III of the mitochondrial electron transport chain (ETC) (Haas et al., 1995; Parker et al., 1989) (Schapira et al., 1989), which leads to decreased ATP generation and increased ROS production. Confirming these findings, PD models of α-syn overexpression indicate reduced activity of complex I and IV of the ETC, possibly through direct binding, and increased ROS production (Chinta et al., 2010; Devi et al., 2008; Di Maio et al., 2016). Like many biochemical processes that require ATP for proper function, the ER imports ATP and uses energy from ATP hydrolysis to achieve protein folding and trafficking of proteins to the Golgi. Therefore, a decline in mitochondrial respiration due to α-syn can negatively affect ER function and lead to increased accumulation of misfolded proteins collectively contributing to neurotoxicity.

Although the direct mechanisms by which α-syn can alter mitochondrial morphology remain to be further investigated, one possibility is through the aberrant localization and

association of α-syn to mitochondria. For one, mitochondria within the substantia nigra and striatum of post-mortem PD brains accumulate α-syn (Devi *et al.*, 2008). More recently, α-syn has been found to specifically localize to mitochondria-associated membranes (MAMs) of neurons (Guardia-Laguarta *et al.*, 2014). MAMs bridge the mitochondria to the ER and play an important role in calcium transport and lipid metabolism between the two organelles. Both WT and mutant (A53T, A30P) forms of α-syn can interact with MAM tethering proteins and disrupt MAM formation, leading to defects in cellular calcium regulation (Paillusson *et al.*, 2017). Moreover, α-syn-MAM interactions disrupt mitochondrial ATP production (Paillusson *et al.*, 2017), providing a more direct potential mechanism for how α-syn itself can lead to ER proteostasis dysfunction downstream.

5.6 Final remarks

The etiology of PD is likely multifactorial and involves the interplay of genetics, aging, and the cellular environment. Findings from genetic studies have greatly enhanced our understanding of the processes involved in PD pathogenesis, including α-syn accumulation and organellar dysfunction. Indeed, multiple organelles are affected by α-syn toxicity, making it more difficult to decipher which insults are the first to occur during pathology. Moreover, the wide crosstalk between organelles and vicious cycles that occur when one becomes dysfunctional further complicate the understanding of PD pathogenesis. Therefore, a thorough understanding of the basic molecular processes that occur in health and disease will be necessary for the development of future therapeutic targets to treat this complex disease.

CO-AUTHORED PUBLICATIONS

1) Reversible Conformational Conversion of α-synuclein into Toxic Assemblies by Glucosylceramide

Friederike Zunke[1], Alexandra C. Moise[1], Nandkishore R. Belur[1], Eilrayna Gelyana[1], Iva Stojkovska[1], Haris Dzaferbegovic[1], Nicholas J. Toker[1], Sohee Jeon[1], Kristina Fredriksen[1], Joseph R. Mazzulli[1]

[1]Ken and Ruth Davee Department of Neurology, Northwestern University Feinberg School of Medicine, Chicago, IL 60611, USA

This manuscript was published in *Neuron*, Volume 97, Issue 1, on 3 January 2018 (Zunke *et al.*, 2018).

ABSTRACT

α-Synuclein (α-syn) aggregation is a key event in Parkinson's disease (PD). Mutations in glycosphingolipid (GSL)-degrading glucocerebrosidase are risk factors for PD, indicating that disrupted GSL clearance plays a key role in α-syn aggregation. However, the mechanisms of GSL-induced aggregation are not completely understood. We document the presence of physiological α-syn conformers in human midbrain dopamine neurons and tested their contribution to the aggregation process. Pathological α-syn assembly mainly occurred through the conversion of high molecular weight (HMW) physiological α-syn conformers into compact, assembly-state intermediates by glucosylceramide (GluCer), without apparent disassembly into free monomers. This process was reversible *in vitro* through GluCer depletion. Reducing GSLs

in PD patient neurons with and without *GBA1* mutations diminished pathology and restored physiological α-syn conformers that associated with synapses. Our work indicates that GSLs control the toxic conversion of physiological α-syn conformers in a reversible manner that is amenable to therapeutic intervention by GSL reducing agents.

CONTRIBUTIONS

- Contributed by performing transmission electron microscopy studies that appear in Figure 1C, D and Supplemental Figure 1G-J of the manuscript (termed Figure S1-1 and S1-2, respectively, in this dissertation), showing the accumulation of vesicles and fibrillogranular material within enlarged vacuoles in iPSC-derived dopaminergic neurons treated with the β-glucocerebrosidase inhibitor conduritol-β-epoxide (CBE).
- Contributed by performing immuno-electron microscopy studies that appear in Supplemental Figure 3F of the manuscript (termed Figure S1-3 in this dissertation), showing the close association of glucosylceramide with pathological forms of α-synuclein.

FIGURES

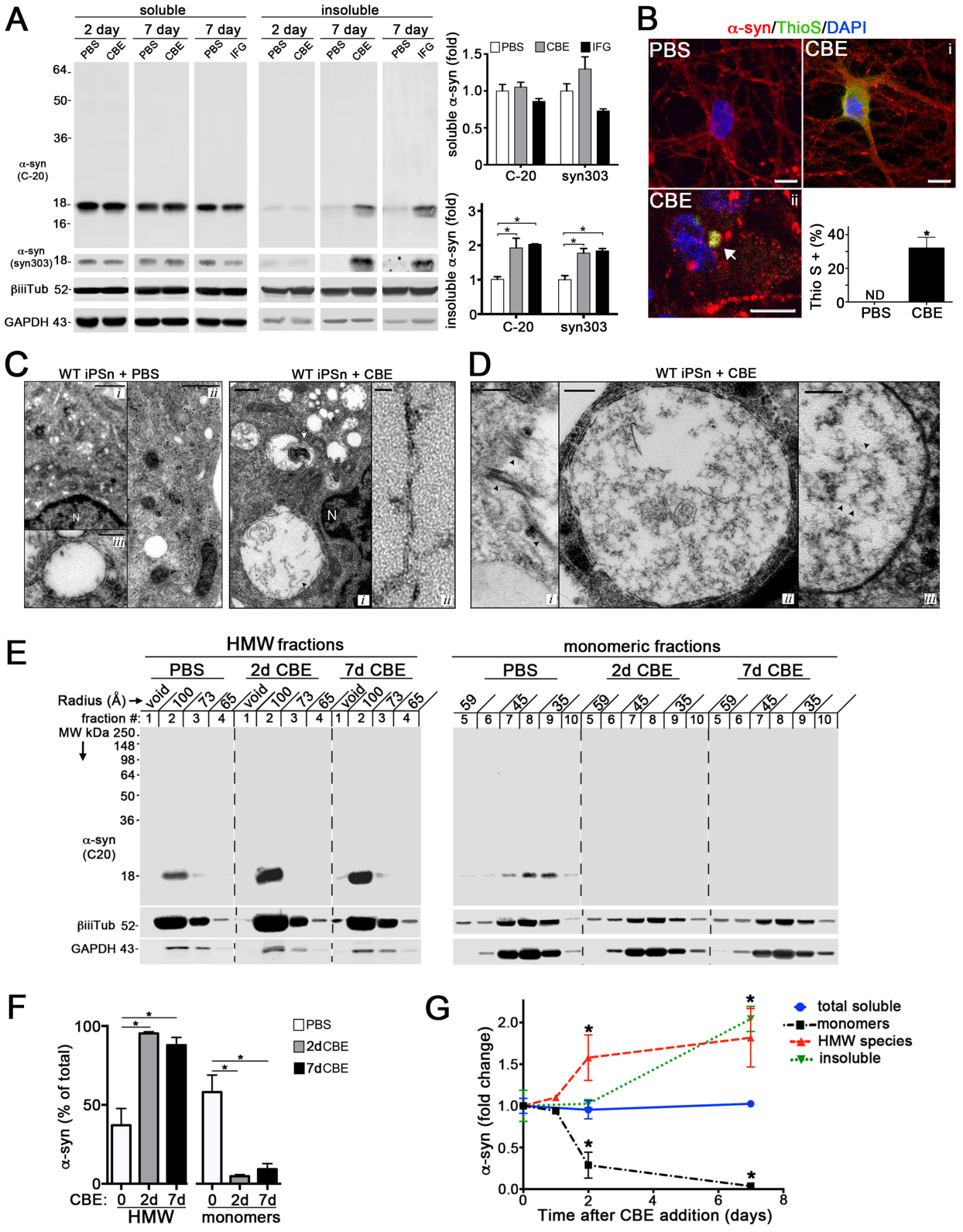
A
soluble
insoluble
2 day
7 day
PBS
CBE
IFG
α-syn (C-20)
α-syn (syn303)
βiiiTub
GAPDH
soluble α-syn (fold)
insoluble α-syn (fold)
C-20
syn303
B
α-syn/ThioS/DAPI
PBS
CBE
Thio S + (%)
ND
C
WT iPSn + PBS
WT iPSn + CBE
D
WT iPSn + CBE
E
HMW fractions
monomeric fractions
PBS
2d CBE
7d CBE
Radius (Å)
fraction #:
MW kDa
α-syn (C20)
βiiiTub
GAPDH
F
α-syn (% of total)
PBS
2dCBE
7dCBE
CBE:
HMW
monomers
G
α-syn (fold change)
Time after CBE addition (days)
total soluble
monomers
HMW species
insoluble

Figure S1-1. GSL accumulation induces pathological α-syn aggregates in human midbrain iPSns.

(A) iPSC-derived midbrain dopamine neurons from healthy control lines were treated for 2 or 7 days with GCase inhibitors CBE or IFG (50μM) and phosphate buffered saline (PBS) as a control. Neurons were subjected to sequential extraction followed by western blot using α-syn antibodies C-20 and syn303. β3-tubulin (tub) and GAPDH were used as loading controls. Right: quantification of the blots (n = 4).

(B) Immunofluorescence analysis of α-syn- (red) or thioflavin S- (Thio S, green) positive neurons as diffuse (i) or punctated inclusions (ii) after a 7-day treatment with 50 μM CBE. Nuclei were detected with DAPI (blue). The arrow indicates a representative amyloidogenic inclusion. Scale bars, 5 μm.

(C) Left: transmission electron microscopy (TEM) analysis of WT control iPSns showing normal morphology of vesicles in the cytoplasm (i and ii) and a close-up of membrane delimited electron lucent vesicles (iii). Scale bars, 1 (i), 0.5 (ii), and 0.25 μm (iii). N, nucleus. Right: TEM analysis of 7-day CBE-treated WT iPSns showing accumulation of vesicles and multilamellar membrane inclusions (i, white arrow) or fibrillogranular material accumulating in enlarged vacuoles. (ii) shows a close-up of the fibrillar material indicated with the black arrow in (i). Scale bars, 200 (i) and 25 nm (ii).

(D) Tubular (i) or fibrillar (ii and iii) accumulations indicated by black arrows within enlarged vacuoles of 7-day CBE-treated iPSns. Scale bars, 100 (i and iii) and 200 nm (ii).

(E) Soluble lysates were analyzed by native SEC (inputs shown in A). HMW (#1–4) and monomeric fractions (#5–10) were analyzed by western blot. Molecular radius is shown horizontally in angstroms (Å).

(F) Quantification of western blot in (E) (n = 5).

(G) Measurement of α-syn from CBE-treated iPSns by SEC/ELISA (soluble monomers or HMW species) or sequential extraction (total soluble or insoluble) (n = 4). For all quantifications, values are the mean ± SEM, *$p < 0.05$. For all blots, MW is shown vertically in kilodaltons (kDa).

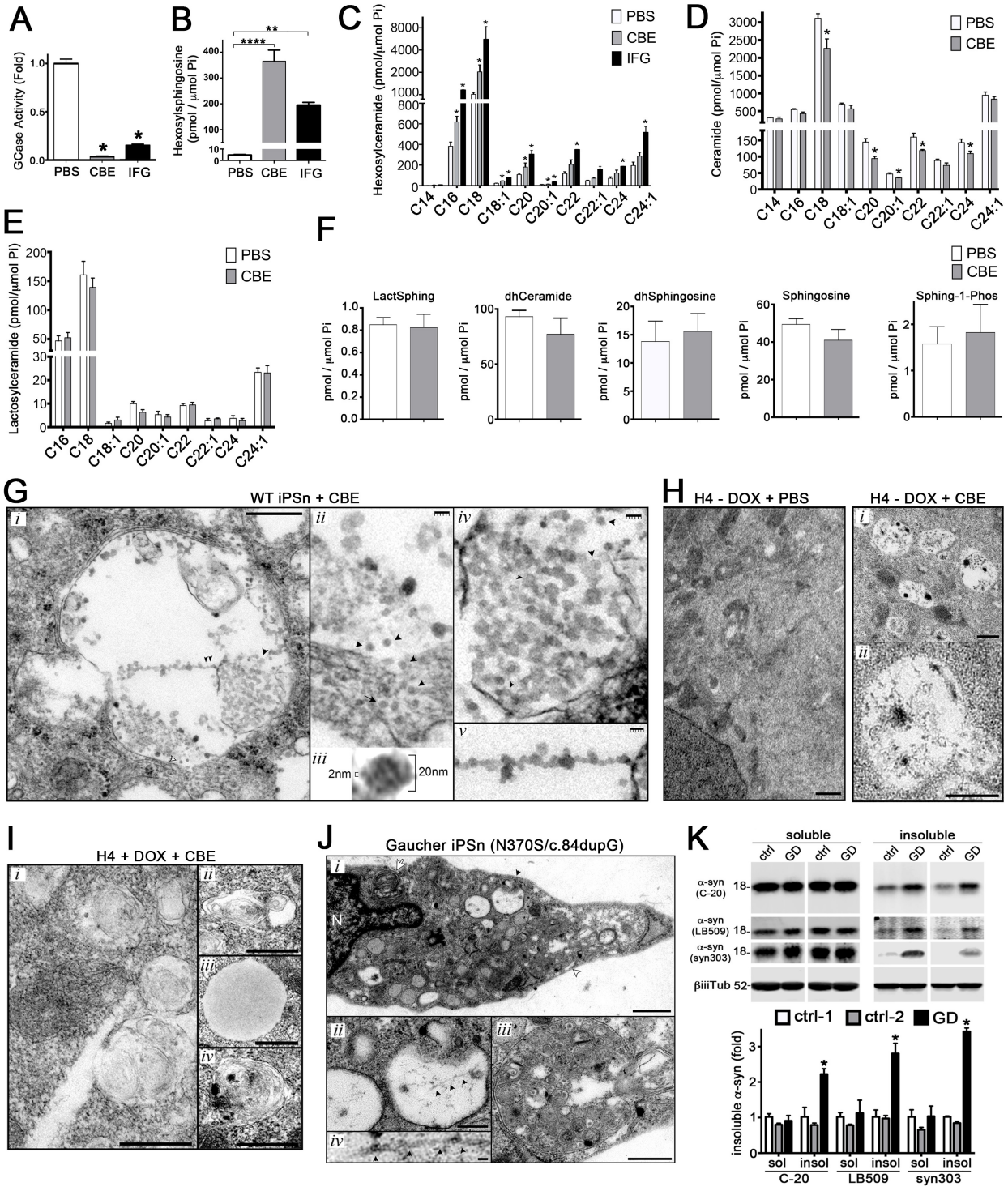
A
GCase Activity (Fold)
PBS
CBE
IFG
B
Hexosylsphingosine (pmol / µmol Pi)
C
Hexosylceramide (pmol/µmol Pi)
D
Ceramide (pmol/µmol Pi)
E
Lactosylceramide (pmol/µmol Pi)
F
LactSphing
dhCeramide
dhSphingosine
Sphingosine
Sphing-1-Phos
G
WT iPSn + CBE
H
H4 - DOX + PBS
H4 - DOX + CBE
I
H4 + DOX + CBE
J
Gaucher iPSn (N370S/c.84dupG)
K
soluble
insoluble
α-syn (C-20)
α-syn (LB509)
α-syn (syn303)
βiiiTub 52
ctrl-1
ctrl-2
GD
insoluble α-syn (fold)
C-20
LB509
syn303

Figure S1-2. Lipid accumulation and pathological analysis of iPSn treated with GCase inhibitors and GD patient neurons.

(A) iPSC midbrain cultures from healthy controls were treated with 50 μM conduritol-β-epoxide (CBE) or isofagomine (IFG) for 7 days. GCase activity was measured from whole-cell lysates from neurons treated with CBE or IFG, using an artificial GCase substrate that fluoresces upon cleavage, 4-MU-Gluc (n=4).

(B) Hexosylsphingosine species were measured by high performance liquid chromatography- tandem mass spectrometry (HPLC-MS/MS) after CBE or IFG treatment and expressed as picomole substrate / micromole of inorganic phosphate (Pi).

(C) HPLC-MS/MS measurement of hexosylceramide species separated by N-acyl fatty acid chain length after CBE or IFG treatment, expressed as pmol / mol Pi (n=4). Hexosylsphingosine and hexosylceramides include both glucosyl and galactosyl species, however glucosylceramides make up ca. 90% of the total hexosylceramide species in neuronal cultures.

(D, E) HPLC-MS/MS measurement of ceramide or lactosylceramide species separated by N-acyl fatty acid chain length.

(F) HPLC-MS/MS measurement of sphingolipids related to the glucosylceramide metabolic pathway, demonstrating specificity of CBE at the utilized time and concentration.

(G) 2-day CBE-treated neurons demonstrate accumulation of annular structures within vacuoles (i, black arrowhead) that occasionally coalesce in a linear manner (i, double arrow head) and surround disrupted regions of the vacuole (i, white arrow head). Higher magnification of structures indicated by the white arrow (ii), a single annular structure of 20nm in diameter with the appearance of a 2nm pore (iii), higher magnification of annular structures (iv), and linear alignment (v). Scale bars = 500nm (i), 50nm with 10nm ticks (ii, iv, v).

(H) Left, TEM of H4 cells expressing α-syn treated with PBS. Scale bar = 100nm. Right, H4 cells treated with CBE for 5 days showing fibrillogranular inclusions. Scale bars = 500nm.

(I) CBE-treated H4 cells depleted of α-syn through doxycycline addition demonstrate membrane accumulations of multilamellar structure (ii, iv) or electron lucent vacuoles (iii) in the absence of fibrillar material. Scale bars = 500nm.

(J) TEM analysis of GD patient neurons (N370S / c.84dupG) showing enlarged vacuoles containing multiple vesicular bodies (white arrowhead in panel (i), close up shown in panel (iii)), multilamellar body (white arrow in panel (i)), and a disrupted vacuole containing fibrillar material (black arrowhead in panel (i), close up shown in panel (ii) and fibrillar material shown in (iv). Scale bar = 1μm.

(K) Elevated insoluble α-syn in GD iPSn. Sequential extraction of GD iPSC midbrain neurons (expressing N370S / c.84dupG mutations) by 1% Triton X-100 (soluble), then 2% SDS buffer (insoluble) followed by western blot analysis. GD samples were compared to two separate iPSC control lines previously characterized (Mazzulli *et al.*, 2016). The blots were quantified below (n=4). For all blots, the molecular weight is shown in kilodaltons. All quantifications represent the mean ± SEM. *p<0.05, **p<0.01, ***p<0.001, ****p<0.0001.

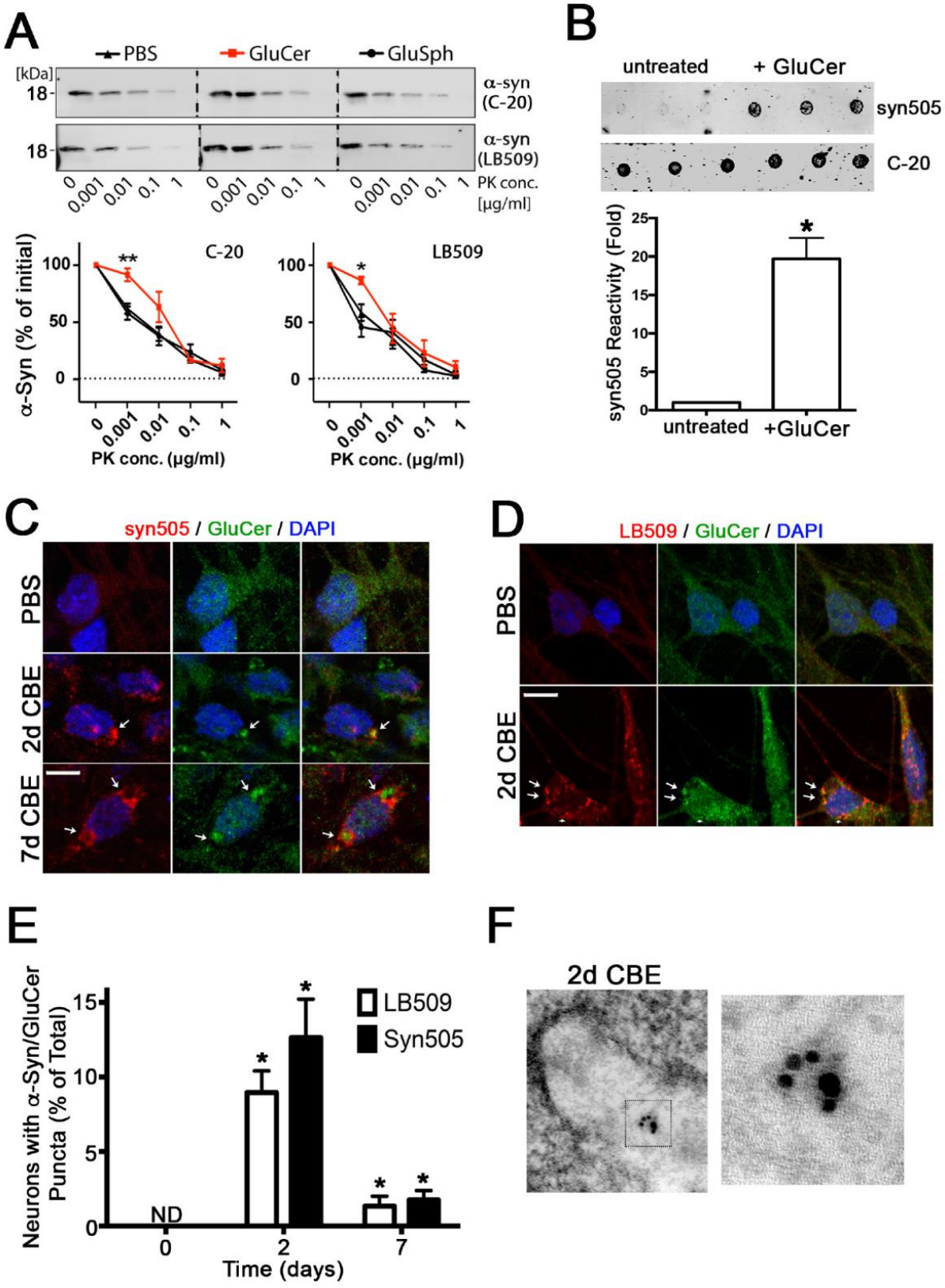
A
PBS
GluCer
GluSph
[kDa]
18
α-syn (C-20)
α-syn (LB509)
0 0.001 0.01 0.1 1
PK conc. [μg/ml]
α-Syn (% of initial)
C-20
LB509
PK conc. (μg/ml)
B
untreated
+ GluCer
syn505
C-20
syn505 Reactivity (Fold)
untreated
+GluCer
C
syn505 / GluCer / DAPI
PBS
2d CBE
7d CBE
D
LB509 / GluCer / DAPI
PBS
2d CBE
E
Neurons with α-Syn/GluCer Puncta (% of Total)
LB509
Syn505
ND
Time (days)
F
2d CBE

Figure S1-3. Conversion of α-syn species by GluCer *in vitro* and in neurons.

(A) GluCer directly converts α-syn into PK resistant species. Recombinant purified α-syn (*E. coli* derived) was incubated with GluCer or GluSph at pH 5.5 with sample agitation, followed by PK digest and western blot. (n=3, *p< 0.05, **p<0.01, GluCer compared to GluSph and PBS).

(B) Native dot blot analysis of recombinant α-syn mixed with GluCer using the same conditions as in A) showing increased reactivity with syn505. Three replicates are shown and quantified below. C-20 was used to detect total α-syn.

(C) Immunostaining analysis of iPSn treated with 50μM CBE for 2 or 7 days, with syn505 (red) and anti-GluCer antibodies (green). Nuclei are stained with DAPI in blue.

(D) iPSn were analyzed for α-syn -GluCer colocalization using LB509 and anti-GluCer after 2 days of CBE treatment.

(E) Quantification of neurons containing α-syn / GluCer colocalized puncta (n=3).

(F) Immunoelectron microscopy analysis of 2-day CBE treated cells using syn505 (6 nm gold secondary) and anti-GluCer (10 nm gold secondary). For all quantifications, values are the mean +/- SEM, *p<0.05, **p<0.01. Student's t-test (B) or ANOVA with Tukey's post-hoc test (A, E) was used for statistical analysis.

2) Patient-Customized Oligonucleotide Therapy for a Rare Genetic Disease

Jinkuk Kim, Chunguang Hu, Christelle Moufawad El Achkar, Lauren E. Black, Julie Douville, Austin Larson, Mary K. Pendergast, Sara F. Goldkind, Eunjung A. Lee, Ashley Kuniholm, Aubrie Soucy, Jai Vaze, Nandkishore R. Belur, Kristina Fredriksen, Iva Stojkovska, Alla Tsytsykova, Myriam Armant, Renata L. DiDonato, Jaejoon Choi, Laura Cornelissen, Luis M. Pereira, Erika F. Augustine, Casie A. Genetti, Kira Dies, Brenda Barton, Lucinda Williams, Benjamin D. Goodlett, Bobbie L. Riley, Amy Pasternak, Emily R. Berry, Kelly A. Pflock, Stephen Chu, Chantal Reed, Kimberly Tyndall, Pankaj B. Agrawal, Alan H. Beggs, P. Ellen Grant, David K. Urion, Richard O. Snyder, Susan E. Waisbren, Annapurna Poduri, Peter J. Park, Al Patterson, Alessandra Biffi, Joseph R. Mazzulli, Olaf Bodamer, Charles B. Berde, and Timothy W. Yu

This manuscript was published in *The New England Journal of Medicine*, on 24 October 2019 (Kim et al., 2019).

ABSTRACT

Genome sequencing is often pivotal in the diagnosis of rare diseases, but many of these conditions lack specific treatments. We describe how molecular diagnosis of a rare, fatal neurodegenerative condition led to the rational design, testing, and manufacture of milasen, a splice-modulating antisense oligonucleotide drug tailored to a particular patient. Proof-of-concept experiments in cell lines from the patient served as the basis for launching an “N-of-1” study of milasen within 1 year after first contact with the patient. There were no serious adverse events, and treatment was associated with objective reduction in seizures (determined by

electroencephalography and parental reporting). This study offers a possible template for the rapid development of patient-customized treatments. (Funded by Mila's Miracle Foundation and others.)

CONTRIBUTIONS

- Contributed by performing transmission electron microscopy studies that appear in Figure 2D of the manuscript (termed Figure S2-1 in this dissertation), showing a reduction of intracellular vacuoles and lipid storage in Batten's disease patient fibroblasts treated with the antisense oligonucleotide termed milasen.

FIGURES

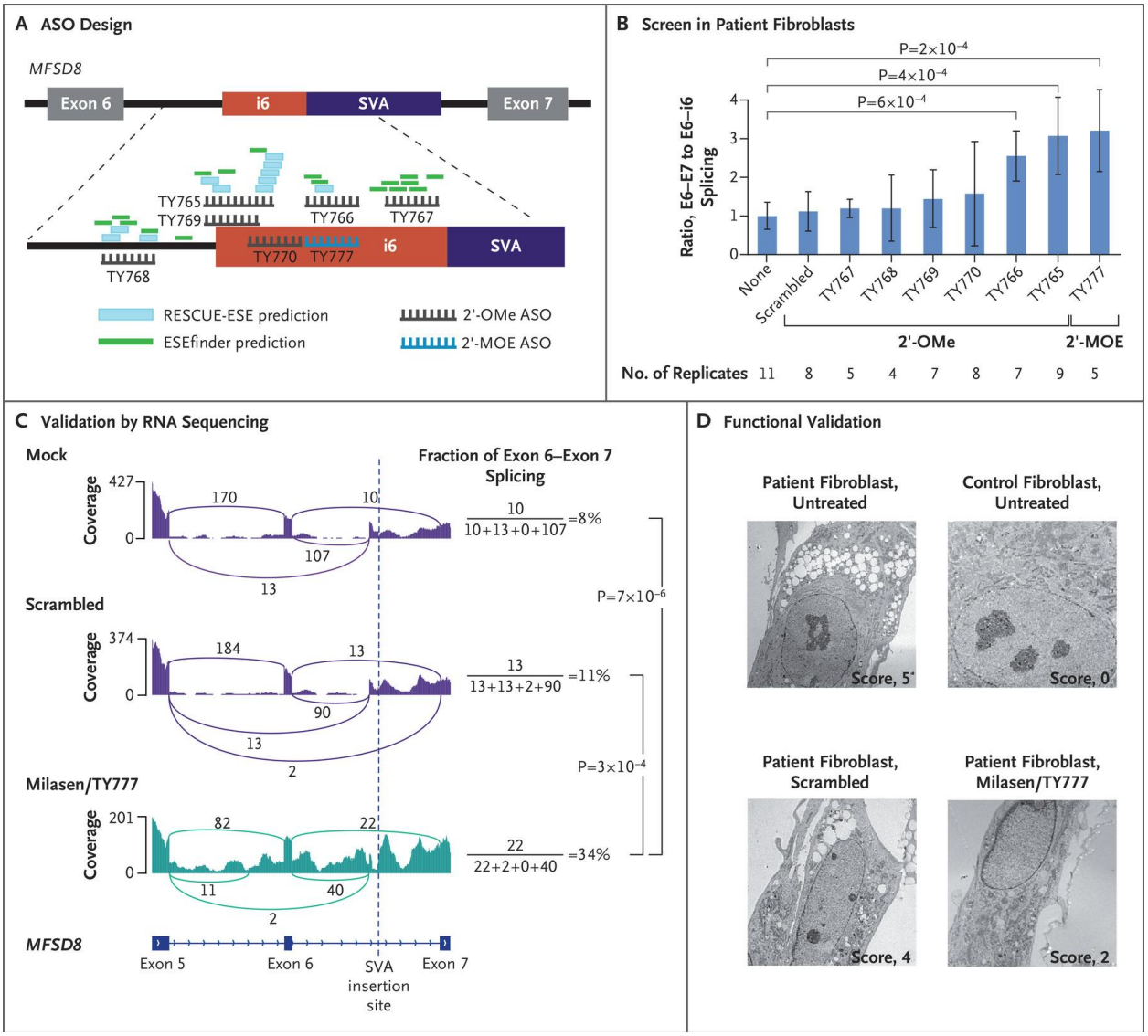

Figure S2-1. Antisense oligonucleotide drug development.

(A) Location and chemistry of the ASOs that were designed to block the i6.SA splice acceptor site or exonic splicing enhancer (ESE) elements. (Additional details are provided in Table S1.) The ESE elements were predicted with RESCUE-ESE and ESEfinder. 2′-MOE denotes 2′-*O*-methoxyethyl, and 2′-OMe 2′-*O*-methyl.

(B) Ratio of the normal exon 6–exon 7 (E6–E7) splicing to the abnormal exon 6–intron 6 (E6–i6) splicing (normalized to a no-transfection control), measured in patient fibroblasts that were transfected (for 24 hours at 100 nmol per liter) as indicated. To measure splice isoform-specific levels, multiplex reverse-transcriptase polymerase chain reactions were conducted with isoform-specific primer sets, and then the intensity of the isoform-specific bands was quantified by gel electrophoresis (Fig. S6). "Scrambled" indicates a nontargeting oligonucleotide (TY772). I bars indicate 95% confidence intervals of the means. P values were calculated by two-sided t-test.

(C) RNA sequencing (RNA-seq) analysis validation of the splice-correcting effect of milasen (TY777). For the calculation of the fraction of normal splicing (exon 6–exon 7), three other splicing events that are mutually exclusive with the normal splicing were considered. Splicing events supported by only one read are not shown. P values were calculated by Fisher's exact test.

(D) Intracellular vacuoles, visualized by electron microscopy, in control fibroblasts (*MFSD8* wild-type human foreskin fibroblast; BJ cell line) and in patient fibroblasts that are either untreated or transfected with the indicated oligonucleotide. Scoring was performed on a scale of 0 to 5, with 0 representing the lowest and 5 representing the highest level of vacuole accumulation.

Supplementary Tables

Table S1. Protocol for the differentiation of iPSCs to midbrain dopaminergic neurons.

Volume Per Well	Day	Media	Factors
3 mL	0	KSR	LDN, SB
	1	KSR	LDN, SB, SHH, PURM, FGF8a
	2	KSR	LDN, SB, SHH, PURM, FGF8a
	3	KSR	LDN, SB, SHH, PURM, FGF8a, CHIR
	4	KSR	LDN, SB, SHH, PURM, FGF8a, CHIR
4 mL	5	3:1 KSR:SM1	LDN, SHH, PURM, FGF8a, CHIR
	6	3:1 KSR:SM1	LDN, SHH, PURM, FGF8a, CHIR
	7	1:1 KSR:SM1	LDN, CHIR
	8	1:1 KSR:SM1	LDN, CHIR
5 mL	9	1:3 KSR:SM1	LDN, CHIR
	10	1:3 KSR:SM1	LDN, CHIR
	11	SM1	CHIR, BAGTCD
	12	SM1	CHIR, BAGTCD
6 mL	13	SM1	BAGTCD
	14	SM1	BAGTCD
	15	SM1	BAGTCD

Factor	Full name	Final Concentration	Company
LDN	LDN193189	100 nM	Stemgent
SB	SB431542	10 uM	R&D
SHH	Sonic Hedgehog	100 ng/ml	R&D
PURM	Purmorphamine	2 uM	Stemgent
FGF8a	Fibroblast growth factor 8a	100 ng/ml	R&D
CHIR	CHIR99021	3 uM	Stemgent
B	Brain derived neurotrophic factor	20 ng/ml	R&D
A	Ascorbic acid	0.4 uM	Sigma
G	Glial cell-derived neurotrophic	5 ng/ml	R&D
T	Transforming growth factor	1 ng/ml	R&D
C	Dibutyrul cyclic adenosine	500 uM	Enzo / Santa Cruz /
D	DAPT	10 uM	Stemgent

Table S2. List of reagents and resources used in the study.

REAGENT or RESOURCE	SOURCE	CATALOG #
Antibodies		
Rabbit polyclonal anti-alpha synuclein (C-20)	Santa Cruz	Cat #sc-7011-R RRID: AB_2192953
Mouse monoclonal anti-alpha synuclein (LB509)	Abcam	Cat #ab27766 RRID: AB_727020
Mouse monoclonal anti-alpha synuclein (syn211)	Sigma Aldrich	Cat #S5566 RRID: AB_261518
Mouse monoclonal anti-alpha synuclein (303)	Biolegend	Cat #824301 RRID: AB_2564879
Mouse monoclonal anti-β3-tubulin	Biolegend	Cat #802001 RRID: AB_2564645
Rabbit polyclonal anti-calnexin (CANX)	Cell Signaling	Cat #2433S RRID: AB_2243887
Mouse monoclonal anti-calnexin (CANX) (E-10)	Santa Cruz	Cat #sc-46669 RRID: AB_626784
Mouse monoclonal anti-cathepsin D	Sigma	Cat #C0715 RRID: AB_258707
Mouse monoclonal anti-EDEM1	Santa Cruz	Cat #sc-377394
Rabbit polyclonal anti-p-eIF2α (ser51)	Cell Signaling	Cat #3398 RRID: AB_2096481
Mouse monoclonal anti-eIF2α	Santa Cruz	Cat #sc-133132 RRID: AB_1562699
Mouse monoclonal anti-FoxA2	Santa Cruz	Cat #sc-101060 RRID: AB_1124660
Mouse monoclonal anti-GAPDH	Millipore	Cat #CB1001 RRID: AB_2107426
Rabbit polyclonal anti-glucocerebrosidase (GCase)	Sigma	Cat #G4171 RRID: AB_1078958
Mouse monoclonal anti-glucocerebrosidase (GCase) (8E4)	N/A (gift from J. Aerts)	N/A
Rabbit polyclonal anti-GRP78	Novus	Cat #NBP1-06274 RRID: AB_1555284
Mouse monoclonal anti-GRP94	Santa Cruz	Cat #sc-393402
Mouse monoclonal anti-Hexosaminidase B (Hex B)	Sigma	Cat #sc-376781
Rabbit polyclonal anti-Nanog	Abcam	Cat #ab21624 RRID: AB_446437
Neurofilament Marker	Biolegend	Cat #SMI-312R RRID: AB_2314906
Rabbit polyclonal anti-Oct4	Abcam	Cat #ab19857 RRID: AB_445175
Rabbit polyclonal anti-PDI	Abcam	Cat #ab11432 RRID: AB_298038
Rabbit polyclonal anti-Sox2	Abcam	Cat #ab97959 RRID: AB_2341193
Mouse monoclonal anti-SSEA4	Abcam	Cat #ab16287 RRID: AB_778073
Mouse monoclonal anti-Tra-1-60	Abcam	Cat #ab16288 RRID: AB_778563
Rabbit polyclonal anti-tyrosine hydroxylase (TH)	Millipore	Cat #AB5986 RRID: AB_92190

Rabbit polyclonal anti-ubiquitin	Dako	Cat #Z045801-5
Mouse monoclonal anti-ykt6	Santa Cruz	Cat #SC-365732 RRID: AB_10859388
Secondary antibody: Alexa Fluor 488 Goat anti-rabbit IgG secondary (H+L)	Invitrogen	Cat #A11034 RRID: AB_2576217
Secondary antibody: Alexa Fluor 488 Goat anti-mouse IgG secondary (H+L)	Invitrogen	Cat #A11029 RRID: AB_138404
Secondary antibody: Alexa Fluor 568 Goat anti-rabbit IgG secondary (H+L)	Invitrogen	Cat #A11036 RRID: AB_10563566
Secondary antibody: Alexa Fluor 568 Goat anti-mouse IgG secondary (H+L)	Invitrogen	Cat #A11031 RRID: AB_144696
Secondary antibody: Alexa Fluor 680 Goat anti-mouse IgG secondary (H+L)	Invitrogen	Cat #A21058 RRID: AB_2535724
Secondary antibody: IRdye 800CW goat anti-mouse IgG secondary (H+L)	Li-Cor Biosciences	Cat #926-32210 RRID: AB_621842
Secondary antibody: IRdye 800CW goat anti-rabbit IgG secondary (H+L)	Li-Cor Biosciences	Cat #926-32211 RRID: AB_621843
Bacterial and virus strains		
pER4 (vector) lentivirus	Mazzulli et al., 2011	N/A
pER4 ykt6-CS lentivirus	Cuddy et al., 2019	N/A
Scrambled (scrb) shRNA lentivirus	Stojkovska et al., 2021 (under review)	N/A
RyR3 shRNA lentivirus	Stojkovska et al., 2021 (under review)	N/A
Biological samples		
Human brain tissue of control, DLB, DLB + AD patients	Northwestern University Alzheimer's disease pathology core (CNADC)	N/A
Chemicals, peptides, and recombinant proteins		
Bafilomycin A1	Santa Cruz	Cat #SC-201550
Bovine serum albumin (BSA), heat shock, fatty acid free	Roche	Cat #03117057001
Brefeldin A (BFA)	Cell Signaling	Cat #9972S
Cascade Dextran Blue	Life Technologies	Cat #D1976
CHAPS hydrate	Sigma	Cat #C5070
Conduritol-β-epoxide (CBE)	Millipore	Cat #234599
Doxycycline (DOX)	Sigma	Cat #D3447
Diltiazem hydrochloride (DILT)	Sigma	Cat #D2521
Dantrolene sodium salt (DANT)	Sigma	Cat #D9175
DHBP (1,1'-diheptyl-4,4'-bipyridinium dibromide)	Sigma	Cat #180858
Epoxomicin	Fisher	Cat #10007806
Farnesyl transferase inhibitor (FTI): LNK-754	Link Medicine	N/A
Fetal bovine serum (FBS), heat-inactivated	Thermo Fisher Scientific	Cat #10438026
Geneticin (G418)	Thermo Fisher Scientific	Cat #10131027
L-glutamine	Gibco	Cat #25030081
Glutaraldehyde, 25% aqueous solution	Electron Microscopy Sciences	Cat #16220

Hygromycin B	Thermo Fisher Scientific	Cat #10687010
L-Lysine	Cambridge Isotope Laboratories	Cat #CNLM-291-H-0.5
L-Arginine	Cambridge Isotope Laboratories	Cat #CNLM-539-H-0.5
LX112	Ladd Research Industries	Cat #21310
Normal goat serum (NGS)	Jackson ImmunoResearch	Cat #005-000-121
Osmium tetroxide (OsO_4), 4% aqueous solution	Electron Microscopy Sciences	Cat #19150
Paraformaldehyde (10%, methanol-free)	Polysciences, Inc.	Cat #40181
Penicillin / Streptomycin	Thermo Fisher Scientific	Cat #10378016
Phenylmethylsulfonyl fluoride (PMSF)	Sigma	Cat #78830
Protease Inhibitor Cocktail (PIC)	Roche	Cat #11836170001
N-Lauroylsarcosine sodium salt (sarkosyl)	Sigma	Cat #L9150
SimplyBlue SafeStain (Coomassie)	Thermo Fisher Scientific	Cat #LC6065
Sodium dodecyl sulfate (SDS)	Sigma	Cat #L4509
Sodium orthovanadate (Na_3VO_4)	Sigma	Cat #450243
Sodium fluoride (NaF)	Sigma	Cat #201154
Sucrose	Sigma	Cat #S1888
Triton X-100	Sigma	Cat #T8787
Thapsigargin (Tg)	Sigma	Cat #T9033
Thioflavin S (ThioS)	Sigma	Cat #T1892
Uranyl acetate	Electron Microscopy Sciences	Cat #22400
Methyl-5-Norbornene-2,3-Dicarboxylic Anhydride (NMA)	Electron Microscopy Sciences	Cat #19000
Dodecenyl Succinic Anhydride (DDSA)	Electron Microscopy Sciences	Cat #13700
2,4,6-Tri(dimethylaminomethyl) phenol (DMP-30)	Electron Microscopy Sciences	Cat #13600
5-(pentafluoro-benzoylamino) fluorescein di-β-D-glucopyranoside (PFB-FDGluc)	Life Technologies	Cat #P11947
4-methylumbelliferyl β-glucopyranoside (4-MU-Gluc)	Chem-Impex Int'l Inc.	Cat #21630
Critical commercial assays		
CellTag 700	Li-Cor Biosciences	Cat #926-41090
Concanavalin A (CON-A), biotinylated	Vector Laboratories	Cat #B-1005-5
DNeasy Blood and Tissue Kit	QIAGEN	Cat #69504
Duolink In Situ Red Starter Kit Mouse/Rabbit	Sigma Aldrich	Cat #92101
Endoglycosidase H	New England Biolabs	Cat #P0702L
HIV1-p24 Antigen ELISA Kit	Zeptometrix	Cat #0801111
Pierce BCA Protein Assay Kit	Thermo Fisher Scientific	Cat #23227
PureLink Genomic DNA Kit	Invitrogen	Cat #K182002

RevertAid First Strand cDNA Synthesis Kit	Thermo Fisher Scientific	Cat #K1621
RNeasy Mini Prep Kit	QIAGEN	Cat #74104
T7EI Endonuclease I assay kit	Genecopoeia	Cat #IC005
Quantitative RT-PCR: SNCA (ID: Hs00240906_m1)	Thermo Fisher Scientific	Cat #4331182
Quantitative RT-PCR: GRP78 (ID: Hs99999174_m1)	Thermo Fisher Scientific	Cat #4331182
Quantitative RT-PCR: CANX (ID: Hs01558409_m1)	Thermo Fisher Scientific	Cat #4331182
Quantitative RT-PCR: EDEM1 (ID: Hs00976004_m1)	Thermo Fisher Scientific	Cat #4331182
Quantitative RT-PCR: XBP1-S (ID: Hs03929085_g1)	Thermo Fisher Scientific	Cat #4331182
Quantitative RT-PCR: RyR3 (ID: Hs00168821_m1)	Thermo Fisher Scientific	Cat #4331182
Quantitative RT-PCR: Nanog (ID: Hs04399610_g1)	Thermo Fisher Scientific	Cat #4331182
Quantitative RT-PCR: Puromycin (Custom Assay# gi763524_CCN1FIY)	Thermo Fisher Scientific	Cat #4331182
Quantitative RT-PCR: RNAseP (ID: 4403326)	Thermo Fisher Scientific	Cat #4331182
Quantitative RT-PCR: ACTB (β-actin) (ID: Hs99999903_m1)	Thermo Fisher Scientific	Cat #4331182
Quantitative RT-PCR: GAPDH (ID: Hs02758991_g1)	Thermo Fisher Scientific	Cat #4331182
Experimental models: Cell lines		
H4 neuroglioma cells	Mazzulli et al., 2011; From: Pamela McLean (Mayo Clinic, Jacksonville, Florida, USA)	N/A
iPSC-derived midbrain neurons: GM15845 (Control), GM15010 (*SNCA* Triplication, 3x-1), ND00196 (*SNCA* Triplication, 3x-2), ND00139 (*SNCA* Triplication, 3x-4), and isogenic controls	Stojkovska et al., 2021 (under review); Coriell Cell Repository	N/A
iPSC-derived midbrain neurons: ND34391 (*SNCA* Triplication, Est. 3X).	Mazzulli et al., 2016a; Zunke et al., 2018; Cuddy et al., 2019; Coriell Cell Repository	N/A
iPSC-derived midbrain neurons: GD patients (N370S / 84GG or L444P / L444P)	Mazzulli et al., 2011; Mazzulli et al., 2016a; Coriell Cell Repository	N/A
iPSC-derived midbrain neurons: A53T alpha-synuclein and isogenic control	Soldner et al., 2011	N/A
Recombinant DNA		
pCXLE-hOCT3/4-shp53-F	Addgene	Cat #27077
pCXLE-hUL	Addgene	Cat #27080
pCXLE-hSK	Addgene	Cat #27078
PITX3-2A-eGFP-PGK-Puro	Addgene	Cat #31943
Cas9-nickase plasmid PX335	Addgene	Cat #42335

pLKO.1 scrambled (scrb) shRNA	N/A (gift from J. Mazzulli)	N/A
pLKO.1 RyR3 shRNA (clone ID #TRCN0000053349)	Sigma	Cat #NM_001036
pER4-ykt6-CS	Stojkovska et al., 2021 (under review)	N/A
Software and algorithms		
GraphPad Prism V6.0 software	https://www.graphpad.com/scientific-software/prism/	N/A
ImageJ / Fiji V1.0 software	https://imagej.net/software/fiji/	N/A
Nikon NIS Elements	Nikon; https://www.microscope.healthcare.nikon.com/products/software/nis-elements	N/A
Odyssey software (Image Studio V3.1.4)	Li-Cor Biosciences; https://www.licor.com/bio/image-studio/	N/A
Snapgene V5.3 software	https://www.snapgene.com	N/A
STRING online tool	https://string-db.org	N/A
Other		
Concanavalin-A, biotinylated	Vector Laboratories	Cat #B-1005-5
DAPI Fluoromount mounting media	Southern Biotech	Cat #0100-20
Intercept blocking buffer	Li-Cor Biosciences	Cat #927-70001
Lenti-X concentrator	Clontech	Cat #631232
Lipofectamine 3000	Thermo Fisher Scientific	Cat #L3000008
Matrigel	Fisher	Cat #CB-40234
mTeSR1 media	StemCell Technologies	Cat #85850
Neurobasal SM1 media	Thermo Fisher Scientific	Cat #21103-049
NeuroCult SM1 supplement	StemCell Technologies	Cat #05711
NeutrAvidin agarose beads	Thermo Fisher Scientific	Cat #29204
PVDF transfer membrane, 0.45 mm pore size	Millipore	Cat #IPFL00010
X-tremeGENE HP DNA Transfection Reagent	Roche	Cat #6366236001

Table S3. List of oligonucleotides used in the study.

OLIGONUCLEOTIDES	SOURCE
CRISPR/mutCas9 guide RNAs	
5'-AGCAGCCACAACTCCCTCCTTGG-3'	Cuddy et al., 2019; designed with http://crispr.mit.edu
5'- TGAGAAAACCAAACAGGGTGTGG-3'	Cuddy et al., 2019; designed with http://crispr.mit.edu
PCR primers for iPSC reprogramming factor transgenes	
Oct3/4 Fwd: CCTCACTTCACTGCACTGTA Rev: CATAGCGTAAAAGGAGCAACA	Stojkovska et al., 2021 (under review); Generation: Integrated DNA Technologies
Sox2 Fwd: GCAACGTGCTGGTTATTGTG Rev: GACCACACCATGAAGGCATTCATGGG	Stojkovska et al., 2021 (under review); Generation: Integrated DNA Technologies
Klf4 Fwd: GATGAACTGACCAGGCACTA Rev: CATAGCGTAAAAGGAGCAACA	Stojkovska et al., 2021 (under review); Generation: Integrated DNA Technologies
L-Myc Fwd: GCAACGTGCTGGTTATTGTG Rev: GATGGCACCAGCTCGAATTTC	Stojkovska et al., 2021 (under review); Generation: Integrated DNA Technologies
PCR primers to validate PGK-puromycin insertion	
5' Fwd: CATAAAATCTGTCTGCCCGCTCTC 5' Rev: GTGGGCTTGTACTCGGTC	Stojkovska et al., 2021 (under review); Generation: Integrated DNA Technologies
3' Fwd: CTTCTACGAGCGGCTCGGCTT 3' Rev: TGTGGTCATCCTCCACCTGACT	Stojkovska et al., 2021 (under review); Generation: Integrated DNA Technologies
Sequencing primers for CRISPR/Cas9 off-targets on genomic DNA	
SLC26A1 Fwd: CCTTCTACGAGGATGCCACAGAGT Rev: GCCTTCTGGAAACACAGAGACCCT	Zunke et al., 2018; Generation: Integrated DNA Technologies
SNCG Fwd: ATCGGCGTCAATAGGAGGCATC Rev: GGCCTCTTCCTGCTGTGTCT	Zunke et al., 2018; Generation: Integrated DNA Technologies
SEMA4B Fwd: GAGAGGACCAGGGTGCAGTTAG Rev: GATCACCGAGGGTACCAGTCCC	Zunke et al., 2018; Generation: Integrated DNA Technologies
ARHGAP32 Fwd: GGCCTGGGTTCCAATTCTGACT Rev: GAACGTGCCCAGAACAACCGAA	Zunke et al., 2018; Generation: Integrated DNA Technologies
SLC29A3 Fwd: GCATTCACATGTGCATGGTGCC Rev: AGGAAGGAGGCATGGACAGTGA	Zunke et al., 2018; Generation: Integrated DNA Technologies
ADAMTSL4 Fwd: GGTGGTGTCTGGCGTTCTGT Rev: TCCCTCCTCCTTCCAAGTGCAG	Zunke et al., 2018; Generation: Integrated DNA Technologies
TSC2 Fwd: TGCTCTGCTCTCTGCTCCATGGTA Rev: TCGCAGGTGAAGGGACAGTTTC	Zunke et al., 2018; Generation: Integrated DNA Technologies
SNCB Fwd: AGCTGGGGAAGGGGATGGAAA Rev: CTTTCATCACTGCACTGGTCCCTG	Zunke et al., 2018; Generation: Integrated DNA Technologies

ATG9B Fwd: TTGCAGCTGCGCCACTTCAA Rev: GCGCTTCACATCCATAAGGGCA	Zunke et al., 2018; Generation: Integrated DNA Technologies
Primers for semi-quantitative RT-PCR analysis of XBP1 mRNA	
Fwd: TTACGAGAGAAAACTCATGGCC Rev: GGGTCCAAGTTGTCCAGAATGC	Stojkovska et al., 2021 (under review); Generation: Integrated DNA Technologies
Primers for *GBA1* amplification	
Fwd: TGTGTGCAAGGTCCAGGATCAG Rev: ACCACCTAGAGGGGAAAGTG	Stojkovska et al., 2021 (under review); Generation: Integrated DNA Technologies
Sequencing primers for *GBA1* genotyping	
Exon 8 Fwd: AGTTCCAGAAGCCTGTGTGC Rev: CTTCTGTCAGTCTTTGGTGAAA	Stojkovska et al., 2021 (under review); Generation: Integrated DNA Technologies
Exon 9 Fwd: CCCACATGTGACCCTTACCT Rev: TGTAGGAGATGATAGGCCTGGT	Stojkovska et al., 2021 (under review); Generation: Integrated DNA Technologies
Exons 10+11 Fwd: GGGTCCGTGGGTGGGT Rev: TGCTGTGCCCTCTTTAGTCA	Stojkovska et al., 2021 (under review); Generation: Integrated DNA Technologies

Table S4. Recipes for buffers, solutions and cell culture media.

BUFFER, SOLUTION, OR MEDIA	FINAL CONCENTRATION	AMOUNT
1% Triton Base Buffer		
Triton X-100	1%	0.5 mL
5M NaCl	150 mM	1.5 mL
1M HEPES pH 7.4	20 mM	1 mL
0.5M EDTA	1 mM	100 µL
1M $MgCl_2$	1.5 mM	75 µL
100% Glycerol	10%	5 mL
milliQ H_2O	n/a	41.825 mL
Total		**50 mL**
Triton Extraction Buffer		
1% Triton Base Buffer	n/a	4.425 mL
PIC	n/a	½ tablet
500 mM NaF	50 mM	500 µl
200 mM Na_3VO_4	2 mM	50 µl
0.1M PMSF	0.5 mM	25 µl
Total		**5 mL**
2% SDS Base Buffer		
10% SDS	2%	10 mL
1M Tris pH 7.4	50 mM	2.5 mL
milliQ H_2O	n/a	37.5 mL
Total		**50 mL**
SDS Extraction Buffer		
2% SDS Base Buffer	n/a	5 mL
PIC	n/a	½ tablet
Total		**5 mL**
Sucrose HEPES Lysis Buffer		
Sucrose	0.25 M	171 g
HEPES pH 7.4	10 mM	4.766 g
EDTA	0.01 M	7.4 g
Total		**2 L**
CHAPS Lysis Buffer		
CHAPS	0.30%	150 mg
5M NaCl	120 mM	1.2 mL
1M HEPES pH 7.4	40 mM	2 mL
0.5M EDTA	1 mM	0.1 mL
glycerol	10% v/v	5 mL
milliQ H_2O	n/a	41.7 mL
Total		**50 mL**
PFA Fixative Solution		
10% Formaldehyde (PFA)	0.40%	2 mL
10X PBS	1X	5 mL
milliQ H_2O	n/a	43 mL
Total		**50 mL**

PFA Fixative Solution		
10% Formaldehyde (PFA)	4%	4 mL
10X PBS	1X	1 mL
milliQ H_2O	n/a	5 mL
Total		**10 mL**
5X Laemmli SDS Sample Buffer		
0.5M Tris-HCl pH 6.8	100 mM	2 mL
2-mercaptoethanol	900 mM	630 µL
Glycerol	20%	2 mL
SDS	10%	1 g
Bromophenol Blue	0.02%	1.5 mg
Total		**10 mL**
Media for iPSC dopaminergic neurons		
SM1 neurobasal media	n/a	480 mL
Penicillin / Streptomycin	1%	5 mL
L-Glutamine	1%	5 mL
SM1 supplement	n/a	10 mL
Total		**500 mL**
Media for H4 neuroglioma cells		
Optimem	n/a	466 mL
Heat-inactivated FBS	5%	25 mL
Geneticin (G1418)	200 µg/ml	2 mL
Hygromycin B	200 µg/ml	2 mL
Penicillin / Streptomycin	1%	5 mL
Total		**500 mL**
KSR media		
KO DMEM	n/a	85 mL
Knockout serum (KOSR)	15%	15 mL
L-Glutamine	1%	1 mL
MEM-NEAA	1%	1 mL
Penicillin / Streptomycin	1%	1 mL
2-mercaptoethanol	55 mM	182 µL

REFERENCES

Abeliovich, A., Schmitz, Y., Farinas, I., Choi-Lundberg, D., Ho, W.H., Castillo, P.E., Shinsky, N., Verdugo, J.M., Armanini, M., Ryan, A., et al. (2000). Mice lacking alpha-synuclein display functional deficits in the nigrostriatal dopamine system. Neuron *25*, 239-252. 10.1016/s0896-6273(00)80886-7.

Alexander, G.E. (2004). Biology of Parkinson's disease: pathogenesis and pathophysiology of a multisystem neurodegenerative disorder. Dialogues Clin Neurosci *6*, 259-280.

Apicco, D.J., Shlevkov, E., Nezich, C.L., Tran, D.T., Guilmette, E., Nicholatos, J.W., Bantle, C.M., Chen, Y., Glajch, K.E., Abraham, N.A., et al. (2021). The Parkinson's disease-associated gene ITPKB protects against alpha-synuclein aggregation by regulating ER-to-mitochondria calcium release. Proc Natl Acad Sci U S A *118*. 10.1073/pnas.2006476118.

Bellucci, A., Navarria, L., Zaltieri, M., Falarti, E., Bodei, S., Sigala, S., Battistin, L., Spillantini, M., Missale, C., and Spano, P. (2011). Induction of the unfolded protein response by alpha-synuclein in experimental models of Parkinson's disease. J Neurochem *116*, 588-605. 10.1111/j.1471-4159.2010.07143.x.

Bendikov-Bar, I., Ron, I., Filocamo, M., and Horowitz, M. (2011). Characterization of the ERAD process of the L444P mutant glucocerebrosidase variant. Blood Cells Mol Dis *46*, 4-10. 10.1016/j.bcmd.2010.10.012.

Bergmann, J.E., and Grabowski, G.A. (1989). Posttranslational processing of human lysosomal acid beta-glucosidase: a continuum of defects in Gaucher disease type 1 and type 2 fibroblasts. Am J Hum Genet *44*, 741-750.

Birkmayer, W., and Hornykiewicz, O. (1961). [The L-3,4-dioxyphenylalanine (DOPA)-effect in Parkinson-akinesia]. Wien Klin Wochenschr *73*, 787-788.

Booth, C., and Koch, G.L. (1989). Perturbation of cellular calcium induces secretion of luminal ER proteins. Cell *59*, 729-737. 10.1016/0092-8674(89)90019-6.

Brady, R.O., Gal, A.E., Kanfer, J.N., and Bradley, R.M. (1965). The metabolism of glucocerebrosides. 3. Purification and properties of a glucosyl- and galactosylceramide-cleaving enzyme from rat intestinal tissue. J Biol Chem *240*, 3766-3770.

Brockmann, K., Srulijes, K., Hauser, A.K., Schulte, C., Csoti, I., Gasser, T., and Berg, D. (2011). GBA-associated PD presents with nonmotor characteristics. Neurology *77*, 276-280. 10.1212/WNL.0b013e318225ab77.

Burre, J., Sharma, M., and Sudhof, T.C. (2014). alpha-Synuclein assembles into higher-order multimers upon membrane binding to promote SNARE complex formation. Proc Natl Acad Sci U S A *111*, E4274-4283. 10.1073/pnas.1416598111.

Burre, J., Sharma, M., Tsetsenis, T., Buchman, V., Etherton, M.R., and Sudhof, T.C. (2010). Alpha-synuclein promotes SNARE-complex assembly in vivo and in vitro. Science *329*, 1663-1667. 10.1126/science.1195227.

Butler, E.K., Voigt, A., Lutz, A.K., Toegel, J.P., Gerhardt, E., Karsten, P., Falkenburger, B., Reinartz, A., Winklhofer, K.F., and Schulz, J.B. (2012). The mitochondrial chaperone protein TRAP1 mitigates alpha-Synuclein toxicity. PLoS Genet *8*, e1002488. 10.1371/journal.pgen.1002488.

Calfon, M., Zeng, H., Urano, F., Till, J.H., Hubbard, S.R., Harding, H.P., Clark, S.G., and Ron, D. (2002). IRE1 couples endoplasmic reticulum load to secretory capacity by processing the XBP-1 mRNA. Nature *415*, 92-96. 10.1038/415092a.

Caraveo, G., Auluck, P.K., Whitesell, L., Chung, C.Y., Baru, V., Mosharov, E.V., Yan, X., Ben-Johny, M., Soste, M., Picotti, P., et al. (2014). Calcineurin determines toxic versus beneficial responses to alpha-synuclein. Proc Natl Acad Sci U S A *111*, E3544-3552. 10.1073/pnas.1413201111.

Chandra, S., Gallardo, G., Fernandez-Chacon, R., Schluter, O.M., and Sudhof, T.C. (2005). Alpha-synuclein cooperates with CSPalpha in preventing neurodegeneration. Cell *123*, 383-396. 10.1016/j.cell.2005.09.028.

Chang, D., Nalls, M.A., Hallgrimsdottir, I.B., Hunkapiller, J., van der Brug, M., Cai, F., International Parkinson's Disease Genomics, C., andMe Research, T., Kerchner, G.A., Ayalon, G., et al. (2017). A meta-analysis of genome-wide association studies identifies 17 new Parkinson's disease risk loci. Nat Genet *49*, 1511-1516. 10.1038/ng.3955.

Chartier-Harlin, M.C., Kachergus, J., Roumier, C., Mouroux, V., Douay, X., Lincoln, S., Levecque, C., Larvor, L., Andrieux, J., Hulihan, M., et al. (2004). Alpha-synuclein locus duplication as a cause of familial Parkinson's disease. Lancet *364*, 1167-1169. 10.1016/S0140-6736(04)17103-1.

Chinta, S.J., Mallajosyula, J.K., Rane, A., and Andersen, J.K. (2010). Mitochondrial alpha-synuclein accumulation impairs complex I function in dopaminergic neurons and results in increased mitophagy in vivo. Neurosci Lett *486*, 235-239. 10.1016/j.neulet.2010.09.061.

Chung, C.Y., Khurana, V., Auluck, P.K., Tardiff, D.F., Mazzulli, J.R., Soldner, F., Baru, V., Lou, Y., Freyzon, Y., Cho, S., et al. (2013). Identification and rescue of α-synuclein toxicity in Parkinson patient-derived neurons. Science (New York, N.Y.) *342*, 983-987. 10.1126/science.1245296.

Clayton, D.F., and George, J.M. (1999). Synucleins in synaptic plasticity and neurodegenerative disorders. J Neurosci Res *58*, 120-129.

Cleeter, M.W., Chau, K.Y., Gluck, C., Mehta, A., Hughes, D.A., Duchen, M., Wood, N.W., Hardy, J., Mark Cooper, J., and Schapira, A.H. (2013). Glucocerebrosidase inhibition causes mitochondrial dysfunction and free radical damage. Neurochem Int *62*, 1-7. 10.1016/j.neuint.2012.10.010.

Colla, E., Coune, P., Liu, Y., Pletnikova, O., Troncoso, J.C., Iwatsubo, T., Schneider, B.L., and Lee, M.K. (2012a). Endoplasmic reticulum stress is important for the manifestations of α-synucleinopathy in vivo. The Journal of neuroscience : the official journal of the Society for Neuroscience *32*, 3306-3320. 10.1523/JNEUROSCI.5367-11.2012.

Colla, E., Jensen, P.H., Pletnikova, O., Troncoso, J.C., Glabe, C., and Lee, M.K. (2012b). Accumulation of toxic alpha-synuclein oligomer within endoplasmic reticulum occurs in alpha-synucleinopathy in vivo. J Neurosci *32*, 3301-3305. 10.1523/JNEUROSCI.5368-11.2012.

Colla, E., Panattoni, G., Ricci, A., Rizzi, C., Rota, L., Carucci, N., Valvano, V., Gobbo, F., Capsoni, S., Lee, M.K., and Cattaneo, A. (2018). Toxic properties of microsome-associated alpha-synuclein species in mouse primary neurons. Neurobiol Dis *111*, 36-47. 10.1016/j.nbd.2017.12.004.

Conway, K.A., Harper, J.D., and Lansbury, P.T. (1998). Accelerated in vitro fibril formation by a mutant alpha-synuclein linked to early-onset Parkinson disease. Nat Med *4*, 1318-1320. 10.1038/3311.

Cookson, M.R. (2016). Cellular functions of LRRK2 implicate vesicular trafficking pathways in Parkinson's disease. Biochem Soc Trans *44*, 1603-1610. 10.1042/BST20160228.

Cooper, A.A., Gitler, A.D., Cashikar, A., Haynes, C.M., Hill, K.J., Bhullar, B., Liu, K., Xu, K., Strathearn, K.E., Liu, F., et al. (2006). Alpha-synuclein blocks ER-Golgi traffic and Rab1 rescues neuron loss in Parkinson's models. Science *313*, 324-328. 10.1126/science.1129462.

Credle, J.J., Forcelli, P.A., Delannoy, M., Oaks, A.W., Permaul, E., Berry, D.L., Duka, V., Wills, J., and Sidhu, A. (2015). alpha-Synuclein-mediated inhibition of ATF6 processing into COPII vesicles disrupts UPR signaling in Parkinson's disease. Neurobiol Dis *76*, 112-125. 10.1016/j.nbd.2015.02.005.

Cuddy, L.K., Wani, W.Y., Morella, M.L., Pitcairn, C., Tsutsumi, K., Fredriksen, K., Justman, C.J., Grammatopoulos, T.N., Belur, N.R., Zunke, F., et al. (2019). Stress-Induced Cellular Clearance Is Mediated by the SNARE Protein ykt6 and Disrupted by alpha-Synuclein. Neuron *104*, 869-884 e811. 10.1016/j.neuron.2019.09.001.

Cuervo, A.M., Stefanis, L., Fredenburg, R., Lansbury, P.T., and Sulzer, D. (2004). Impaired degradation of mutant alpha-synuclein by chaperone-mediated autophagy. Science *305*, 1292-1295. 10.1126/science.1101738.

Cullen, V., Sardi, S.P., Ng, J., Xu, Y.H., Sun, Y., Tomlinson, J.J., Kolodziej, P., Kahn, I., Saftig, P., Woulfe, J., et al. (2011). Acid beta-glucosidase mutants linked to Gaucher disease, Parkinson disease, and Lewy body dementia alter alpha-synuclein processing. Ann Neurol *69*, 940-953. 10.1002/ana.22400.

Devi, L., Raghavendran, V., Prabhu, B.M., Avadhani, N.G., and Anandatheerthavarada, H.K. (2008). Mitochondrial import and accumulation of alpha-synuclein impair complex I in human dopaminergic neuronal cultures and Parkinson disease brain. J Biol Chem *283*, 9089-9100. 10.1074/jbc.M710012200.

Di Maio, R., Barrett, P.J., Hoffman, E.K., Barrett, C.W., Zharikov, A., Borah, A., Hu, X., McCoy, J., Chu, C.T., Burton, E.A., et al. (2016). alpha-Synuclein binds to TOM20 and inhibits mitochondrial protein import in Parkinson's disease. Sci Transl Med *8*, 342ra378. 10.1126/scitranslmed.aaf3634.

Dikic, I. (2018). Open questions: why should we care about ER-phagy and ER remodelling? BMC Biol *16*, 131. 10.1186/s12915-018-0603-7.

El-Agnaf, O.M., Salem, S.A., Paleologou, K.E., Curran, M.D., Gibson, M.J., Court, J.A., Schlossmacher, M.G., and Allsop, D. (2006). Detection of oligomeric forms of alpha-synuclein protein in human plasma as a potential biomarker for Parkinson's disease. FASEB J *20*, 419-425. 10.1096/fj.03-1449com.

Emanuele, M., and Chieregatti, E. (2015). Mechanisms of alpha-synuclein action on neurotransmission: cell-autonomous and non-cell autonomous role. Biomolecules *5*, 865-892. 10.3390/biom5020865.

Farfel-Becker, T., Vitner, E.B., Kelly, S.L., Bame, J.R., Duan, J., Shinder, V., Merrill, A.H., Jr., Dobrenis, K., and Futerman, A.H. (2014). Neuronal accumulation of glucosylceramide in a mouse model of neuronopathic Gaucher disease leads to neurodegeneration. Hum Mol Genet *23*, 843-854. 10.1093/hmg/ddt468.

Fernandes, H.J.R., Hartfield, E.M., Christian, H.C., Emmanoulidou, E., Zheng, Y., Booth, H., Bogetofte, H., Lang, C., Ryan, B.J., Sardi, S.P., et al. (2016). ER Stress and Autophagic Perturbations Lead to Elevated Extracellular α-Synuclein in GBA-N370S Parkinson's

iPSC-Derived Dopamine Neurons. Stem cell reports *6*, 342-356. 10.1016/j.stemcr.2016.01.013.

Forno, L.S. (1996). Neuropathology of Parkinson's disease. J Neuropathol Exp Neurol *55*, 259-272.

Fruen, B.R., Mickelson, J.R., and Louis, C.F. (1997). Dantrolene inhibition of sarcoplasmic reticulum Ca2+ release by direct and specific action at skeletal muscle ryanodine receptors. J Biol Chem *272*, 26965-26971. 10.1074/jbc.272.43.26965.

Fuchs, J., Nilsson, C., Kachergus, J., Munz, M., Larsson, E.M., Schule, B., Langston, J.W., Middleton, F.A., Ross, O.A., Hulihan, M., et al. (2007). Phenotypic variation in a large Swedish pedigree due to SNCA duplication and triplication. Neurology *68*, 916-922. 10.1212/01.wnl.0000254458.17630.c5.

Fujiwara, T., Oda, K., Yokota, S., Takatsuki, A., and Ikehara, Y. (1988). Brefeldin A causes disassembly of the Golgi complex and accumulation of secretory proteins in the endoplasmic reticulum. J Biol Chem *263*, 18545-18552.

Garcia-Sanz, P., Orgaz, L., Bueno-Gil, G., Espadas, I., Rodriguez-Traver, E., Kulisevsky, J., Gutierrez, A., Davila, J.C., Gonzalez-Polo, R.A., Fuentes, J.M., et al. (2017). N370S-GBA1 mutation causes lysosomal cholesterol accumulation in Parkinson's disease. Mov Disord *32*, 1409-1422. 10.1002/mds.27119.

Gautier, C.A., Kitada, T., and Shen, J. (2008). Loss of PINK1 causes mitochondrial functional defects and increased sensitivity to oxidative stress. Proc Natl Acad Sci U S A *105*, 11364-11369. 10.1073/pnas.0802076105.

Gegg, M.E., Burke, D., Heales, S.J., Cooper, J.M., Hardy, J., Wood, N.W., and Schapira, A.H. (2012). Glucocerebrosidase deficiency in substantia nigra of parkinson disease brains. Ann Neurol *72*, 455-463. 10.1002/ana.23614.

Ghosh, D., Mondal, M., Mohite, G.M., Singh, P.K., Ranjan, P., Anoop, A., Ghosh, S., Jha, N.N., Kumar, A., and Maji, S.K. (2013). The Parkinson's disease-associated H50Q mutation accelerates alpha-Synuclein aggregation in vitro. Biochemistry *52*, 6925-6927. 10.1021/bi400999d.

Giannini, G., Conti, A., Mammarella, S., Scrobogna, M., and Sorrentino, V. (1995). The ryanodine receptor/calcium channel genes are widely and differentially expressed in murine brain and peripheral tissues. J Cell Biol *128*, 893-904. 10.1083/jcb.128.5.893.

Giasson, B.I., Duda, J.E., Quinn, S.M., Zhang, B., Trojanowski, J.Q., and Lee, V.M. (2002). Neuronal alpha-synucleinopathy with severe movement disorder in mice expressing A53T human alpha-synuclein. Neuron *34*, 521-533. 10.1016/s0896-6273(02)00682-7.

Gitler, A.D., Bevis, B.J., Shorter, J., Strathearn, K.E., Hamamichi, S., Su, L.J., Caldwell, K.A., Caldwell, G.A., Rochet, J.C., McCaffery, J.M., et al. (2008). The Parkinson's disease protein alpha-synuclein disrupts cellular Rab homeostasis. Proc Natl Acad Sci U S A *105*, 145-150. 10.1073/pnas.0710685105.

Goker-Alpan, O., Schiffmann, R., LaMarca, M.E., Nussbaum, R.L., McInerney-Leo, A., and Sidransky, E. (2004). Parkinsonism among Gaucher disease carriers. J Med Genet *41*, 937-940. 10.1136/jmg.2004.024455.

Gorbatyuk, M.S., Shabashvili, A., Chen, W., Meyers, C., Sullivan, L.F., Salganik, M., Lin, J.H., Lewin, A.S., Muzyczka, N., and Gorbatyuk, O.S. (2012). Glucose regulated protein 78 diminishes alpha-synuclein neurotoxicity in a rat model of Parkinson disease. Mol Ther *20*, 1327-1337. 10.1038/mt.2012.28.

Gosavi, N., Lee, H.J., Lee, J.S., Patel, S., and Lee, S.J. (2002). Golgi fragmentation occurs in the cells with prefibrillar alpha-synuclein aggregates and precedes the formation of fibrillar inclusion. J Biol Chem *277*, 48984-48992. 10.1074/jbc.M208194200.

Grabowski, G.A. (2008). Phenotype, diagnosis, and treatment of Gaucher's disease. Lancet *372*, 1263-1271. 10.1016/S0140-6736(08)61522-6.

Grace, M.E., Newman, K.M., Scheinker, V., Berg-Fussman, A., and Grabowski, G.A. (1994). Analysis of human acid beta-glucosidase by site-directed mutagenesis and heterologous expression. J Biol Chem *269*, 2283-2291.

Grandjean, J.M.D., Madhavan, A., Cech, L., Seguinot, B.O., Paxman, R.J., Smith, E., Scampavia, L., Powers, E.T., Cooley, C.B., Plate, L., et al. (2020). Pharmacologic IRE1/XBP1s activation confers targeted ER proteostasis reprogramming. Nat Chem Biol *16*, 1052-1061. 10.1038/s41589-020-0584-z.

Greenbaum, E.A., Graves, C.L., Mishizen-Eberz, A.J., Lupoli, M.A., Lynch, D.R., Englander, S.W., Axelsen, P.H., and Giasson, B.I. (2005). The E46K mutation in alpha-synuclein increases amyloid fibril formation. J Biol Chem *280*, 7800-7807. 10.1074/jbc.M411638200.

Grumati, P., Dikic, I., and Stolz, A. (2018). ER-phagy at a glance. J Cell Sci *131*. 10.1242/jcs.217364.

Guardia-Laguarta, C., Area-Gomez, E., Rub, C., Liu, Y., Magrane, J., Becker, D., Voos, W., Schon, E.A., and Przedborski, S. (2014). alpha-Synuclein is localized to mitochondria-associated ER membranes. J Neurosci *34*, 249-259. 10.1523/JNEUROSCI.2507-13.2014.

Guzman, J.N., Sanchez-Padilla, J., Wokosin, D., Kondapalli, J., Ilijic, E., Schumacker, P.T., and Surmeier, D.J. (2010). Oxidant stress evoked by pacemaking in dopaminergic neurons is attenuated by DJ-1. Nature *468*, 696-700. 10.1038/nature09536.

Ha, T.W., Jeong, J.H., Shin, H., Kim, H.K., Im, J.S., Song, B.H., Hanna, J., Oh, J.S., Woo, D.H., Han, J., and Lee, M.R. (2020). Characterization of Endoplasmic Reticulum (ER) in Human Pluripotent Stem Cells Revealed Increased Susceptibility to Cell Death upon ER Stress. Cells *9*. 10.3390/cells9051078.

Haas, R.H., Nasirian, F., Nakano, K., Ward, D., Pay, M., Hill, R., and Shults, C.W. (1995). Low platelet mitochondrial complex I and complex II/III activity in early untreated Parkinson's disease. Ann Neurol *37*, 714-722. 10.1002/ana.410370604.

Hao, L.Y., Giasson, B.I., and Bonini, N.M. (2010). DJ-1 is critical for mitochondrial function and rescues PINK1 loss of function. Proc Natl Acad Sci U S A *107*, 9747-9752. 10.1073/pnas.0911175107.

Harding, H.P., Zhang, Y., and Ron, D. (1999). Protein translation and folding are coupled by an endoplasmic-reticulum-resident kinase. Nature *397*, 271-274. 10.1038/16729.

Helms, J.B., and Rothman, J.E. (1992). Inhibition by brefeldin A of a Golgi membrane enzyme that catalyses exchange of guanine nucleotide bound to ARF. Nature *360*, 352-354. 10.1038/360352a0.

Heman-Ackah, S.M., Manzano, R., Hoozemans, J.J.M., Scheper, W., Flynn, R., Haerty, W., Cowley, S.A., Bassett, A.R., and Wood, M.J.A. (2017). Alpha-synuclein induces the unfolded protein response in Parkinson's disease SNCA triplication iPSC-derived neurons. Hum Mol Genet *26*, 4441-4450. 10.1093/hmg/ddx331.

Hernandez, I., Luna, G., Rauch, J.N., Reis, S.A., Giroux, M., Karch, C.M., Boctor, D., Sibih, Y.E., Storm, N.J., Diaz, A., et al. (2019). A farnesyltransferase inhibitor activates

lysosomes and reduces tau pathology in mice with tauopathy. Sci Transl Med *11*. 10.1126/scitranslmed.aat3005.

Hidvegi, T., Schmidt, B.Z., Hale, P., and Perlmutter, D.H. (2005). Accumulation of mutant alpha1-antitrypsin Z in the endoplasmic reticulum activates caspases-4 and -12, NFkappaB, and BAP31 but not the unfolded protein response. J Biol Chem *280*, 39002-39015. 10.1074/jbc.M508652200.

Holtz, W.A., and O'Malley, K.L. (2003). Parkinsonian mimetics induce aspects of unfolded protein response in death of dopaminergic neurons. J Biol Chem *278*, 19367-19377. 10.1074/jbc.M211821200.

Hoozemans, J.J., van Haastert, E.S., Eikelenboom, P., de Vos, R.A., Rozemuller, J.M., and Scheper, W. (2007). Activation of the unfolded protein response in Parkinson's disease. Biochem Biophys Res Commun *354*, 707-711. 10.1016/j.bbrc.2007.01.043.

Hubner, C.A., and Dikic, I. (2020). ER-phagy and human diseases. Cell Death Differ *27*, 833-842. 10.1038/s41418-019-0444-0.

Hunn, B.H., Cragg, S.J., Bolam, J.P., Spillantini, M.G., and Wade-Martins, R. (2015). Impaired intracellular trafficking defines early Parkinson's disease. Trends Neurosci *38*, 178-188. 10.1016/j.tins.2014.12.009.

Iwai, A., Masliah, E., Yoshimoto, M., Ge, N., Flanagan, L., de Silva, H.A., Kittel, A., and Saitoh, T. (1995). The precursor protein of non-A beta component of Alzheimer's disease amyloid is a presynaptic protein of the central nervous system. Neuron *14*, 467-475. 10.1016/0896-6273(95)90302-x.

Kahle, P.J., Neumann, M., Ozmen, L., Muller, V., Jacobsen, H., Schindzielorz, A., Okochi, M., Leimer, U., van Der Putten, H., Probst, A., et al. (2000). Subcellular localization of wild-type and Parkinson's disease-associated mutant alpha -synuclein in human and transgenic mouse brain. J Neurosci *20*, 6365-6373.

Kamp, F., Exner, N., Lutz, A.K., Wender, N., Hegermann, J., Brunner, B., Nuscher, B., Bartels, T., Giese, A., Beyer, K., et al. (2010). Inhibition of mitochondrial fusion by alpha-synuclein is rescued by PINK1, Parkin and DJ-1. EMBO J *29*, 3571-3589. 10.1038/emboj.2010.223.

Kang, J.J., Hsu, K.S., and Lin-Shiau, S.Y. (1994). Effects of bipyridylium compounds on calcium release from triadic vesicles isolated from rabbit skeletal muscle. Br J Pharmacol *112*, 1216-1222. 10.1111/j.1476-5381.1994.tb13213.x.

Kim, J., Hu, C., Moufawad El Achkar, C., Black, L.E., Douville, J., Larson, A., Pendergast, M.K., Goldkind, S.F., Lee, E.A., Kuniholm, A., et al. (2019). Patient-Customized Oligonucleotide Therapy for a Rare Genetic Disease. N Engl J Med *381*, 1644-1652. 10.1056/NEJMoa1813279.

Kim, R.H., Smith, P.D., Aleyasin, H., Hayley, S., Mount, M.P., Pownall, S., Wakeham, A., You-Ten, A.J., Kalia, S.K., Horne, P., et al. (2005). Hypersensitivity of DJ-1-deficient mice to 1-methyl-4-phenyl-1,2,3,6-tetrahydropyrindine (MPTP) and oxidative stress. Proc Natl Acad Sci U S A *102*, 5215-5220. 10.1073/pnas.0501282102.

Koch, G.L., Booth, C., and Wooding, F.B. (1988). Dissociation and re-assembly of the endoplasmic reticulum in live cells. J Cell Sci *91 (Pt 4)*, 511-522.

Korkotian, E., Schwarz, A., Pelled, D., Schwarzmann, G., Segal, M., and Futerman, A.H. (1999). Elevation of intracellular glucosylceramide levels results in an increase in endoplasmic

reticulum density and in functional calcium stores in cultured neurons. J Biol Chem *274*, 21673-21678.
Korkotian, E., and Segal, M. (1999). Release of calcium from stores alters the morphology of dendritic spines in cultured hippocampal neurons. Proc Natl Acad Sci U S A *96*, 12068-12072. 10.1073/pnas.96.21.12068.
Kozutsumi, Y., Segal, M., Normington, K., Gething, M.J., and Sambrook, J. (1988). The presence of malfolded proteins in the endoplasmic reticulum signals the induction of glucose-regulated proteins. Nature *332*, 462-464. 10.1038/332462a0.
Kriks, S., Shim, J.W., Piao, J., Ganat, Y.M., Wakeman, D.R., Xie, Z., Carrillo-Reid, L., Auyeung, G., Antonacci, C., Buch, A., et al. (2011). Dopamine neurons derived from human ES cells efficiently engraft in animal models of Parkinson's disease. Nature *480*, 547-551. 10.1038/nature10648.
Lee, A.H., Iwakoshi, N.N., and Glimcher, L.H. (2003). XBP-1 regulates a subset of endoplasmic reticulum resident chaperone genes in the unfolded protein response. Mol Cell Biol *23*, 7448-7459. 10.1128/mcb.23.21.7448-7459.2003.
Lee, H.J., Khoshaghideh, F., Patel, S., and Lee, S.J. (2004). Clearance of alpha-synuclein oligomeric intermediates via the lysosomal degradation pathway. J Neurosci *24*, 1888-1896. 10.1523/JNEUROSCI.3809-03.2004.
Liou, B., Peng, Y., Li, R., Inskeep, V., Zhang, W., Quinn, B., Dasgupta, N., Blackwood, R., Setchell, K.D., Fleming, S., et al. (2016). Modulating ryanodine receptors with dantrolene attenuates neuronopathic phenotype in Gaucher disease mice. Hum Mol Genet *25*, 5126-5141. 10.1093/hmg/ddw322.
Lloyd-Evans, E., Pelled, D., Riebeling, C., Bodennec, J., de-Morgan, A., Waller, H., Schiffmann, R., and Futerman, A.H. (2003). Glucosylceramide and glucosylsphingosine modulate calcium mobilization from brain microsomes via different mechanisms. J Biol Chem *278*, 23594-23599. 10.1074/jbc.M300212200.
Maor, G., Rencus-Lazar, S., Filocamo, M., Steller, H., Segal, D., and Horowitz, M. (2013). Unfolded protein response in Gaucher disease: from human to Drosophila. Orphanet J Rare Dis *8*, 140. 10.1186/1750-1172-8-140.
Maroteaux, L., Campanelli, J.T., and Scheller, R.H. (1988). Synuclein: a neuron-specific protein localized to the nucleus and presynaptic nerve terminal. J Neurosci *8*, 2804-2815.
Marquardt, T., and Helenius, A. (1992). Misfolding and aggregation of newly synthesized proteins in the endoplasmic reticulum. J Cell Biol *117*, 505-513. 10.1083/jcb.117.3.505.
Martin, I., Kim, J.W., Dawson, V.L., and Dawson, T.M. (2014). LRRK2 pathobiology in Parkinson's disease. J Neurochem *131*, 554-565. 10.1111/jnc.12949.
Masliah, E., Rockenstein, E., Veinbergs, I., Mallory, M., Hashimoto, M., Takeda, A., Sagara, Y., Sisk, A., and Mucke, L. (2000). Dopaminergic loss and inclusion body formation in alpha-synuclein mice: implications for neurodegenerative disorders. Science *287*, 1265-1269. 10.1126/science.287.5456.1265.
Matsuoka, Y., Vila, M., Lincoln, S., McCormack, A., Picciano, M., LaFrancois, J., Yu, X., Dickson, D., Langston, W.J., McGowan, E., et al. (2001). Lack of nigral pathology in transgenic mice expressing human alpha-synuclein driven by the tyrosine hydroxylase promoter. Neurobiol Dis *8*, 535-539. 10.1006/nbdi.2001.0392.
Mazzulli, J.R., Xu, Y.-H., Sun, Y., Knight, A.L., McLean, P.J., Caldwell, G.A., Sidransky, E., Grabowski, G.A., and Krainc, D. (2011). Gaucher disease glucocerebrosidase and α-

synuclein form a bidirectional pathogenic loop in synucleinopathies. Cell *146*, 37-52. 10.1016/j.cell.2011.06.001.

Mazzulli, J.R., Zunke, F., Isacson, O., Studer, L., and Krainc, D. (2016). alpha-Synuclein-induced lysosomal dysfunction occurs through disruptions in protein trafficking in human midbrain synucleinopathy models. Proc Natl Acad Sci U S A *113*, 1931-1936. 10.1073/pnas.1520335113.

McNeill, A., Duran, R., Hughes, D.A., Mehta, A., and Schapira, A.H. (2012). A clinical and family history study of Parkinson's disease in heterozygous glucocerebrosidase mutation carriers. J Neurol Neurosurg Psychiatry *83*, 853-854. 10.1136/jnnp-2012-302402.

Melnick, J., Dul, J.L., and Argon, Y. (1994). Sequential interaction of the chaperones BiP and GRP94 with immunoglobulin chains in the endoplasmic reticulum. Nature *370*, 373-375. 10.1038/370373a0.

Middleton, E.R., and Rhoades, E. (2010). Effects of curvature and composition on alpha-synuclein binding to lipid vesicles. Biophys J *99*, 2279-2288. 10.1016/j.bpj.2010.07.056.

Mitsumoto, A., and Nakagawa, Y. (2001). DJ-1 is an indicator for endogenous reactive oxygen species elicited by endotoxin. Free Radic Res *35*, 885-893. 10.1080/10715760100301381.

Mu, T.W., Ong, D.S., Wang, Y.J., Balch, W.E., Yates, J.R., 3rd, Segatori, L., and Kelly, J.W. (2008). Chemical and biological approaches synergize to ameliorate protein-folding diseases. Cell *134*, 769-781. 10.1016/j.cell.2008.06.037.

Murphy, D.D., Rueter, S.M., Trojanowski, J.Q., and Lee, V.M. (2000). Synucleins are developmentally expressed, and alpha-synuclein regulates the size of the presynaptic vesicular pool in primary hippocampal neurons. J Neurosci *20*, 3214-3220.

Murphy, K.E., Gysbers, A.M., Abbott, S.K., Tayebi, N., Kim, W.S., Sidransky, E., Cooper, A., Garner, B., and Halliday, G.M. (2014). Reduced glucocerebrosidase is associated with increased alpha-synuclein in sporadic Parkinson's disease. Brain *137*, 834-848. 10.1093/brain/awt367.

Nakamura, K., Nemani, V.M., Azarbal, F., Skibinski, G., Levy, J.M., Egami, K., Munishkina, L., Zhang, J., Gardner, B., Wakabayashi, J., et al. (2011). Direct membrane association drives mitochondrial fission by the Parkinson disease-associated protein alpha-synuclein. J Biol Chem *286*, 20710-20726. 10.1074/jbc.M110.213538.

Nalls, M.A., Blauwendraat, C., Vallerga, C.L., Heilbron, K., Bandres-Ciga, S., Chang, D., Tan, M., Kia, D.A., Noyce, A.J., Xue, A., et al. (2019). Identification of novel risk loci, causal insights, and heritable risk for Parkinson's disease: a meta-analysis of genome-wide association studies. Lancet Neurol *18*, 1091-1102. 10.1016/S1474-4422(19)30320-5.

Nalls, M.A., Duran, R., Lopez, G., Kurzawa-Akanbi, M., McKeith, I.G., Chinnery, P.F., Morris, C.M., Theuns, J., Crosiers, D., Cras, P., et al. (2013). A multicenter study of glucocerebrosidase mutations in dementia with Lewy bodies. JAMA Neurol *70*, 727-735. 10.1001/jamaneurol.2013.1925.

Nalls, M.A., Pankratz, N., Lill, C.M., Do, C.B., Hernandez, D.G., Saad, M., DeStefano, A.L., Kara, E., Bras, J., Sharma, M., et al. (2014). Large-scale meta-analysis of genome-wide association data identifies six new risk loci for Parkinson's disease. Nat Genet *46*, 989-993. 10.1038/ng.3043.

Narendra, D., Tanaka, A., Suen, D.F., and Youle, R.J. (2008). Parkin is recruited selectively to impaired mitochondria and promotes their autophagy. J Cell Biol *183*, 795-803. 10.1083/jcb.200809125.

Neudorfer, O., Giladi, N., Elstein, D., Abrahamov, A., Turezkite, T., Aghai, E., Reches, A., Bembi, B., and Zimran, A. (1996). Occurrence of Parkinson's syndrome in type I Gaucher disease. QJM *89*, 691-694.

Neumann, J., Bras, J., Deas, E., O'Sullivan, S.S., Parkkinen, L., Lachmann, R.H., Li, A., Holton, J., Guerreiro, R., Paudel, R., et al. (2009). Glucocerebrosidase mutations in clinical and pathologically proven Parkinson's disease. Brain *132*, 1783-1794. 10.1093/brain/awp044.

Nussbaum, R.L., and Ellis, C.E. (2003). Alzheimer's disease and Parkinson's disease. N Engl J Med *348*, 1356-1364. 10.1056/NEJM2003ra020003.

Ong, D.S.T., Mu, T.-W., Palmer, A.E., and Kelly, J.W. (2010). Endoplasmic reticulum Ca2+ increases enhance mutant glucocerebrosidase proteostasis. Nature chemical biology *6*, 424-432. 10.1038/nchembio.368.

Osellame, L.D., Rahim, A.A., Hargreaves, I.P., Gegg, M.E., Richard-Londt, A., Brandner, S., Waddington, S.N., Schapira, A.H., and Duchen, M.R. (2013). Mitochondria and quality control defects in a mouse model of Gaucher disease--links to Parkinson's disease. Cell Metab *17*, 941-953. 10.1016/j.cmet.2013.04.014.

Ou, W.J., Cameron, P.H., Thomas, D.Y., and Bergeron, J.J. (1993). Association of folding intermediates of glycoproteins with calnexin during protein maturation. Nature *364*, 771-776. 10.1038/364771a0.

Outeiro, T.F., and Lindquist, S. (2003). Yeast cells provide insight into alpha-synuclein biology and pathobiology. Science *302*, 1772-1775. 10.1126/science.1090439.

Paillusson, S., Gomez-Suaga, P., Stoica, R., Little, D., Gissen, P., Devine, M.J., Noble, W., Hanger, D.P., and Miller, C.C.J. (2017). alpha-Synuclein binds to the ER-mitochondria tethering protein VAPB to disrupt Ca(2+) homeostasis and mitochondrial ATP production. Acta Neuropathol *134*, 129-149. 10.1007/s00401-017-1704-z.

Parker, W.D., Jr., Boyson, S.J., and Parks, J.K. (1989). Abnormalities of the electron transport chain in idiopathic Parkinson's disease. Ann Neurol *26*, 719-723. 10.1002/ana.410260606.

Parkinson, J. (2002). An essay on the shaking palsy. 1817. J Neuropsychiatry Clin Neurosci *14*, 223-236; discussion 222. 10.1176/jnp.14.2.223.

Pelled, D., Trajkovic-Bodennec, S., Lloyd-Evans, E., Sidransky, E., Schiffmann, R., and Futerman, A.H. (2005). Enhanced calcium release in the acute neuronopathic form of Gaucher disease. Neurobiol Dis *18*, 83-88. 10.1016/j.nbd.2004.09.004.

Polymeropoulos, M.H., Lavedan, C., Leroy, E., Ide, S.E., Dehejia, A., Dutra, A., Pike, B., Root, H., Rubenstein, J., Boyer, R., et al. (1997). Mutation in the alpha-synuclein gene identified in families with Parkinson's disease. Science *276*, 2045-2047.

Pozo Devoto, V.M., Dimopoulos, N., Alloatti, M., Pardi, M.B., Saez, T.M., Otero, M.G., Cromberg, L.E., Marin-Burgin, A., Scassa, M.E., Stokin, G.B., et al. (2017). alphaSynuclein control of mitochondrial homeostasis in human-derived neurons is disrupted by mutations associated with Parkinson's disease. Sci Rep *7*, 5042. 10.1038/s41598-017-05334-9.

Price, B.D., Mannheim-Rodman, L.A., and Calderwood, S.K. (1992). Brefeldin A, thapsigargin, and AIF4- stimulate the accumulation of GRP78 mRNA in a cycloheximide dependent

manner, whilst induction by hypoxia is independent of protein synthesis. J Cell Physiol *152*, 545-552. 10.1002/jcp.1041520314.
Quinn, N., Critchley, P., and Marsden, C.D. (1987). Young onset Parkinson's disease. Mov Disord *2*, 73-91. 10.1002/mds.870020201.
Rajagopalan, S., Xu, Y., and Brenner, M.B. (1994). Retention of unassembled components of integral membrane proteins by calnexin. Science *263*, 387-390. 10.1126/science.8278814.
Reczek, D., Schwake, M., Schroder, J., Hughes, H., Blanz, J., Jin, X., Brondyk, W., Van Patten, S., Edmunds, T., and Saftig, P. (2007). LIMP-2 is a receptor for lysosomal mannose-6-phosphate-independent targeting of beta-glucocerebrosidase. Cell *131*, 770-783. 10.1016/j.cell.2007.10.018.
Rocha, E.M., Smith, G.A., Park, E., Cao, H., Brown, E., Hallett, P., and Isacson, O. (2015). Progressive decline of glucocerebrosidase in aging and Parkinson's disease. Ann Clin Transl Neurol *2*, 433-438. 10.1002/acn3.177.
Rockenstein, E., Clarke, J., Viel, C., Panarello, N., Treleaven, C.M., Kim, C., Spencer, B., Adame, A., Park, H., Dodge, J.C., et al. (2016). Glucocerebrosidase modulates cognitive and motor activities in murine models of Parkinson's disease. Hum Mol Genet *25*, 2645-2660. 10.1093/hmg/ddw124.
Ron, D., and Walter, P. (2007). Signal integration in the endoplasmic reticulum unfolded protein response. Nat Rev Mol Cell Biol *8*, 519-529. 10.1038/nrm2199.
Ron, I., and Horowitz, M. (2005). ER retention and degradation as the molecular basis underlying Gaucher disease heterogeneity. Hum Mol Genet *14*, 2387-2398. 10.1093/hmg/ddi240.
Rutherford, N.J., Moore, B.D., Golde, T.E., and Giasson, B.I. (2014). Divergent effects of the H50Q and G51D SNCA mutations on the aggregation of alpha-synuclein. J Neurochem *131*, 859-867. 10.1111/jnc.12806.
Samali, A., Fitzgerald, U., Deegan, S., and Gupta, S. (2010). Methods for monitoring endoplasmic reticulum stress and the unfolded protein response. Int J Cell Biol *2010*, 830307. 10.1155/2010/830307.
Sanchez-Martinez, A., Beavan, M., Gegg, M.E., Chau, K.Y., Whitworth, A.J., and Schapira, A.H. (2016). Parkinson disease-linked GBA mutation effects reversed by molecular chaperones in human cell and fly models. Sci Rep *6*, 31380. 10.1038/srep31380.
Schapira, A.H., Cooper, J.M., Dexter, D., Jenner, P., Clark, J.B., and Marsden, C.D. (1989). Mitochondrial complex I deficiency in Parkinson's disease. Lancet *1*, 1269. 10.1016/s0140-6736(89)92366-0.
Schondorf, D.C., Aureli, M., McAllister, F.E., Hindley, C.J., Mayer, F., Schmid, B., Sardi, S.P., Valsecchi, M., Hoffmann, S., Schwarz, L.K., et al. (2014). iPSC-derived neurons from GBA1-associated Parkinson's disease patients show autophagic defects and impaired calcium homeostasis. Nat Commun *5*, 4028. 10.1038/ncomms5028.
Schuck, S., Prinz, W.A., Thorn, K.S., Voss, C., and Walter, P. (2009). Membrane expansion alleviates endoplasmic reticulum stress independently of the unfolded protein response. J Cell Biol *187*, 525-536. 10.1083/jcb.200907074.
Schultheis, P.J., Fleming, S.M., Clippinger, A.K., Lewis, J., Tsunemi, T., Giasson, B., Dickson, D.W., Mazzulli, J.R., Bardgett, M.E., Haik, K.L., et al. (2013). Atp13a2-deficient mice

exhibit neuronal ceroid lipofuscinosis, limited alpha-synuclein accumulation and age-dependent sensorimotor deficits. Hum Mol Genet *22*, 2067-2082. 10.1093/hmg/ddt057.

Scott, L., Dawson, V.L., and Dawson, T.M. (2017). Trumping neurodegeneration: Targeting common pathways regulated by autosomal recessive Parkinson's disease genes. Exp Neurol. 10.1016/j.expneurol.2017.04.008.

Sidransky, E., Nalls, M.A., Aasly, J.O., Aharon-Peretz, J., Annesi, G., Barbosa, E.R., Bar-Shira, A., Berg, D., Bras, J., Brice, A., et al. (2009). Multicenter analysis of glucocerebrosidase mutations in Parkinson's disease. N Engl J Med *361*, 1651-1661. 10.1056/NEJMoa0901281.

Simon-Sanchez, J., Schulte, C., Bras, J.M., Sharma, M., Gibbs, J.R., Berg, D., Paisan-Ruiz, C., Lichtner, P., Scholz, S.W., Hernandez, D.G., et al. (2009). Genome-wide association study reveals genetic risk underlying Parkinson's disease. Nat Genet *41*, 1308-1312. 10.1038/ng.487.

Singleton, A., and Gwinn-Hardy, K. (2004). Parkinson's disease and dementia with Lewy bodies: a difference in dose? Lancet *364*, 1105-1107. 10.1016/S0140-6736(04)17117-1.

Singleton, A.B., Farrer, M., Johnson, J., Singleton, A., Hague, S., Kachergus, J., Hulihan, M., Peuralinna, T., Dutra, A., Nussbaum, R., et al. (2003). alpha-Synuclein locus triplication causes Parkinson's disease. Science *302*, 841. 10.1126/science.1090278.

Smith, M.H., Ploegh, H.L., and Weissman, J.S. (2011). Road to ruin: targeting proteins for degradation in the endoplasmic reticulum. Science *334*, 1086-1090. 10.1126/science.1209235.

Soldner, F., Laganiere, J., Cheng, A.W., Hockemeyer, D., Gao, Q., Alagappan, R., Khurana, V., Golbe, L.I., Myers, R.H., Lindquist, S., et al. (2011). Generation of isogenic pluripotent stem cells differing exclusively at two early onset Parkinson point mutations. Cell *146*, 318-331. 10.1016/j.cell.2011.06.019.

Spillantini, M.G., Divane, A., and Goedert, M. (1995). Assignment of human alpha-synuclein (SNCA) and beta-synuclein (SNCB) genes to chromosomes 4q21 and 5q35. Genomics *27*, 379-381. 10.1006/geno.1995.1063.

Spillantini, M.G., Schmidt, M.L., Lee, V.M., Trojanowski, J.Q., Jakes, R., and Goedert, M. (1997). Alpha-synuclein in Lewy bodies. Nature *388*, 839-840. 10.1038/42166.

Steger, M., Tonelli, F., Ito, G., Davies, P., Trost, M., Vetter, M., Wachter, S., Lorentzen, E., Duddy, G., Wilson, S., et al. (2016). Phosphoproteomics reveals that Parkinson's disease kinase LRRK2 regulates a subset of Rab GTPases. Elife *5*. 10.7554/eLife.12813.

Stojkovska, I., Krainc, D., and Mazzulli, J.R. (2017). Molecular mechanisms of alpha-synuclein and GBA1 in Parkinson's disease. Cell Tissue Res. 10.1007/s00441-017-2704-y.

Stojkovska, I., and Mazzulli, J.R. (2021). Detection of pathological alpha-synuclein aggregates in human iPSC-derived neurons and tissue. STAR Protoc *2*, 100372. 10.1016/j.xpro.2021.100372.

Sun, Y., Liou, B., Quinn, B., Ran, H., Xu, Y.H., and Grabowski, G.A. (2009). In vivo and ex vivo evaluation of L-type calcium channel blockers on acid beta-glucosidase in Gaucher disease mouse models. PLoS One *4*, e7320. 10.1371/journal.pone.0007320.

Suzuki, M., Fujikake, N., Takeuchi, T., Kohyama-Koganeya, A., Nakajima, K., Hirabayashi, Y., Wada, K., and Nagai, Y. (2015). Glucocerebrosidase deficiency accelerates the accumulation of proteinase K-resistant alpha-synuclein and aggravates neurodegeneration

in a Drosophila model of Parkinson's disease. Hum Mol Genet *24*, 6675-6686. 10.1093/hmg/ddv372.

Taira, T., Saito, Y., Niki, T., Iguchi-Ariga, S.M., Takahashi, K., and Ariga, H. (2004). DJ-1 has a role in antioxidative stress to prevent cell death. EMBO Rep *5*, 213-218. 10.1038/sj.embor.7400074.

Takahashi, K., and Yamanaka, S. (2006). Induction of pluripotent stem cells from mouse embryonic and adult fibroblast cultures by defined factors. Cell *126*, 663-676. 10.1016/j.cell.2006.07.024.

Tan, E.K., Tong, J., Fook-Chong, S., Yih, Y., Wong, M.C., Pavanni, R., and Zhao, Y. (2007). Glucocerebrosidase mutations and risk of Parkinson disease in Chinese patients. Arch Neurol *64*, 1056-1058. 10.1001/archneur.64.7.1056.

Tan, Y.L., Genereux, J.C., Pankow, S., Aerts, J.M., Yates, J.R., 3rd, and Kelly, J.W. (2014). ERdj3 is an endoplasmic reticulum degradation factor for mutant glucocerebrosidase variants linked to Gaucher's disease. Chem Biol *21*, 967-976. 10.1016/j.chembiol.2014.06.008.

Thayanidhi, N., Helm, J.R., Nycz, D.C., Bentley, M., Liang, Y., and Hay, J.C. (2010). Alpha-synuclein delays endoplasmic reticulum (ER)-to-Golgi transport in mammalian cells by antagonizing ER/Golgi SNAREs. Mol Biol Cell *21*, 1850-1863. 10.1091/mbc.E09-09-0801.

Theillet, F.X., Binolfi, A., Bekei, B., Martorana, A., Rose, H.M., Stuiver, M., Verzini, S., Lorenz, D., van Rossum, M., Goldfarb, D., and Selenko, P. (2016). Structural disorder of monomeric alpha-synuclein persists in mammalian cells. Nature *530*, 45-50. 10.1038/nature16531.

Tsunemi, T., and Krainc, D. (2014). Zn(2)(+) dyshomeostasis caused by loss of ATP13A2/PARK9 leads to lysosomal dysfunction and alpha-synuclein accumulation. Hum Mol Genet *23*, 2791-2801. 10.1093/hmg/ddt572.

Vidal, R.L., Sepulveda, D., Troncoso-Escudero, P., Garcia-Huerta, P., Gonzalez, C., Plate, L., Jerez, C., Canovas, J., Rivera, C.A., Castillo, V., et al. (2021). Enforced dimerization between XBP1s and ATF6f enhances the protective effects of the UPR in models of neurodegeneration. Mol Ther. 10.1016/j.ymthe.2021.01.033.

Vilarino-Guell, C., Wider, C., Ross, O.A., Dachsel, J.C., Kachergus, J.M., Lincoln, S.J., Soto-Ortolaza, A.I., Cobb, S.A., Wilhoite, G.J., Bacon, J.A., et al. (2011). VPS35 mutations in Parkinson disease. Am J Hum Genet *89*, 162-167. 10.1016/j.ajhg.2011.06.001.

Vogiatzi, T., Xilouri, M., Vekrellis, K., and Stefanis, L. (2008). Wild type alpha-synuclein is degraded by chaperone-mediated autophagy and macroautophagy in neuronal cells. J Biol Chem *283*, 23542-23556. 10.1074/jbc.M801992200.

Walter, P., and Ron, D. (2011). The unfolded protein response: from stress pathway to homeostatic regulation. Science *334*, 1081-1086. 10.1126/science.1209038.

Wang, F., Agnello, G., Sotolongo, N., and Segatori, L. (2011). Ca2+ homeostasis modulation enhances the amenability of L444P glucosylcerebrosidase to proteostasis regulation in patient-derived fibroblasts. ACS Chem Biol *6*, 158-168. 10.1021/cb100321m.

Wang, M., and Kaufman, R.J. (2016). Protein misfolding in the endoplasmic reticulum as a conduit to human disease. Nature *529*, 326-335. 10.1038/nature17041.

Webb, J.L., Ravikumar, B., Atkins, J., Skepper, J.N., and Rubinsztein, D.C. (2003). Alpha-Synuclein is degraded by both autophagy and the proteasome. J Biol Chem *278*, 25009-25013. 10.1074/jbc.M300227200.

Westbroek, W., Gustafson, A.M., and Sidransky, E. (2011). Exploring the link between glucocerebrosidase mutations and parkinsonism. Trends Mol Med *17*, 485-493. 10.1016/j.molmed.2011.05.003.

Wiesmann, U., Vassella, F., and Herschkowitz, N. (1971a). "I-cell" disease: leakage of lysosomal enzymes into extracellular fluids. N Engl J Med *285*, 1090-1091. 10.1056/NEJM197111042851922.

Wiesmann, U.N., Lightbody, J., Vassella, F., and Herschkowitz, N.N. (1971b). Multiple lysosomal enzyme deficiency due to enzyme leakage? N Engl J Med *284*, 109-110. 10.1056/NEJM197101142840220.

Wong, K., Sidransky, E., Verma, A., Mixon, T., Sandberg, G.D., Wakefield, L.K., Morrison, A., Lwin, A., Colegial, C., Allman, J.M., and Schiffmann, R. (2004). Neuropathology provides clues to the pathophysiology of Gaucher disease. Mol Genet Metab *82*, 192-207. 10.1016/j.ymgme.2004.04.011.

Wood-Kaczmar, A., Gandhi, S., Yao, Z., Abramov, A.Y., Miljan, E.A., Keen, G., Stanyer, L., Hargreaves, I., Klupsch, K., Deas, E., et al. (2008). PINK1 is necessary for long term survival and mitochondrial function in human dopaminergic neurons. PLoS One *3*, e2455. 10.1371/journal.pone.0002455.

Xie, W., and Chung, K.K. (2012). Alpha-synuclein impairs normal dynamics of mitochondria in cell and animal models of Parkinson's disease. J Neurochem *122*, 404-414. 10.1111/j.1471-4159.2012.07769.x.

Xu, Y.H., Sun, Y., Ran, H., Quinn, B., Witte, D., and Grabowski, G.A. (2011). Accumulation and distribution of alpha-synuclein and ubiquitin in the CNS of Gaucher disease mouse models. Mol Genet Metab *102*, 436-447. 10.1016/j.ymgme.2010.12.014.

Xu, Y.H., Xu, K., Sun, Y., Liou, B., Quinn, B., Li, R.H., Xue, L., Zhang, W., Setchell, K.D., Witte, D., and Grabowski, G.A. (2014). Multiple pathogenic proteins implicated in neuronopathic Gaucher disease mice. Hum Mol Genet *23*, 3943-3957. 10.1093/hmg/ddu105.

Yoshida, H., Matsui, T., Yamamoto, A., Okada, T., and Mori, K. (2001). XBP1 mRNA is induced by ATF6 and spliced by IRE1 in response to ER stress to produce a highly active transcription factor. Cell *107*, 881-891. 10.1016/s0092-8674(01)00611-0.

Youle, R.J., and Narendra, D.P. (2011). Mechanisms of mitophagy. Nat Rev Mol Cell Biol *12*, 9-14. 10.1038/nrm3028.

Zambon, F., Cherubini, M., Fernandes, H.J.R., Lang, C., Ryan, B.J., Volpato, V., Bengoa-Vergniory, N., Vingill, S., Attar, M., Booth, H.D.E., et al. (2019). Cellular alpha-synuclein pathology is associated with bioenergetic dysfunction in Parkinson's iPSC-derived dopamine neurons. Hum Mol Genet *28*, 2001-2013. 10.1093/hmg/ddz038.

Zimprich, A., Benet-Pages, A., Struhal, W., Graf, E., Eck, S.H., Offman, M.N., Haubenberger, D., Spielberger, S., Schulte, E.C., Lichtner, P., et al. (2011). A mutation in VPS35, encoding a subunit of the retromer complex, causes late-onset Parkinson disease. Am J Hum Genet *89*, 168-175. 10.1016/j.ajhg.2011.06.008.

Zunke, F., and Mazzulli, J.R. (2019). Modeling neuronopathic storage diseases with patient-derived culture systems. Neurobiol Dis *127*, 147-162. 10.1016/j.nbd.2019.01.018.

Zunke, F., Moise, A.C., Belur, N.R., Gelyana, E., Stojkovska, I., Dzaferbegovic, H., Toker, N.J., Jeon, S., Fredriksen, K., and Mazzulli, J.R. (2018). Reversible Conformational Conversion of alpha-Synuclein into Toxic Assemblies by Glucosylceramide. Neuron *97*, 92-107 e110. 10.1016/j.neuron.2017.12.012.